THE UNIVERSITY OF MICHIGAN
COLLEGE OF LITERATURE, SCIENCE, AND THE ARTS
Department of Physics

Technical Report No. 26

DEUTERON PRODUCTION IN PROTON-PROTON COLLISIONS FROM 1.5 TO 3 GeV

David E. Pellett

ORA Project 03106

under contract with:

DEPARTMENT OF THE NAVY
OFFICE OF NAVAL RESEARCH
WASHINGTON, D.C.

CONTRACT NO. Nonr-1224(23)
NR-022-274

administered through:

OFFICE OF RESEARCH ADMINISTRATION ANN ARBOR

August 1966

This report was also a dissertation submitted in partial fulfillment of the requirements for the degree of Doctor of Philosophy in The University of Michigan, 1966.

ABSTRACT

The differential cross section for deuteron production in proton-proton collisions was measured for incident proton kinetic energies of 1.55, 2.5, and 2.9 GeV. Measurements were made at laboratory angles of 5.9°, 11.55°, 15.72°, and at the two higher energies, at 20° relative to the beam direction for deuteron laboratory momenta in the range 1.0-2.4 GeV/c.

The experiment was performed in an external proton beam of the cosmotron at Brookhaven National Laboratory. A system of scintillation and Čerenkov counters was used to identify deuterons by momentum analysis and time-of-flight techniques.

The differential cross sections are presented in the laboratory and center of mass (c.m.) systems. Plots are given of the cross section versus the invariant mass of the system of particles formed with the deuteron in the collisions. Total cross sections were obtained by integrating a smooth function fitted to the c.m. data at each energy.

The deuteron distributions in the laboratory system were peaked at small angles relative to the beam direction. All deuterons were formed with momenta >1.0 GeV/c.

The c.m. differential cross section distributions obtained at the three energies of this experiment showed a general similarity to one another. The cross section was

sharply peaked in the forward and backward directions for large c.m. momenta. The maximum became more broad as the momentum decreased until the cross section was almost isotropic. There was evidence of structure in the broad maximum at intermediate momenta.

The total deuteron production cross section decreased monotonically with incident proton kinetic energy from 310 ± 25 μb at 1.5 GeV to 137 ± 21 μb at 2.9 GeV. The interpolated value at 2.3 GeV was consistent with the statistical model prediction. The cross section for production of deuterons associated with two or more pions had a maximum near 2 GeV.

A search for pion resonances of unit isotopic spin in the mass range 400-1000 MeV through reactions of the form $p + p \rightarrow d + x^+$ yielded evidence for ρ production. At 2.5 GeV, the ρ production cross section was small ($\sigma_{total} \lesssim 9$ μb) and did not appear to be sharply peaked in the forward and backward directions. Upper limits were set for the production of the ζ (560 MeV) and the X^+ (960 MeV) resonances.

The laboratory distributions in momentum and angle of deuterons produced in proton-proton collisions at 2.9 GeV were found to be much different from those arising from proton-beryllium and proton-platinum collisions at the same energy. The total deuteron production cross section per nucleon was approximately six times greater in collisions of protons with beryllium than in collisions with other protons, indicating that specifically nuclear processes are at work in the former case.

ACKNOWLEDGMENTS

I would especially like to thank Dr. Oliver E. Overseth for his continual guidance during the entire course of the experiment. His fine personal qualities both as scientist and friend have been a source of inspiration during my graduate studies.

I would like to express my gratitude to Dr. Martin Perl for his invaluable contributions to the planning and performance of this experiment. In addition, I am grateful to Dr. Lawrence Jones and Dr. Michael Longo for many useful discussions.

I am indebted to my colleagues, particularly Dr. Richard Heinz, but also Dr. Homer Neal, Dr. Howard Saxer, and Fred Martin, for their help in various stages of the work.

I am grateful to Walter Merkle, John Harris, and the entire staff of the Brookhaven Cosmotron for their expert skills which were called upon in setting up and running the experiment. Also, I wish to thank the staff of the Stanford Linear Accelerator Center for their help in the design and construction of the experimental apparatus.

TABLE OF CONTENTS

TABLE OF CONTENTS CONT'D

LIST OF TABLES

LIST OF TABLES CONT'D

LIST OF FIGURES

LIST OF FIGURES CONT'D

LIST OF FIGURES CONT'D

LIST OF FIGURES CONT'D

LIST OF APPENDICES

CHAPTER I

INTRODUCTION

A. Deuteron Production in Proton-Proton Collisions

Differential and total cross sections for the production of deuterons in proton-proton collisions were obtained in this experiment for three values of incident proton kinetic energy in the range 1.5 to 3 GeV. The important partial cross sections contributing to deuteron production at these energies are

$$\begin{aligned} p + p \rightarrow\ & d + \pi^+ && (1)\\ & d + \pi^+ + \pi^\circ && (2)\\ & d + \pi^+ + \pi^+ + \pi^- && (3)\\ & d + \pi^+ + \pi^\circ + \pi^\circ && (4)\ . \end{aligned}$$

A detailed study of reaction (1) has been made in this energy range by Heinz, et al.[1,2] This paper will be primarily concerned with reactions in which two or more particles are formed with the deuteron.

There are several reasons why deuteron production in proton-proton collisions is of interest:

1) A number of bubble chamber experiments[3,4,5] have yielded data on inelastic proton-proton scattering leading to an unbound proton and neutron in the final state. Comparison of the angular distributions of deuterons with those of the

unbound nucleons may give insight into how the deuteron is formed at high energies. Theoretical interpretation of the data could yield information concerning the short range components of the deuteron wave function.

2) The differential cross section for deuteron production can be used to study resonance formation in the system of pions created with the deuteron. For a given incident proton energy, a reaction of the form $p + p \rightarrow d + X^+$, where X^+ is a short lived resonance of unit isotopic spin which decays into two or more pions, will lead to an enhancement of the deuteron production cross section in a range of deuteron center of mass (c.m.) momenta determined by the mass and width of the resonance.

3) Deuteron production in collisions of protons with complex nuclei has been studied both experimentally and theoretically at high energies. The nature of deuteron production in elementary proton-proton interactions is basic to the understanding of this process.

B. Survey of Existing Data

Several bubble chamber experiments have measured total cross sections for some of the reactions listed on page 1 in the energy range 1 to 3 GeV. The most comprehensive information comes from the experiment of Sechi Zorn[6,7] at 2.05 GeV. Total cross sections were measured for each of the four reactions. A sufficient number of events were found to establish a pion system invariant mass spectrum for

reactions (2) and (3). The $\pi^+\pi^\circ$ invariant mass spectrum showed evidence of the ρ meson and a narrow resonance at a mass of 560 MeV. Other authors[8,9,10] have reported a two pion resonance with an isotopic spin of one in this mass region. Although it has been given a name, the ζ, its existence is not well established, since none of the experiments observed it with a high level of statistical significance. No evidence was reported of resonance formation in the $\pi^+\pi^+\pi^-$ invariant mass spectrum.

Other bubble chamber experiments reporting deuteron formation are those of Hart, et al.,[5] who report a cross section for the $d\pi^+\pi^+\pi^-$ and $d\pi^+\pi^+\pi^-\pi^\circ$ final states at an incident proton kinetic energy of 2.85 GeV, Eisner, et al.,[3] who report a cross section for the $d\pi^+\pi^-$ final state at 1.48 GeV, and Bugg, et al.,[11] who report a single event of the type $p + p \rightarrow d + \pi^+ + \pi^\circ$ at 970 MeV. The paper of Pickup, et al.[4] reports partial cross sections for deuteron production at 2.05 GeV, but these data were obtained from the same bubble chamber exposure studied in detail by Sechi Zorn. The number of events seen in each of these experiments was small, so neither invariant mass nor angular distributions were given. The results of these experiments will be discussed in Chapter V.

Turkot, et al.,[12,13] using scintillation counters, made a study of deuterons produced in proton-proton collisions at an angle of 0° relative to the incident beam. The differential cross section for deuteron production was

obtained as a function of deuteron momentum for incident proton kinetic energies of 1.55, 1.93, 2.11, and 2.50 GeV. A search for resonances showed clear evidence of ρ production, but no strong indication of the ζ. Graphs of the results of the experiment at 1.55 and 2.50 GeV are given in Chapter IV.

At considerably higher energies, Diddens, et al.[14] have measured differential cross sections for deuteron production at a fixed laboratory angle of 6.6° using scintillation counters. Measurements were made for three values of deuteron momentum at an incident proton momentum of 19 GeV/c and for four values at 24 GeV/c.

A wide literature exists on deuteron production by protons incident on complex nuclei. Of particular interest is a recent experiment of Piroué and Smith[15] to study deuteron production in collisions of protons with beryllium and platinum nuclei at 2.9 GeV. The reader is referred to the paper of Glassgold[16] for a review of other work in this field.

C. Theory

Theories have been developed to explain the reaction $p + p \rightarrow d + \pi^+$ and to explain some features of inelastic proton-proton collisions without deuteron formation in the energy range 1-3 GeV, but at present, little theoretical work has been done on deuteron production when two or more pions occur in the final state.

Hagedorn [17] has studied deuteron production in proton-proton collisions on the basis of a statistical model. In this theory, the dynamics of the interaction are not considered. The probability for producing a final state of a certain type (for example, one made up of a deuteron and two pions), is determined by the number of states of that type relative to the total number of final states allowed by the various conservation laws. For a given energy of the incident proton, the theory relates the total deuteron production cross section and the partial cross sections for the reactions $p + p \rightarrow d + \pi^+$ and $p + p \rightarrow d + \pi^+ + \pi^\circ$ to the total proton-proton inelastic cross section. Also, a prediction was made for the ratio of deuteron to proton flux as a function of momentum at a fixed laboratory production angle. These predictions are compared with experiment in Chapter V.

The isobar model of Sternheimer and Lindenbaum[18] has been used by many authors[3,4,5] in interpreting the results of experiments on proton-proton inelastic collisions in the energy range 1-3 GeV. The theory assumes that nucleon isobars, primarily the $N^*_{3/2}(1238)$, but also the $N^*_{1/2}(1512)$ and the $N^*_{1/2}(1688)$, are formed in the collision, and all pions result from their subsequent decay. More than one pion can be produced if two isobars are formed, or if a transition occurs from one isobaric state to another with the emission of a pion. The probability for the formation of two pions at a single

vertex is assumed small. The production and decay of the isobars are treated according to statistical and phenomenological methods. The model predicts momentum distributions for the particles in the final state and relationships among the various partial cross sections. The fact that the theory is in rather good agreement with experimental results shows the importance of the formation of nucleon isobars, particularly the $N^*_{3/2}(1238)$, in inelastic proton-proton collisions in this energy range. Sternheimer and Lindenbaum did not predict cross sections for deuteron production, but the theory could presumably be extended to calculate the number of deuterons produced in the various neutron-proton final states.

When only a single pion is formed in the final state, more detailed calculations can be made which, unlike those previously mentioned, predict the angular dependence of the cross section. The one pion exchange model has been useful for describing single pion formation in inelastic proton-proton scattering (see, for example, references 3 and 11). It predicts the observed peaking of the nucleon production cross section at 0 and 180° in the c.m. system (The cross section is symmetric about 90° in the c.m. if the beam is unpolarized since the protons in the initial state are identical particles). The angular distribution of deuterons from the reaction $p + p \rightarrow d + \pi^+$ is somewhat different in the energy range 1.3-2.5 GeV, in that the maximum occurs away from 180° (0°).[1,2]

For example, at an energy of 1.5 GeV, it appears at 148° (32°). Yao[19] has extended the theory to include deuteron production through a final state interaction between the neutron and proton after a positive pion has been formed through one pion exchange. In terms of Feynman diagrams, the reaction proceeds through either

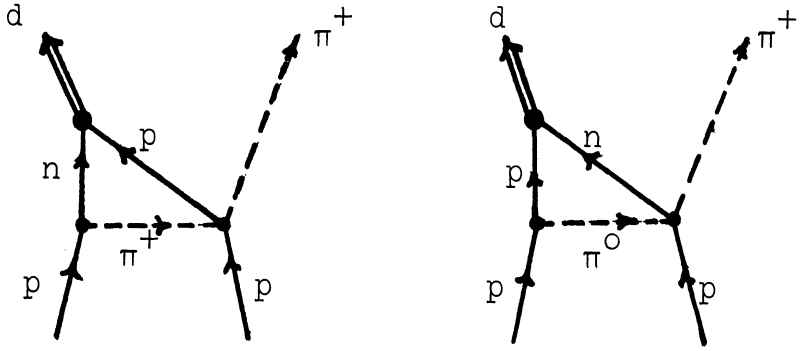

(a) or (b).

Deuteron production can also occur through one nucleon exchange:

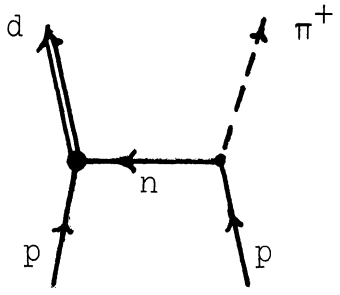

This diagram has been calculated by Heinz,[2] who found it to produce a larger deuteron production cross section than one pion exchange. Qualitative agreement with the experimental angular distributions could be obtained with a suitable choice of deuteron wave function, but the quantitative agreement was not striking for either the one pion exchange or the one nucleon exchange calculations. This is not surprising since many approximations were involved in both.

Modification of such models to include multiple pion production would probably be difficult, but is the only means at present to explain deuteron angular distributions such as those observed in this experiment.

CHAPTER II

EXPERIMENTAL TECHNIQUE

A system of quadrupoles and bending magnets directed protons from the cosmotron at Brookhaven National Laboratory onto a liquid hydrogen target. Deuterons produced in the target were identified by momentum analysis and time of flight techniques in a spectrometer consisting of a bending magnet and a system of scintillation and Čerenkov counters.

A. The Beam

For this experiment, the cosmotron produced an external beam of protons of variable energy in the range 1.0 to 2.9 GeV. The particles arrived at the target in repetitive bursts spaced several seconds apart. Each burst lasted approximately 250 msec. and contained up to 5×10^9 protons.

The energy of the beam could be determined by measurement of a) the path length and revolution frequency of the particle orbit inside the cosmotron, or b) the radius of curvature in the (known) cosmotron magnetic field.[20] The application of one or both of these procedures allowed a measurement of the average incident proton kinetic energy to within $\pm$.05 GeV. The spread in energy about this central value was of the order of 2 MeV full width at half maximum (FWHM).

After extraction from the machine, the beam was directed onto the target by the series of bending and focussing magnets depicted in Fig. 1. The magnet specifications are listed in Table I. At the target, the diameter and angular divergence of the beam must be small in order that the production angle of the deuterons observed by the spectrometer be well defined. Focusing was accomplished by the quadrupole triplet, magnets Q201, Q202, and Q203. The bending magnets, H204 and H205, directed the beam onto the target along the desired beam line in the horizontal plane. They also swept secondary particles of low momentum out of the beam. Protons which did not interact in the target were guided by magnet C207 into a large absorber consisting of lead bricks and steel plates. This beam stopper was placed at a slight angle with respect to the original beam direction to allow clearance for the rear counter assembly.

The angle at which the beam emerges from the cosmotron varies with energy. The current in magnet H200 was adjusted to correct for this effect and bring the beam into the quadrupoles along the desired axis. H200 also served as a collimator. The pole faces of this magnet limited the vertical dimension of the beam to 1.5 in. The beam width was defined by a pair of thick brass absorbers which filled the gap of H200 except for a narrow slot in the center. The width of this slot was varied from .75 to 2.0 in. according to the focusing requirements at the various energies.

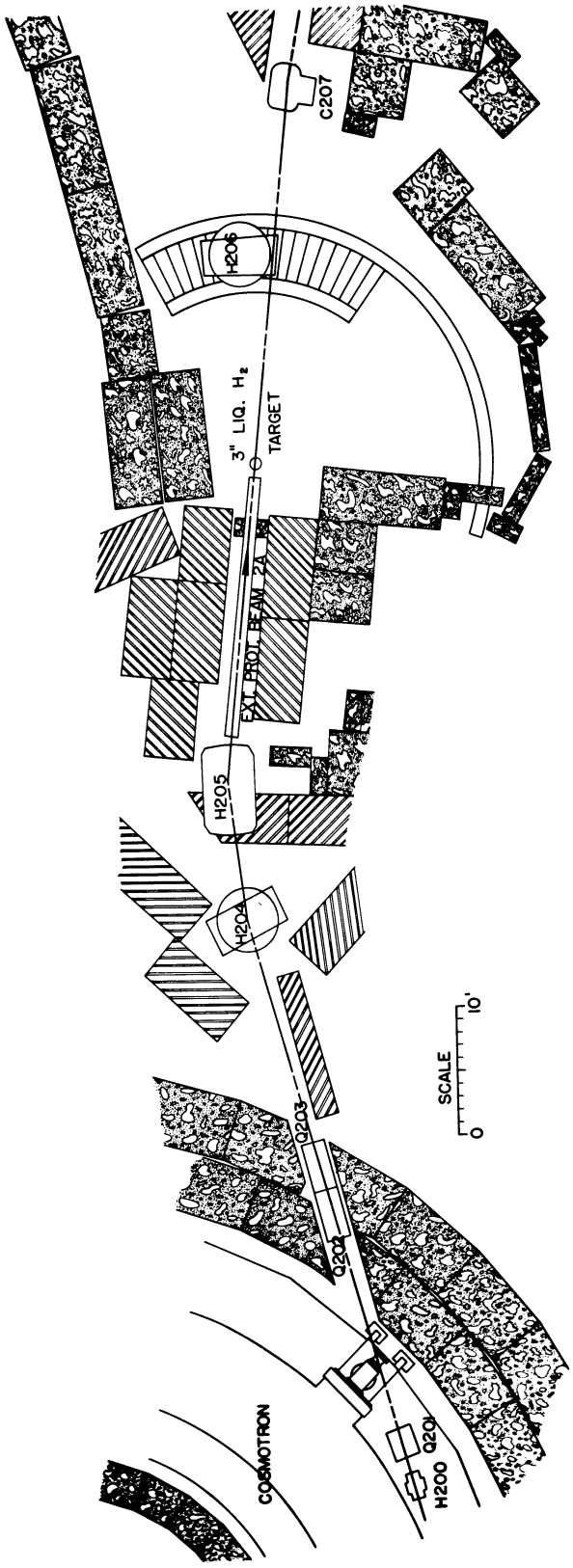

Fig. 1. The beam layout.

TABLE I

MAGNET DATA

MAGNET (See Fig. 1)	PURPOSE	DIMENSIONS OF GAP (HxWxD or Dia.xD) (in.)
H 200	BENDING	1.5 x 6 x 12
Q 201	HORIZ. FOCUSING	8 x 16
Q 202	VERT. FOCUSING	8 x 32
Q 203	HORIZ. FOCUSING	8 x 32
H 204	BENDING	6 x 18 x 36
H 205	BENDING	6 x 12 x 60
H 206	MOMENTUM ANALYSIS	10.5 x 18 x 36
C 207	BENDING	6 x 12 x 24

Collimation was necessary because of the double requirement of small spot size (cross sectional area of the beam) and small angular divergence of the beam particles at the target. One could adjust the vertical position of the beam at the target by moving H200 up or down.

H206 is the momentum analyzing magnet of the spectrometer. The beam traveled in vacuum pipes or polyethylene bags filled with helium wherever possible to reduce multiple Coulomb scattering.

A computer program gave initial values for the currents in the magnet string at each value of beam energy. Then the location and size of the beam spot were determined at the exit of Q203, at the target, and at the entrance of C207 by exposing Polaroid film in the beam. The currents were adjusted until the beam traveled along the desired path and showed a diameter at the target of less than 1.5 in. The divergence was measured by comparing the diameter of the beam spot at the target with its value at the entrance of C207. This quantity was generally of the order of .2°.

B. The Liquid Hydrogen Target

The target consisted of a cylinder 3.03 in. long and 4 in. in diameter made of .010 in. mylar which could be filled with liquid hydrogen. It was suspended in an evacuated aluminum box by its filling lines from the liquid hydrogen reservoir. In addition to the vacuum, thermal insulation was provided by wrapping the target with one

layer of aluminum foil and twenty layers of .00025 in. aluminized mylar. The box containing the target was provided with a circular window of .010 in. mylar for the incoming beam, and a wide, curved, rectangular window of .015 in. mylar for the emergent particles. A photograph of the target assembly is shown in Fig. 2.

C. The Spectrometer

Deuterons are recognized in the background of pions and protons by selecting only particles with momenta in a specified range, and then measuring the time-of-flight spectrum of these particles over a flight path of approximately forty feet. If the momentum acceptance of the spectrometer is sufficiently narrow and the velocities of the particles not too close to the speed of light, the time-of-flight distributions of particles of different mass will be distinct. If, for example, deuterons are present, a peak will appear in the time-of-flight spectrum corresponding to the arrival of particles of the deuteron mass with various momenta, and it will be separate from the peak corresponding to protons or pions. The distribution of counts in this peak can then be related to the differential cross section for deuteron production as a function of momentum. A typical time-of-flight spectrum is shown in Fig. 3.

The spectrometer is shown in Fig. 4. The objects labeled A_1', A_1°, A_2, B_1, and B_2 are scintillation counters through which pass deuterons produced in the target by the beam of protons. The counters are made of commercial plastic

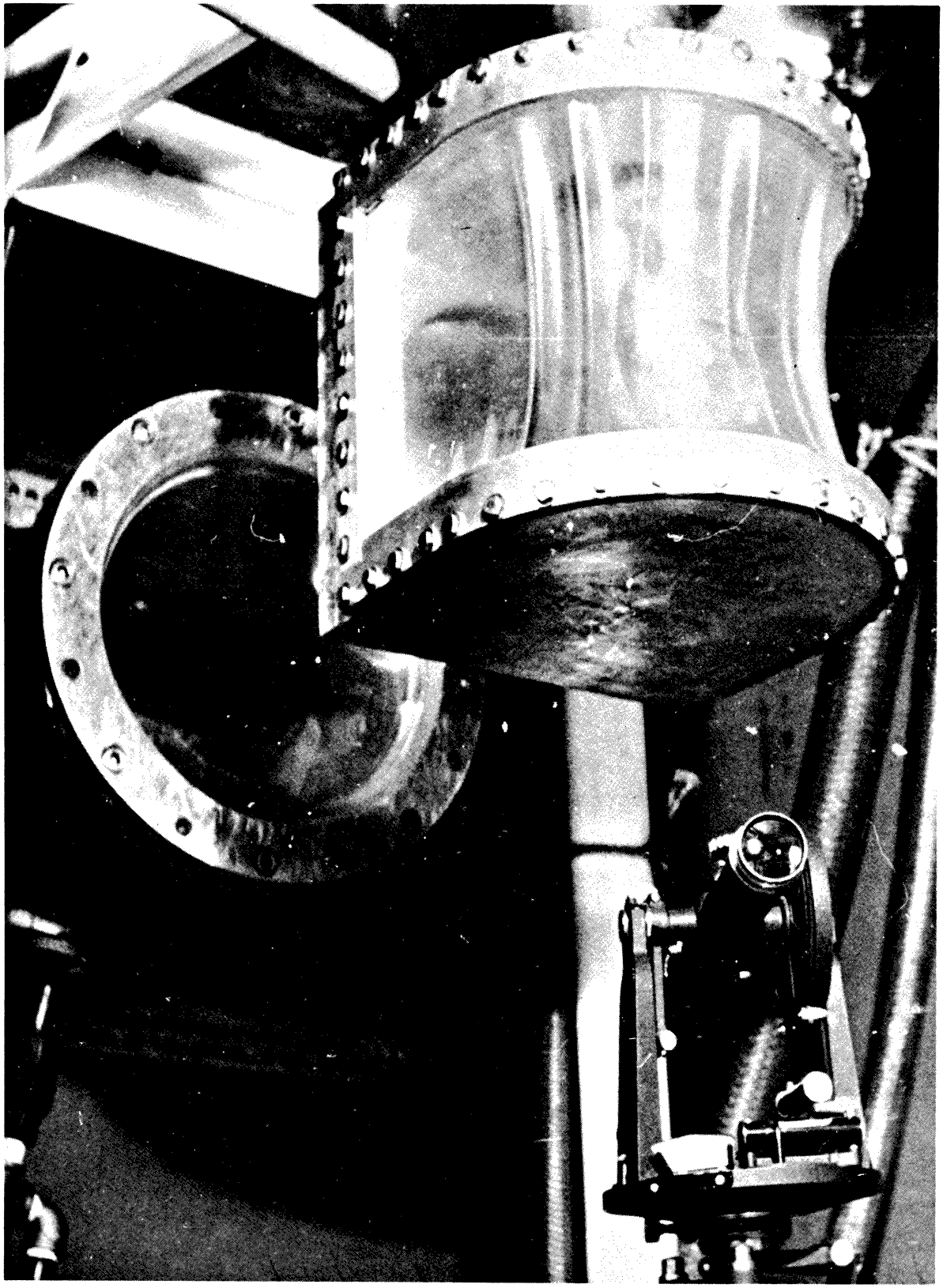

Fig. 2. The liquid hydrogen target.

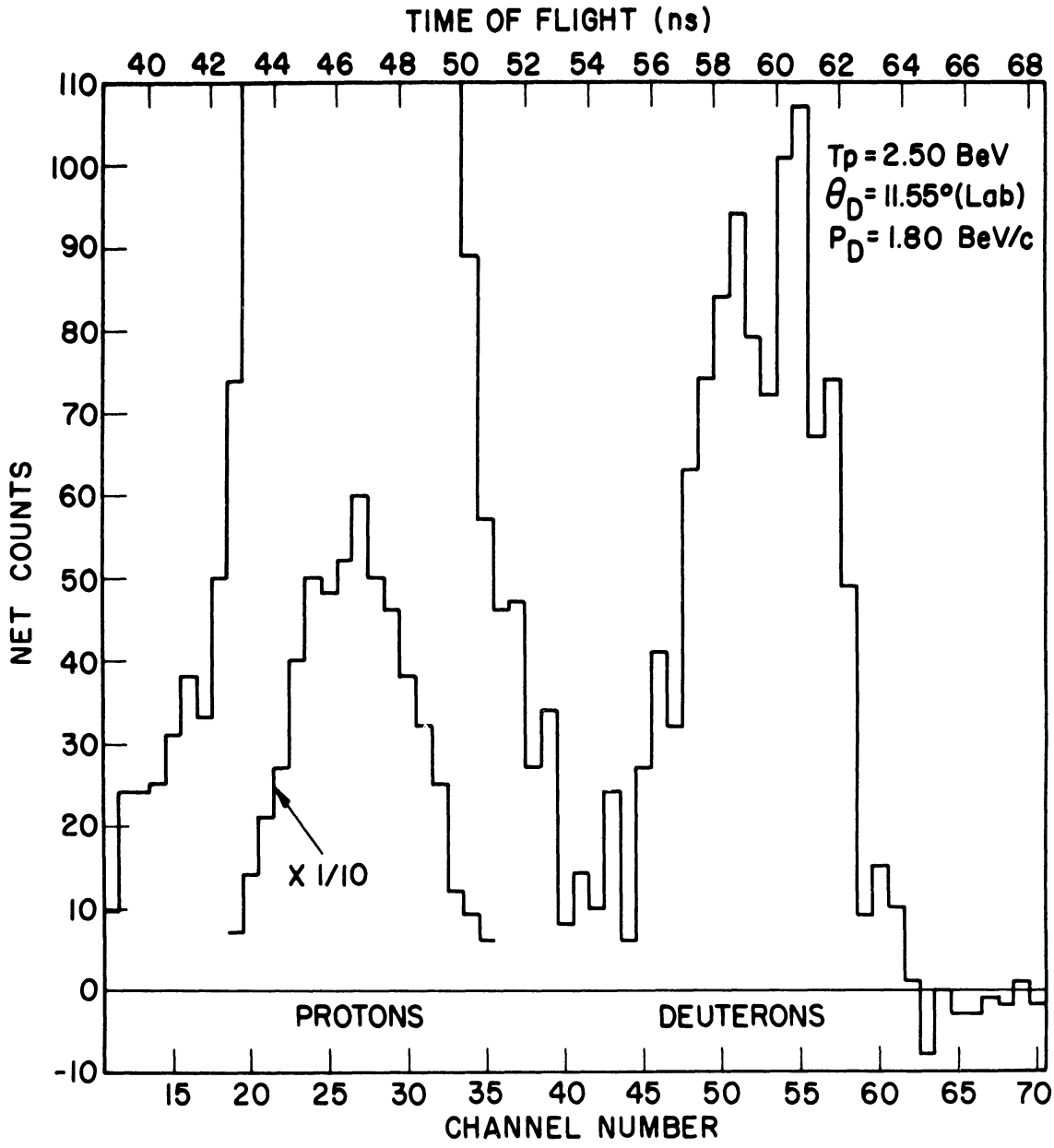

Fig. 3. TYPICAL TIME-OF-FLIGHT SPECTRUM

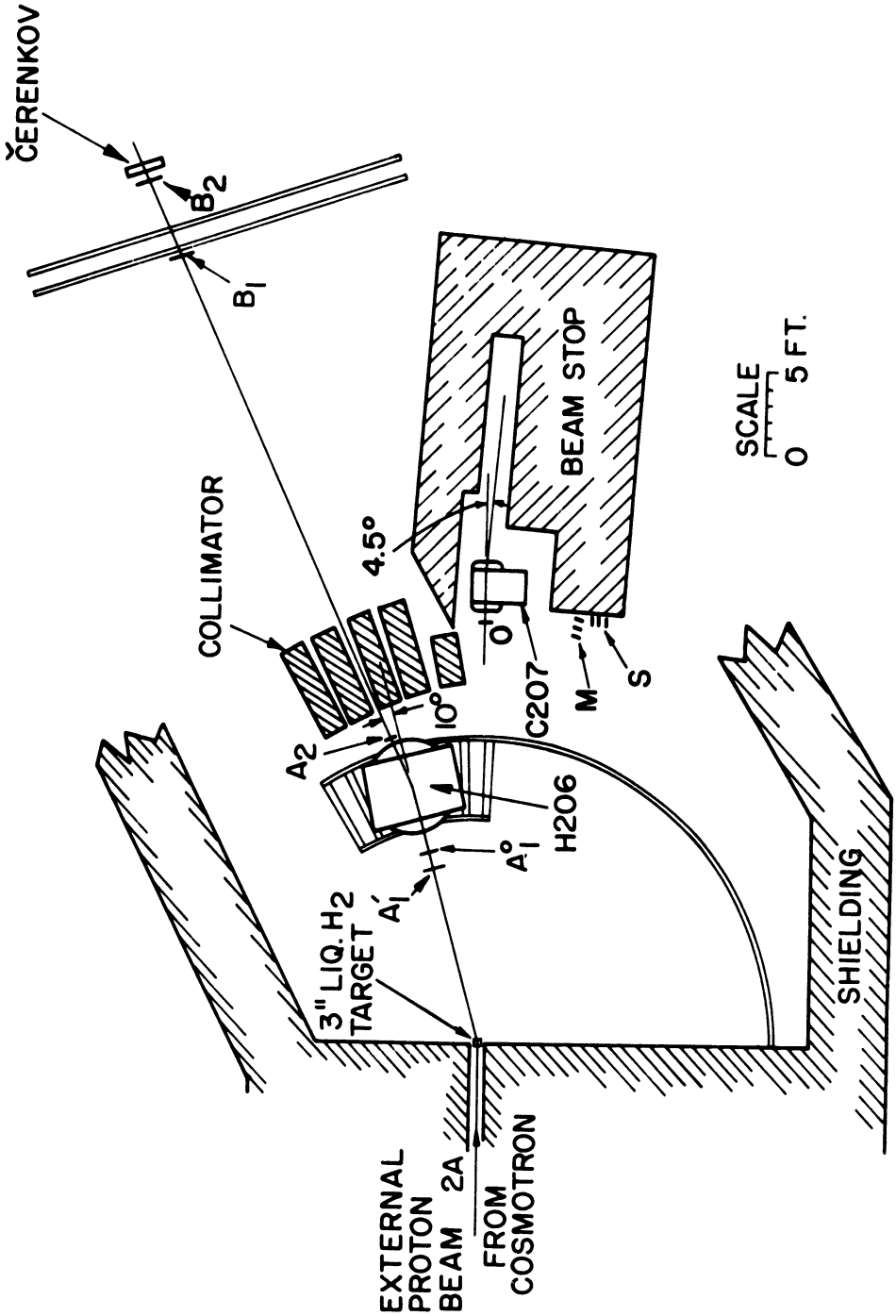

Fig. 4. THE EXPERIMENTAL LAYOUT

scintillating material, and except for A2 are connected to 14-stage photomultiplier tubes by means of Lucite light pipes. The counter A2 defines the solid angle acceptance of the spectrometer. Deuterons with momentum greater than 1.7 GeV/c passing through a thick Lucite light pipe would produce spurious counts through Čerenkov radiation. To avoid this, the block of scintillating material was supported by a thin walled polystyrene tube. Light was conducted to the photomultiplier through a hollow cylinder covered on the inside surface with a thin sheet of highly polished aluminum.

The Čerenkov counter is of the threshold type. It consists of a rectangular box constructed of Lucite, with thin front and back walls. The outside of the box is painted with a white reflective coating. The box is filled with FC-75, a liquid fluorocarbon compound manufactured by the Minnesota Mining and Manufacturing Company. Six photomultipliers are affixed to the box to detect Čerenkov radiation. Since the refractive index of FC-75 is 1.276, the minimum momentum for Čerenkov emission is 2.38 GeV/c for deuterons, 1.19 GeV/c for protons, and .177 GeV/c for charged pions. The counter is used in anticoincidence with the pulses from counters B1 and B2 to cut down the background counting rate from pions and protons. The range of deuteron momenta analyzed by the spectrometer is 1.0 to 2.4 GeV/c, so the deuteron counting rate is not affected.

The counter labeled 0 is a circular scintillator placed in the proton beam. Its output is integrated and

displayed on an oscilloscope to give a visual indication of the instantaneous beam flux as a function of time during the burst of particles from the cosmotron (known as the "spill"). The counting rate in the beam is too high to be recorded accurately by this counter. Rather, the beam flux is monitored indirectly by the two counter telescopes, M and S. Each telescope consists of three small scintillators in line spaced several inches apart, and placed in electronic coincidence. M counts particles produced in the liquid hydrogen target. S counts particles produced by the beam in the scintillator, O. The flux in each telescope is proportional to the beam flux. Since only about 1% of the beam interacts in the target, the flux in S is nearly independent of whether or not the target is filled with liquid hydrogen. It is used to measure the beam rate during runs with the target empty for background measurements. The monitor telescopes are calibrated by the radioactive foil technique (described in Appendix I) to provide an absolute determination of the number of particles passing through the target during each cross section measurement.

The dimensions and other pertinent data concerning the various counters used in the experiment are listed in Table II. The intercounter distances are listed in Table III.

Magnet H206 is used to momentum analyze the particles. It is a standard Brookhaven bending magnet (type H 18x36 Mk I), and is described in Brookhaven literature.[21] The polefaces have dimensions 18x36 in., the gap is 10.5 in., the effective length of the magnetic field is 43 in., and the maximum

TABLE II

COUNTER SPECIFICATIONS

COUNTER	MATERIAL	DIMENSIONS (H x W x D) (in.)	PHOTOMULTIPLIER	
			NUMBER	TYPE
A1°,A1'	S[1]	6.5 x 3 x .375	1	6810A
A2	S	6 x 1 x .5	1	6810A
B1	S	25.875 x 8 x .375	1	6810A
B2	S	32 x 11 x .5	2	56AVP
S1,S2,S3	S	1.5 x 1.5 x .375	1	6810A
M1,M2,M3	S	1 x 1 x .25	1	53AVP
O	S	8 (dia.) x .5	1	6810A
Cerenkov	FC - 75[2]	31 x 11.5 x 4	6	6810A

[1]Plastic scintillating material manufactured by Semielements Inc., Saxonburg, Pa.

[2]Liquid fluorocarbon compound (see text)

TABLE III
INTERCOUNTER DISTANCES

FROM	TO	DISTANCE (ft.)
Target	A1'	12.17
A1'	A1°	.87
A1°	Magnet center	3.53
Magnet center	A2	3.29
A2	B1	34.05 (5.9°)
		33.86 (11.55°)
		34.01 (15.72°)
		34.49 (20.0°)
B1	B2	5.1
B2	Čerenkov	.8

field is 15.2×10^3 gauss at a current of 1000 A. The particle trajectories pass through the central field region, which is quite uniform.

The spectrometer is made sensitive to particles of different momenta by changing the current in the magnet. The central ray, originating in the center of the target and passing through the centers of all counters in the spectrometer, is bent through an angle of 10° in the magnet. The momentum setting of the spectrometer is specified by giving the momentum, p_o, of a particle which follows this ray. Since the target and counters have finite widths and the direction of a particle can be altered by multiple Coulomb scattering, particles of momentum $p \neq p_o$, whose trajectories bend through angles other than 10°, will also be counted. The probability of counting an off-momentum particle is a bell-shaped function of p/p_o with FWHM of 13.2% The exact shape of the function varies slowly with p_o. It is described in detail in Chapter III.

All elements of the spectrometer are movable so cross sections can be measured at various angles relative to the direction of the incident beam. The magnet and counters A1', A1°, and A2 are mounted on a carriage that rolls on a circular arc of railroad track. It is driven by a fractional horsepower electric motor to facilitate the change of angles, since the assembly weighs about 20 tons. Counters B1 and B2 are attached to a table which slides on a pair of aluminum

I-beams. B2 is connected to the table by a pair of swinging arms so that it can be aligned with the other counters at each angle. The Čerenkov counter is mounted separately on a rolling table.

In order to reduce the number of particles traversing the rear counter assembly, a collimator six feet thick was constructed of shielding blocks behind the magnet. Four slits were provided corresponding to deuteron production angles of 5.9°, 11.55°, 15.72°, and 20.0°. Additional collimation and shielding for A2 was provided by lead bricks stacked in the magnet gap. Ample clearance was allowed for the desired particle trajectories. When the magnet carriage was in the 5.9° position, the proton beam passed through the gap of H206 in an open space of low magnetic field between the edge of the pole face and the return yoke.

Fig. 5 is a view of the area around the spectrometer magnet. In addition to H206 and its carriage, it shows the collimator, the monitor telescopes, the beam stopper, and the helium bag for the proton beam. Fig. 6 shows counters A1' and A1°, as well as the collimator in the gap of H206. The rear counter assembly is shown in Fig. 7. These photographs were taken with the counters in the 5.9° position.

In setting up the experiment, the counter supports were positioned and the counters aligned with transits. The railroad track was leveled by suitably placing shims under the steel ties. A steel measuring tape was attached to the outside rail which could be sighted through a special indicator attached to the magnet carriage. This scale was

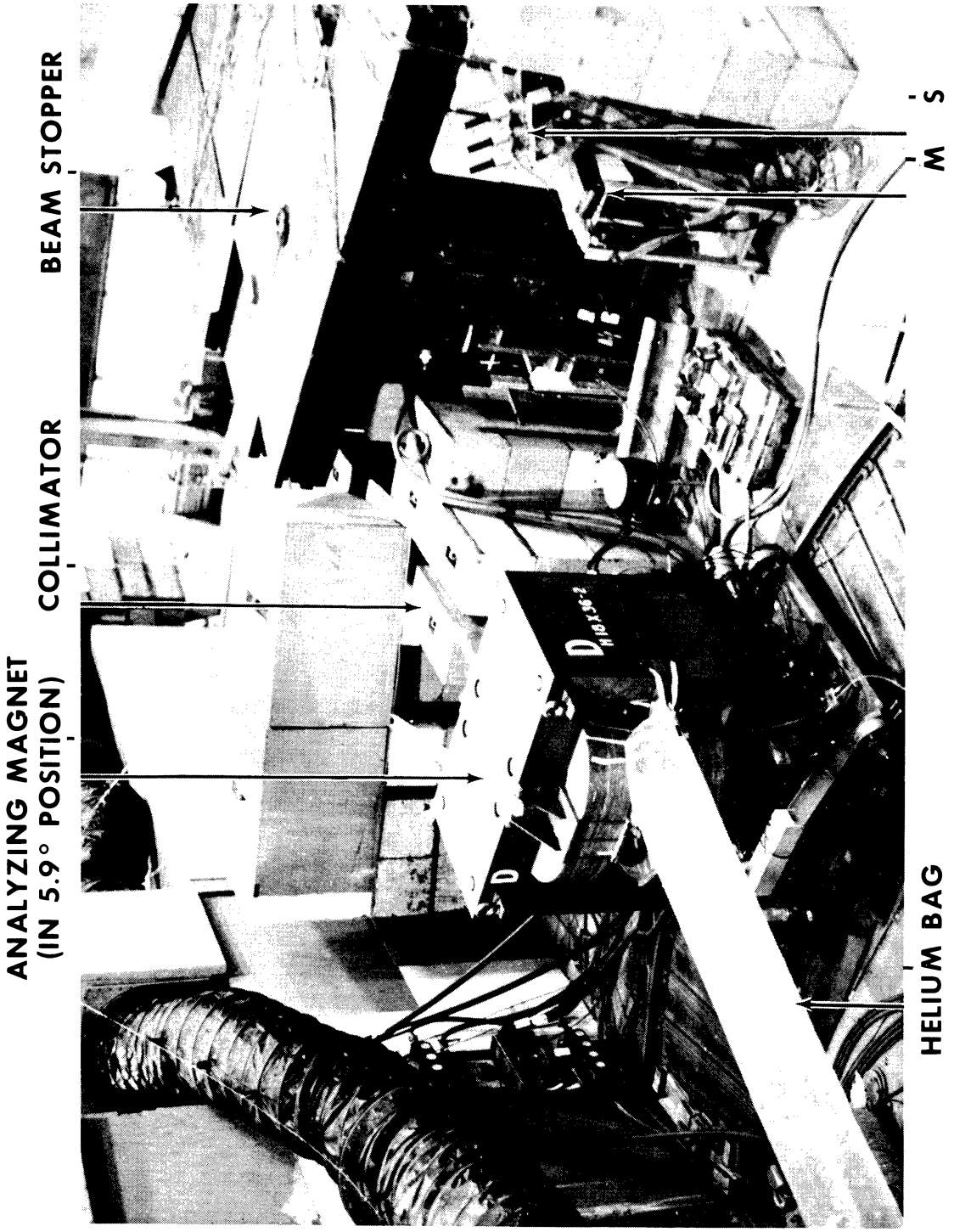

Fig. 5. The experimental area.

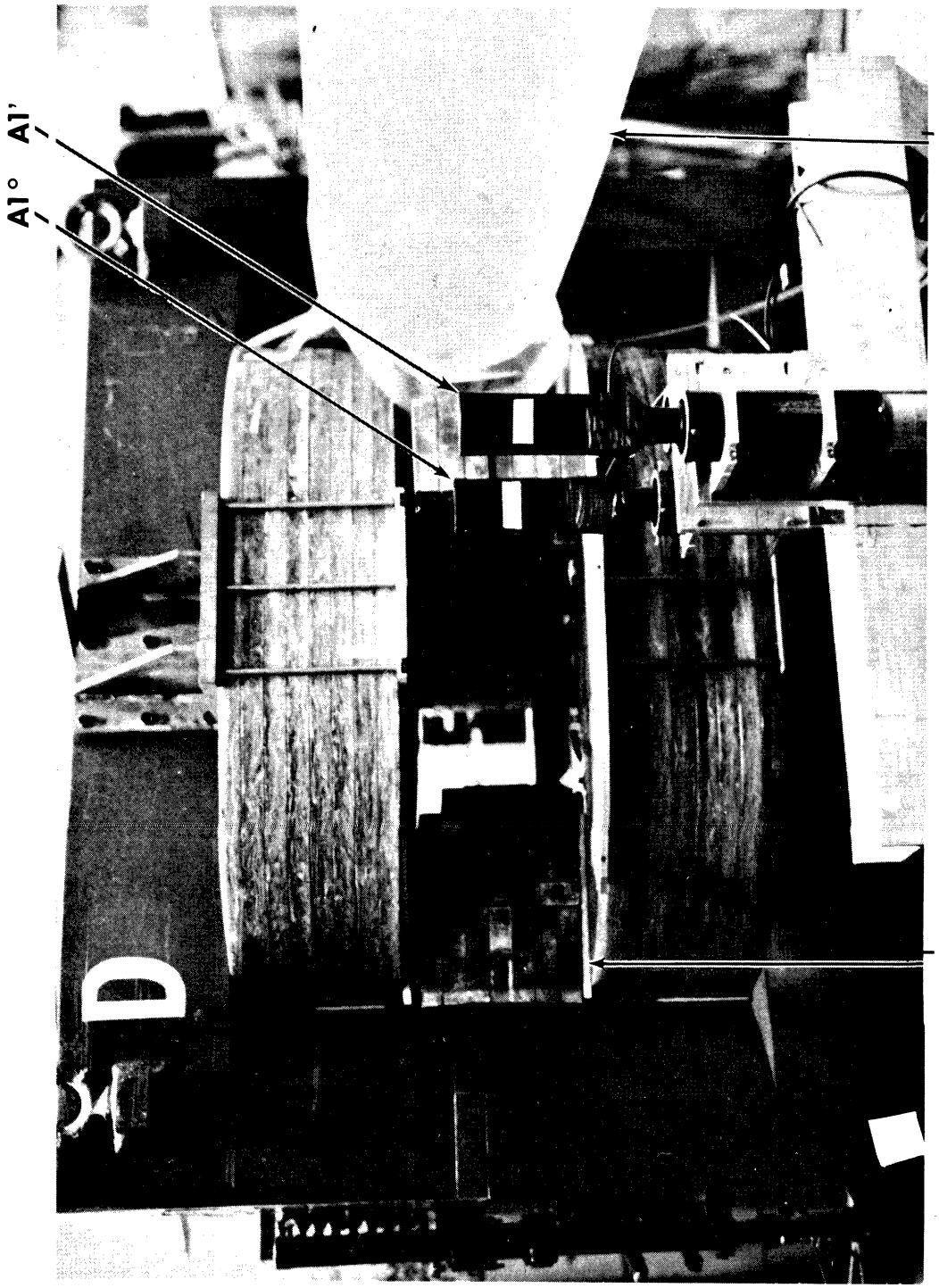

Fig. 6. The momentum analyzing magnet.

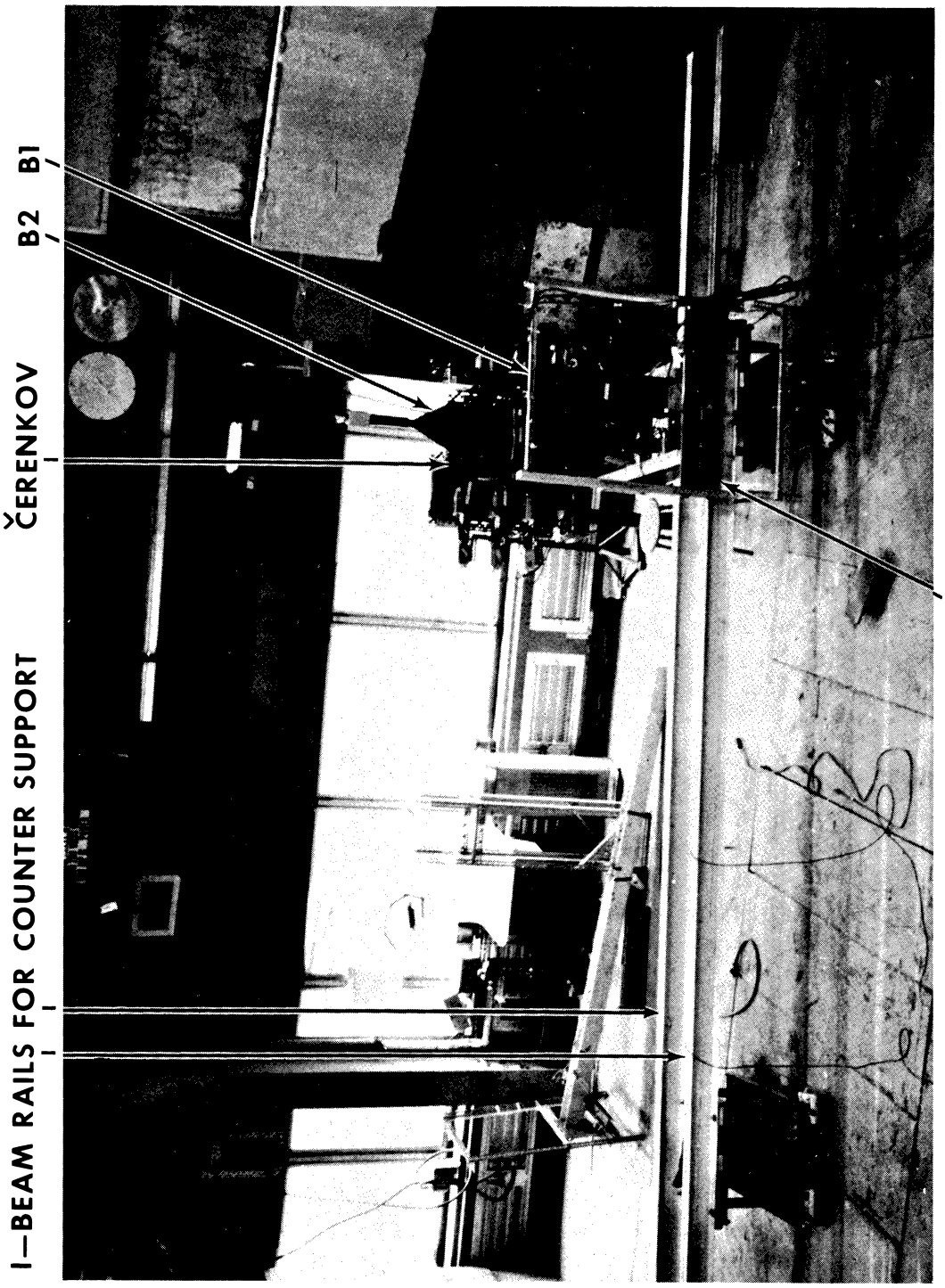

Fig. 7. The rear counter assembly.

calibrated by comparing its reading with the angle between the center of A1' and the beam line as measured with a transit located directly below the liquid hydrogen target. Rulers attached to the front I-beam provided a scale for positioning the rear counter assembly. Another scale attached to the sliding table allowed B2 to be accurately aligned relative to B1. After these counters were set, the Čerenkov counter was rolled to a position behind B2 in line with the direction of particles and as close to B2 as possible.

The wire orbit technique[22] was used to find the relation between the magnet current and the central momentum of the spectrometer. Before the scintillation counters were installed on the magnet, a fine wire was stretched from the target to a point just in front of the center of B1. When a current was passed through it, the wire simulated the trajectory of a singly charged particle of momentum

$$p(\mathrm{GeV/c}) = 3 \times 10^{-6} T(\mathrm{dynes})/I(\mathrm{amperes})$$

where T is the tension and I is the current in the wire. For a given value of magnet current, I was adjusted until the wire passed along the central ray of the spectrometer, bending through an angle of 10° in the magnet. The corresponding momentum was calculated and a graph of magnet current versus momentum was made.

D. The Electronic Logic

Figs. 8 and 9 show the block diagram of the electronic

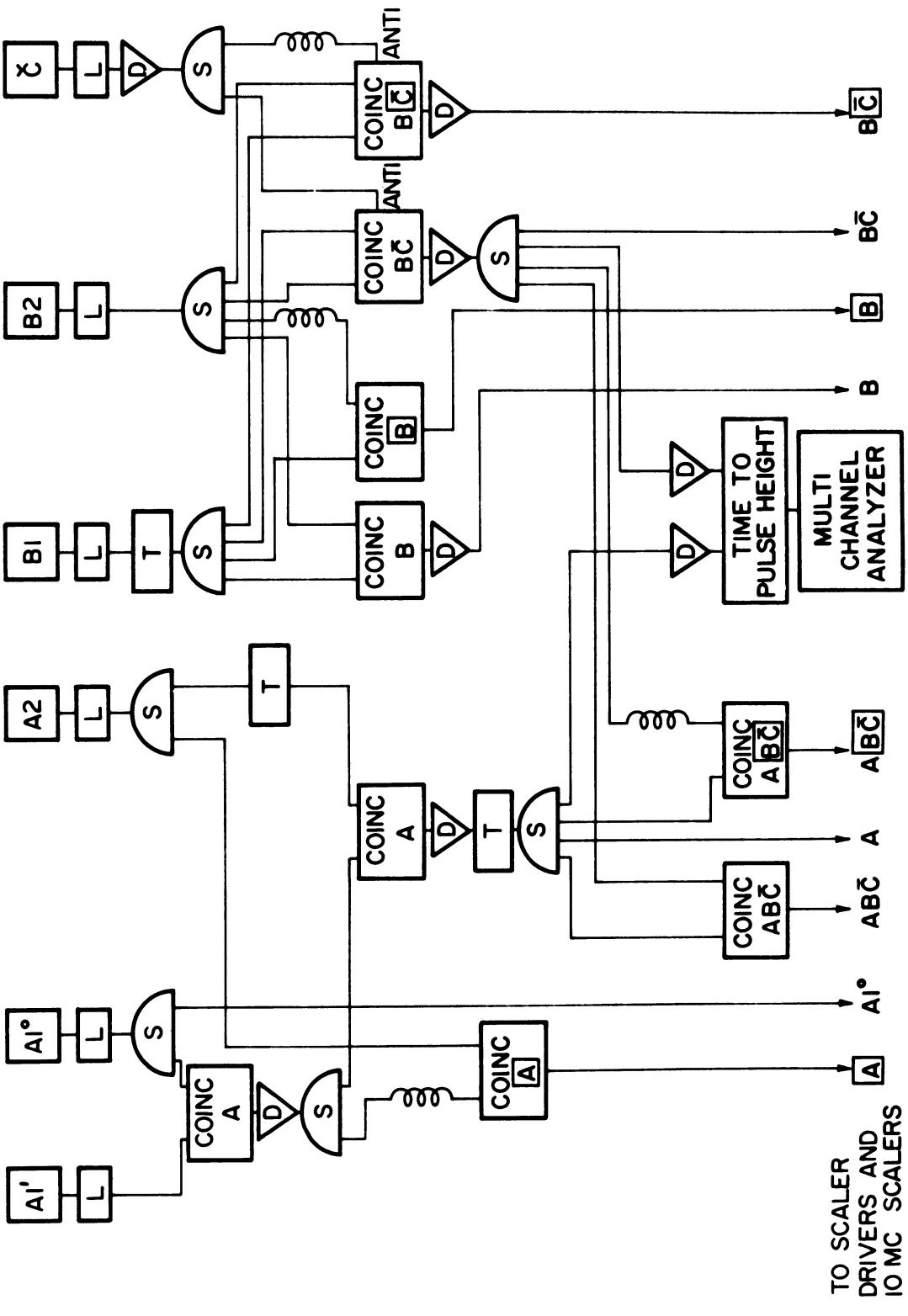

Fig. 8. Logic circuit block diagram: Main channel.

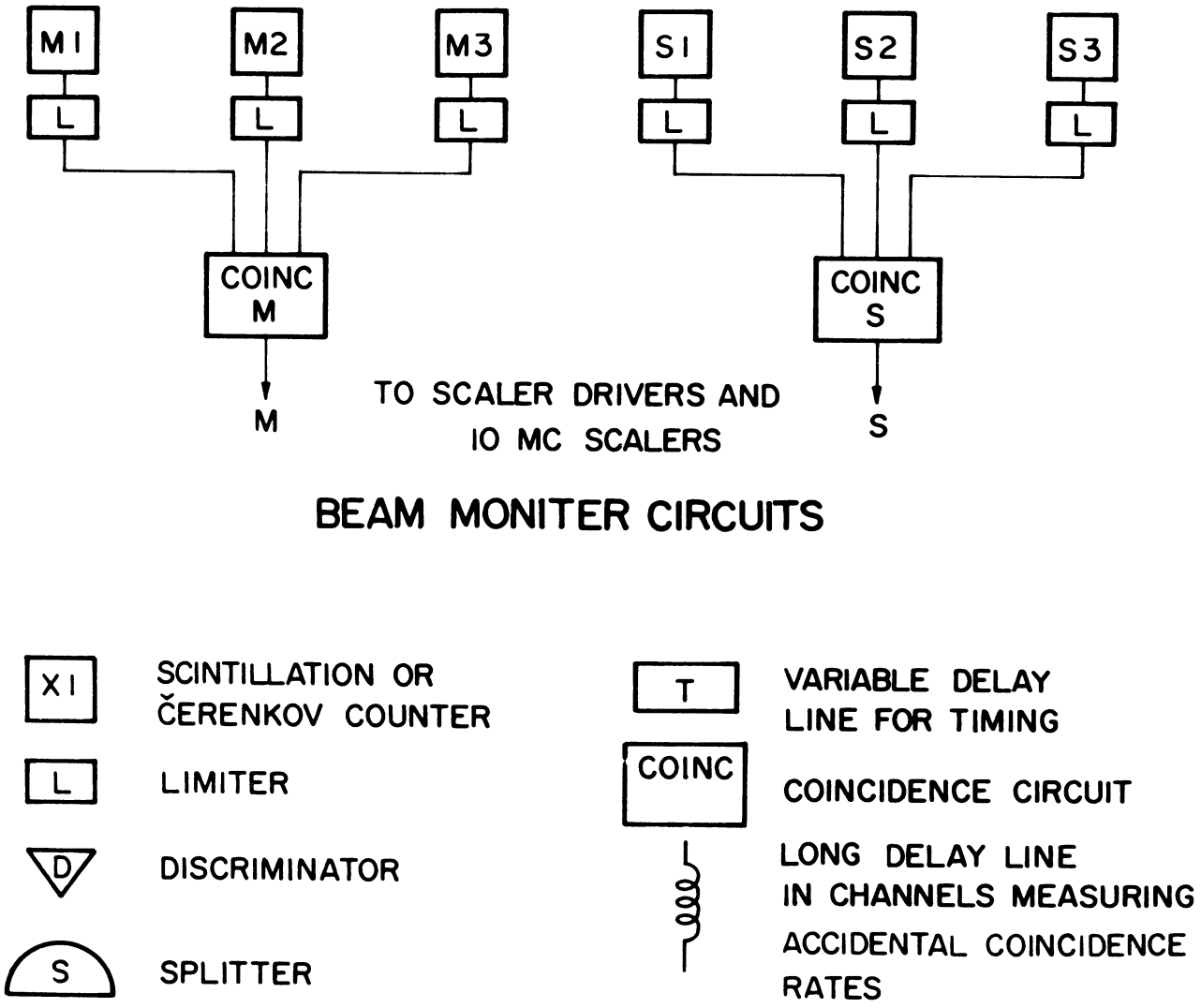

Fig. 9. Logic circuit block diagram: Monitor circuits and table of symbols.

circuitry for the experiment. Most of the circuits were standard units manufactured by General Applied Science Laboratories and described in detail by Sugarman, et al.[23] The 10 Mc scalars were manufactured by Transistor Specialties, Inc.

The main channel consists of the time to pulse height converter driven by a signal from the counters on the magnet carriage and a signal from the rear counter assembly. When a deuteron of the central momentum, p_o, traverses the system of counters along the central ray, it produces a pulse from each in turn. These pulses travel through cables to the electronics area outside the shielded enclosure. Additional cable is inserted in the space marked "τ" in the B1 circuit so the pulse from B1 and from B2 arrive simultaneously at the coincidence circuit $B\overline{C}$, which then sends a pulse to the time to pulse height converter. Similarly, the other input to this circuit is driven by a coincidence among A1', A1°, and A2. The proper values for the variable delay lines were calculated as a function of p_o before beginning the experiment.

The $B\overline{C}$ coincidence circuit also has an input from the Čerenkov counter in anticoincidence to reject pulses from pions and protons. This produced a 20% to 80% reduction in the $B\overline{C}$ counting rate, depending on the momentum. Only about 1% of the counts were lost due to accidental anti-coincidences. This was determined from a comparison of the rates recorded by scalers B and $B\boxed{\overline{C}}$. B counted coincidences between counters B1 and B2. In $B\boxed{\overline{C}}$, a pulse was added from

the Čerenkov in anticoincidence but out of time by 50 nsec. The two scalers then counted alike except when a random pulse from the Čerenkov counter vetoed the $B\overline{C}$ output.

The resolving time of the coincidence circuits was made sufficiently broad so that all deuterons within the 13.2% momentum acceptance of the spectrometer would be counted despite 1) the variation in flight time of the particles, 2) the variation in time for light to reach the photomultiplier from different points in each scintillator, and 3) the time jitter of the photomultiplier response. All time of flight information was then obtained from the time to pulse height converter and multichannel analyzer (MCA). Each of the discriminators driving the time to pulse height converter produced a pulse 40 nsec wide. If the pulses overlapped in time, the time to pulse height converter produced an output pulse of amplitude

$$V_{pulse} = V_{max}(1- |\tau_A-\tau_{B\overline{C}}| /40 \text{ nsec}),$$

i.e., the output was linear in the overlap time of the two input pulses and maximum when they overlapped completely. This pulse then drove a Technical Measurements Corporation 256 channel pulse height analyzer adjusted so V_{max} corresponded to channel 78. The time to pulse height converter-MCA combination was tested at the beginning of the experiment. Its response was found to be essentially linear in the pulse overlap time, with each channel subtending a .5 nsec interval. The variable delay following the A coincidence

circuit was adjusted for each setting of the spectrometer so the deuteron time-of-flight distribution would be centered near channel 52, with faster particles counted in lower channels. A typical time-of-flight spectrum is shown in Fig. 3. Some protons were counted because the Čerenkov counter was only about 90% efficient at this momentum and the production cross section was much greater for protons than for deuterons.

Various counting rates were observed to provide a check on the proper operation of the apparatus in the course of the experiment. Counters Al° and Al' were subjected to the highest flux of particles in the spectrometer. The beam intensity was adjusted to keep the counting rate of Al' less than 250,000 counts per burst. The scaler $AB\overline{C}$ counted coincidences between the A and $B\overline{C}$ coincidence circuits with a resolving time of 14 nsec. Thus it subtended a time interval roughly equivalent to channels 39 through 66 of the multichannel analyzer. It provided a check on the operation of that device and also an approximate running total of the number of deuterons counted during an experimental run. $A\boxed{B\overline{C}}$ counted accidental coincidences between A and $B\overline{C}$. By adjusting the beam intensity, this rate was held to about 10% of the $AB\overline{C}$ rate.

The scalers and discriminators were gated by a signal from a Brookhaven predetermined timer synchronized with the cosmotron cycle. The gating signal was displayed on an

oscilloscope along with the signal from the beam spill monitor counter, O. Occasionally, the spill began with a short period of excessive intensity, which showed up as a "spike" in the spill monitor display. The gate was timed so the electronics would not be turned on until after the "spike" had occurred, and would be turned off at the conclusion of the spill.

At the beginning of the experiment, curves of counting rate versus photomultiplier voltage were obtained for all counters to determine the settings for maximum counting efficiency. The counters were timed initially on the protons passing through the spectrometer when set for a momentum of 1.7 GeV/c. The changes necessary in the variable delay lines were then calculated to time the counters for deuterons of the desired momenta for the experiment.

A small hydrogen lamp was attached to each counter in the spectrometer. When triggered appropriately, the lamps produced a signal of several nanoseconds duration simulating the burst of light produced by a charged particle traversing the counter. The driving pulses were timed by means of delay cables to cause the lamps to flash in sequence and simulate a 1.7 GeV/c proton traversing the spectrometer. This light pulser system was used periodically to check the operation of the counters and electronics in the course of the experiment.

E. Running the Experiment

The experiment was performed for three values of incident proton kinetic energy: 1.55, 2.5, and 2.9 GeV. The deuteron yield was measured for various values of momentum in the range 1.0 to 2.4 GeV/c at laboratory angles of 5.9°, 11.55°, 15.72°, and 20.0° (except that the 20.0° run was omitted at 1.55 GeV). At each setting, data was taken both with the target full of liquid hydrogen and with it empty. The data consisted of the readings of the various scalers indicated in the electronics block diagram plus the spectrum from the MCA.

The monitor counters were calibrated at each energy by the radioactive foil technique (see Appendix I). Also, a polyethylene foil cut into vertical strips $\frac{1}{4}$ in. wide was exposed to the beam. By measuring the radioactive activation of each strip, we obtained the horizontal intensity distribution of the beam spot. These distributions are shown in Fig. 10. Two separate runs were performed at 2.9 GeV. For the second run, the beam conditions were improved and the electronic circuitry was modified slightly.

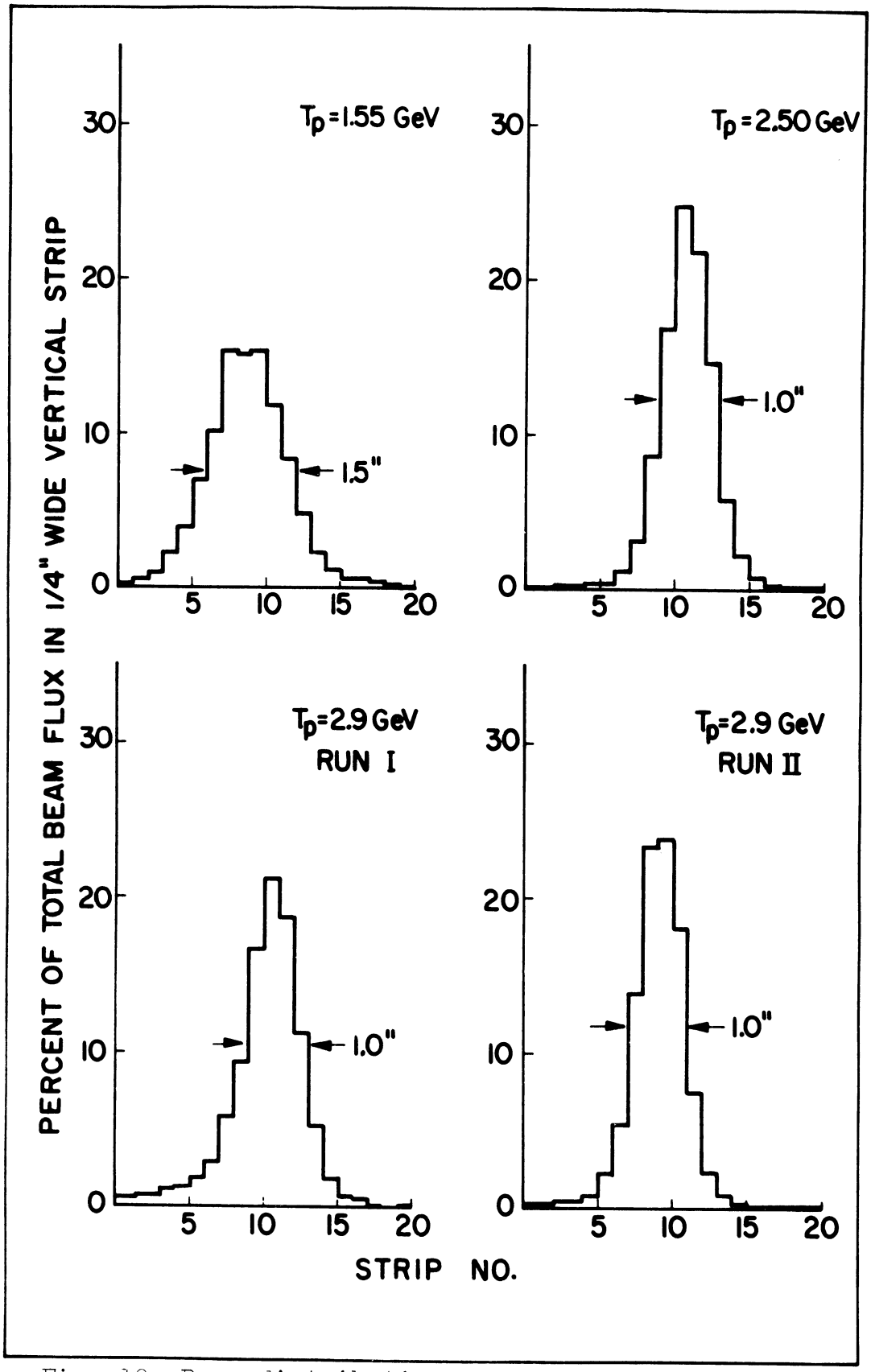

Fig. 10. Beam distributions at the target.

CHAPTER III

ANALYSIS OF DATA

In order to obtain cross sections from the time of flight spectra produced in the experiment, the momentum and time resolution of the spectrometer must be determined. In addition, corrections must be made for electronic inefficiencies, loss of particles through nuclear interactions and multiple Coulomb scattering, and for various kinds of background effects.

A. Background Subtraction

Deuterons were observed passing through the spectrometer with the target empty of liquid hydrogen. Therefore, spectra were obtained both with the target full and empty for each cross section measurement. The counting rate recorded by the beam telescope S was nearly independent of the target condition, so was used to normalize the two runs to the same total beam flux. Then the target empty spectrum was subtracted channel by channel from the one obtained with the target full. A small amount of background remained, attributable in part to accidental coincidences due to the finite resolving time of the electronic logic. Another possible cause was from particles, not necessarily deuterons, of incorrect angle or momentum that were scattered into the spectrometer by the collimators. The background was estimated

by adding the remaining counts in channels 71 through 78 of the multichannel analyzer (MCA) output.

For example, in a typical run with the target full, a total of 2373 counts was registered in channels 50 through 57 of the MCA. The target empty background for the same beam flux was 384 counts in these channels. Ninty-eight counts remained in channels 71 through 78 after the subtraction of this background, of which 41 were attributable to accidental coincidences. An additional subtraction of 98/8 = 12.3 counts was then made from each channel to give the final data. A histogram of the resulting deuteron spectrum is shown in Fig. 14.

B. Time Resolution

There are two important effects which broaden the time resolution of the spectrometer. First, light produced in a scintillator at different distances from the photomultiplier will arrive at the photomultiplier at different times. Second, there are random fluctuations in the time required for the electronic apparatus to respond to the light signal after it reaches the photomultiplier.

A ray tracing program for the IBM 7090 computer was written to simulate these aspects of the spectrometer. Only vertical dimensions were considered since all counters were considerably longer than wide. The velocity of light in a polystyrene scintillator is approximately 8 in./nsec. Most of the light, however, must undergo a series of internal reflections at surfaces of the scintillator and light pipe

before reaching the photomultiplier, so its average rate of progress toward the photomultiplier is somewhat slower. A value of 4.6 in./nsec was chosen for use in the calculation. The response time distribution for each photomultiplier was taken to be Gaussian with a standard deviation of 0.6 nsec. This value produced an excellent fit to the shape of an experimental two-fold coincidence curve.

The predicted response of the system to particles of identical velocity, but originating at the target with different positions and angles, is shown in Fig. 11. Also shown is the experimental time of flight distribution of deuterons from the reaction

$$p + p \rightarrow \pi^+ + d$$

for an incident proton kinetic energy of 1.55 GeV and a deuteron production angle of 11.55° in the laboratory. The spectrometer setting was 1.10 GeV/c. The predicted response distribution is normalized to the number of counts in channels 52 through 62 of the experimental spectrum. The full width at half maximum of the experimental curve predicted by relativistic kinematics and the spread in production angles of the deuterons was .6 nsec.

C. Momentum Resolution

A Monte Carlo program was written to find the collection efficiency of the spectrometer for deuterons of momentum p when the magnet current was set to bend deuterons of momentum p_o through 10°. The program traced deuterons of

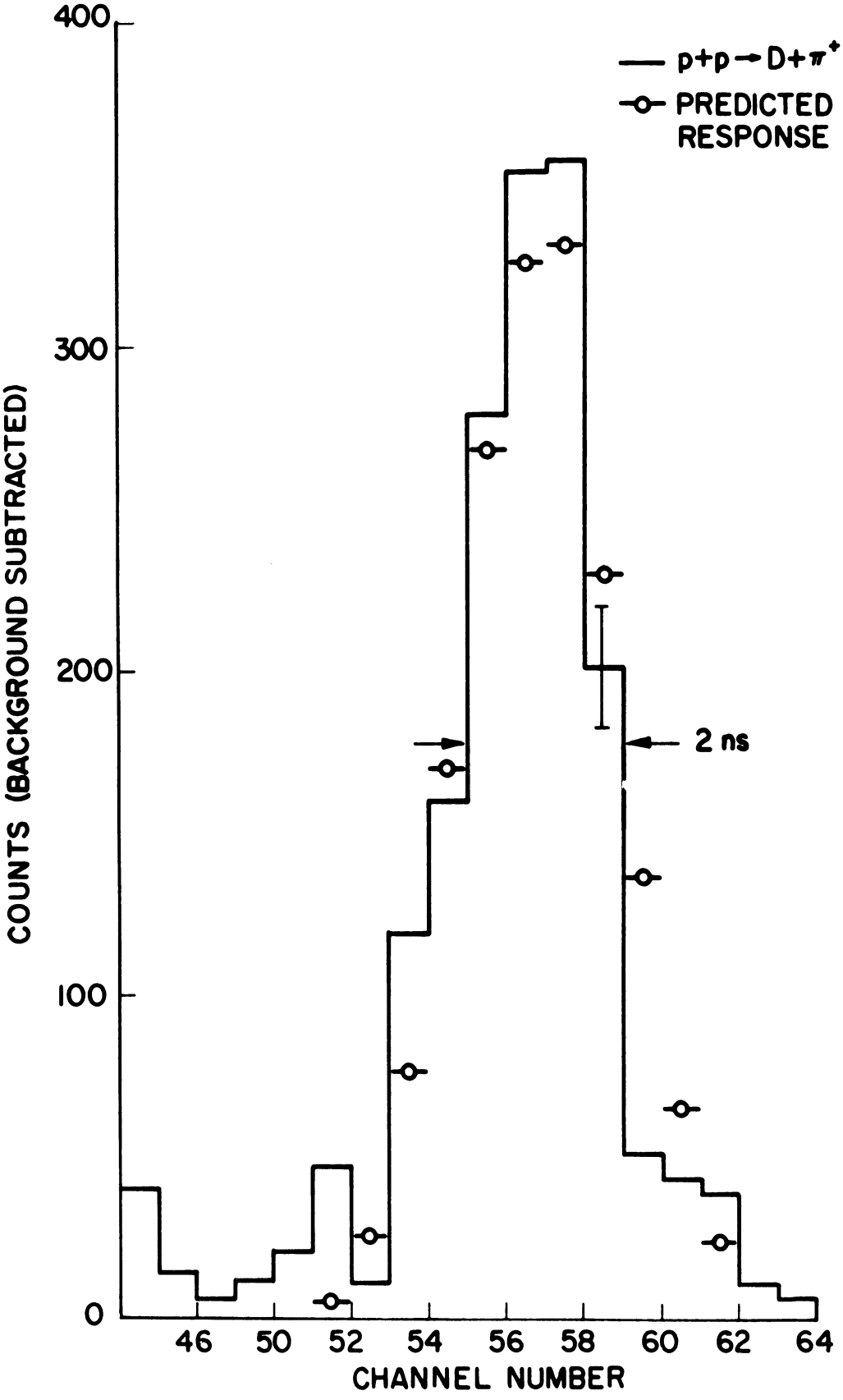

Fig. 11. Time resolution of spectrometer.

a given fixed momentum produced in the target at an arbitrary angle as they passed or failed to pass through the series of counters. Counter A2 defined the acceptance angle of the spectrometer in the vertical plane for particles produced in the target. All other counters were made at least 20% longer than the sizes dictated by straight line geometry in order to catch all but a negligibly small fraction of the particles deflected by multiple Coulomb scattering. Hence only horizontal dimensions were considered in the Monte Carlo calculation. The program took into account the beam intensity distribution at the target, bending of the deuteron trajectories in the magnetic field, and multiple Coulomb scattering in the air between the target and counter A1', in counters A1', A1°, and A2, and in the air between A2 and B1. For a given value of p and p_o, 10 000 rays were generated, each leaving the target with an angle chosen at random from a uniform distribution over the interval $\theta_o \pm 15$ mrad, where θ_o is the angular setting of the spectrometer. Distributions were made of the horizontal position in the plane of counter B1 and of the initial angle at the target for all rays which passed through counters A1', A1°, and A2. Of the original 10 000 rays, approximately 1400 fell in these distributions. This number was determined (except for random fluctuations) by the horizontal angle subtended by counter A2 about the center of the target. The collection efficiency for these rays was given by the number which fell within the limits of counter B1 divided by the total number in the distribution.

Multiple Coulomb scattering in the air was treated according to the approximate method of Scott.[24] Scott gives a bivariate distribution of the scattering induced displacement and angle of a ray projected in the plane of observation (the horizontal plane) as a function of the distance traveled in the scattering medium. The distribution is Gaussian in each random variable when the other is held fixed.

The distribution of projected angles induced by multiple Coulomb scattering in a .5 in. thick polystyrene scintillator was calculated according to the theory of Moliere[25,26,27] for deuterons of momentum 1.1 GeV/c. The result was a Gaussian distribution with standard deviation 3.28 mrad plus two correction terms which sharpened the peak and increased the contribution from the tails; their integral was zero. The correction terms were small, so they were neglected in the Monte Carlo calculation. The standard deviation of the Gaussian term depended in a complicated way on the momentum, p, and velocity, v, of the deuteron. The approximation of this dependence by $(pv)^{-1}$ led to a maximum error of 3.6% at high momenta, where the scattering correction was least important.

The calculated distribution of particles in the plane of B1 had a full width at half maximum (FWHM) of 6 in. when $p=p_o=1.1$ GeV/c* 95% of the particles fell within a width of

---

* Calculated for a spectrometer angle of 11.55° with the 1.55 GeV proton beam distribution.

8.4 in. At 2.2 GeV/c, the deflection of rays by multiple scattering was less, so the FWHM of the B1 distribution decreased to 3.6 in., with 95% of the particles falling within 6.2 in. The distribution of angles on leaving the target for the accepted rays had a FWHM of 8 mrad regardless of momentum. For a fixed value of p_o, the effect of changing p/p_o was to leave the shape of the distribution in the B1 plane unchanged, but to shift the mean of the distribution in a predictable way. Thus it was necessary to run the Monte Carlo program only once with $p/p_o = 1$ for each momentum, angle, and proton beam distribution of interest.

The resulting efficiency function for $p_o = 1.1$ GeV/c is shown compared with experiment in Fig. 12. The peak corresponding to deuterons from the reaction

$$p + p \longrightarrow d + \pi^+$$

was observed for an incident proton kinetic energy of 1.55 GeV and a deuteron production angle in the laboratory of 11.55° in time of flight spectra obtained for four values of p_o: 1.05, 1.10, 1.15, and 1.20 GeV/c. The average momentum of the deuterons in the peak was taken to be 1.08 GeV/c. The number of counts in each peak divided by the beam flux and multiplied by an arbitrary normalization constant is shown plotted as open squares against $1.08/p_o$ for each of the four runs. The error flags represent the uncertainty in the points due to counting statistics. Part

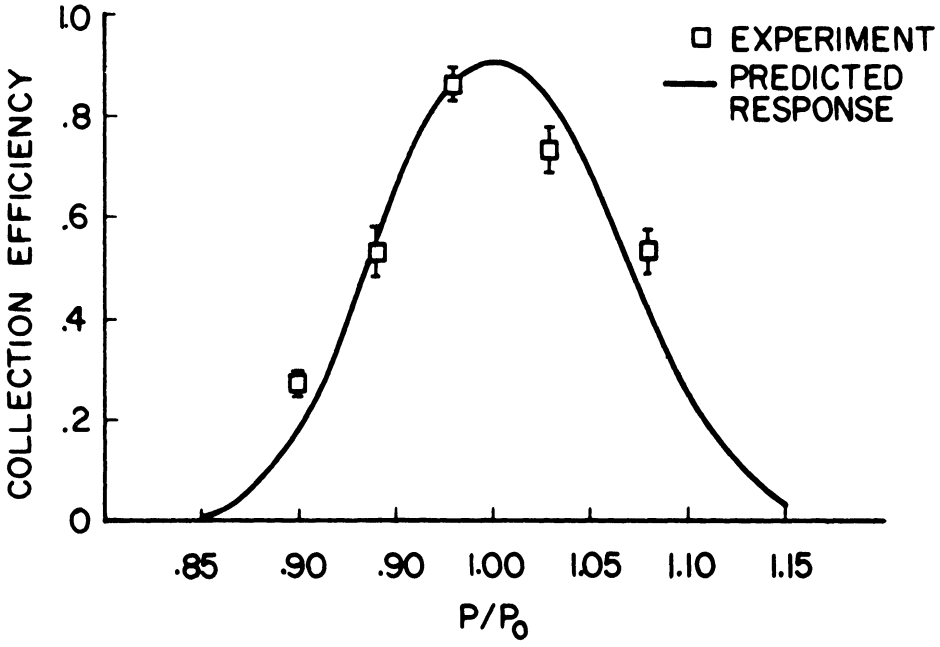

Fig. 12. Comparison of momentum efficiency function with experiment. p_o=1.10 GeV/c, T_p=1.55 GeV, θd=11.55°

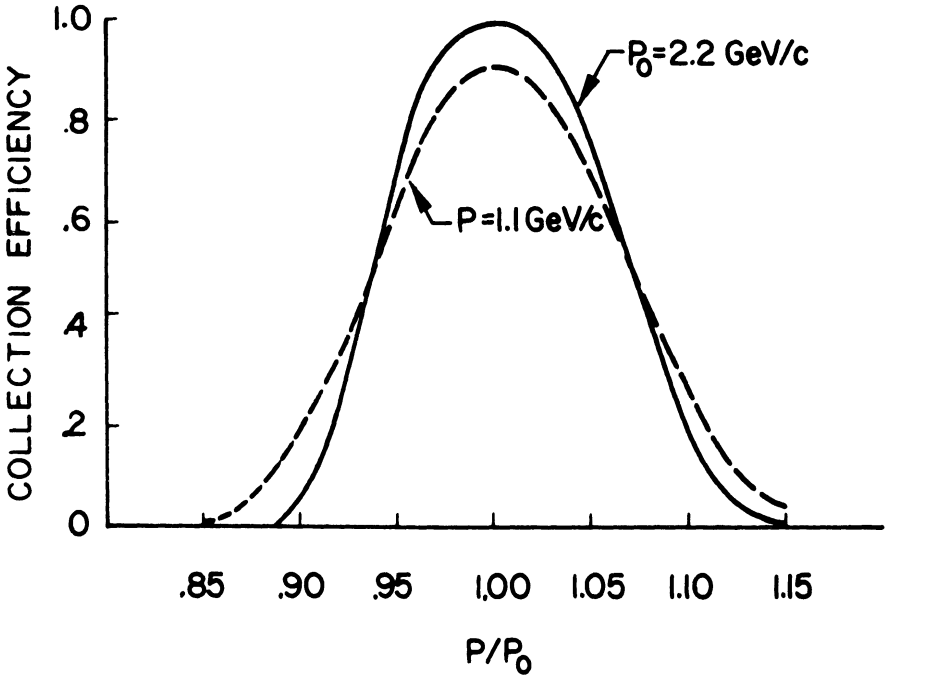

Fig. 13. Momentum efficiency function for two values of p_o. T_p=1.55 GeV, θd=5.9°.

of the disagreement between the experimental points and the efficiency curve may be due to the following facts: 1) the deuteron production cross section from the above reaction is a strong function of angle in this region, although it was assumed to be independent of angle in the calculation; 2) the deuterons observed have a spread in momentum with FWHM of about .01 GeV/c; 3) the momentum and production angle of the deuterons are correlated by relativistic kinematics in such a way as to spread out the particle distribution in the plane of B1.

Fig. 13 shows a comparison of the efficiency distributions obtained for two different values of p_o.

D. Interpreting the Time-of-Flight Spectra

If the time resolution function of the spectrometer had been infinitesimally narrow, the spectrum of deuterons recorded by the MCA would represent the differential cross section for deuteron production as a function of momentum multiplied point by point by the momentum efficiency function and re-expressed as a function of flight time. Each channel in the spectrum would then correspond uniquely to a definite momentum interval, and the average value of the differential cross section in the interval would be proportional to the number of counts divided by the average efficiency for the channel. Different channels would correspond to separate, nonoverlapping momentum intervals. In this experiment, however, the time resolution function has a FWHM of 2 nsec. Particles of the same momentum produce counts in several

different channels; the correspondence between channel and momentum interval is no longer one-to-one. In this case, the momentum and time resolution functions were folded to give the efficiency, ϵ_i, and average momentum, $\bar{p}_i$, for each channel that would obtain if the deuteron production cross section were constant in momentum. The experimental value for the differential cross section in the laboratory is then given by

$$\frac{d^2\sigma}{d\Omega dp}(\bar{p}_i, \theta, T_p) = \frac{C\, N_i}{\rho L_{eff} F\, p_o\, \epsilon_i \Delta\Omega}$$

where N_i is the number of counts in the i^{th} channel of a time-of-flight spectrum obtained for an incident proton kinetic energy T_p, deuteron production angle θ, and momentum setting p_o. C is a correction factor applied to account for deuteron absorption and electronic inefficiencies, ρ is the proton density in the target, L_{eff} is its effective length (see Section I of this chapter), F is the proton flux during the run, and $\Delta\Omega$ is the solid angle subtended by counter A2. The factor p_o enters because the ϵ_i were obtained from the momentum efficiency function in terms of p/p_o. This method of analysis gives a good determination of the differential cross section, provided that quantity is not changing rapidly in a momentum interval corresponding to the width of the time resolution function (an interval of 37 MeV/c for p_o = 1.1 GeV/c and 200 MeV/c for p_o = 2.2 GeV/c). Finer structure will be broadened, since the time spread of the system has not been unfolded. But the momentum resolution is better than the

13% provided by magnetic analysis alone. The values of $\overline{p}_i$ were corrected for energy losses of the deuterons in the target, air, and counters.

Fig. 14 shows a comparison of the predicted efficiency distribution with an actual spectrum in a region where the differential cross section is fairly constant (T_p = 1.55 GeV, p_o = 1.6 GeV/c, θ = 11.55°). Typical statistical errors are indicated in two places on the histogram. The fit is quite good except in the region of channel 42 where the tail of the adjacent proton distribution causes background. The area of the efficiency distribution has been normalized to agree with that of the experimental spectrum in channels 45 through 65.

The cross section spectrum obtained in this run from dividing the number of counts in each channel by the channel efficiency is shown in the center graph of Fig. 15. In the wings of the distribution where the efficiency was less than half that of the central channel, the data were disregarded.

The other two graphs in Fig. 15 show the effect of improper positioning of the efficiency distribution relative to the deuteron spectrum. The center of the efficiency distribution must be located at the MCA channel corresponding to the average flight time of deuterons with momentum p_o. This would have been channel 52 in all cases, had the timing calculations and cabling been done to perfect accuracy. The cables were adjusted only to the nearest nanosecond, however, and the calculations were made neglecting energy losses of

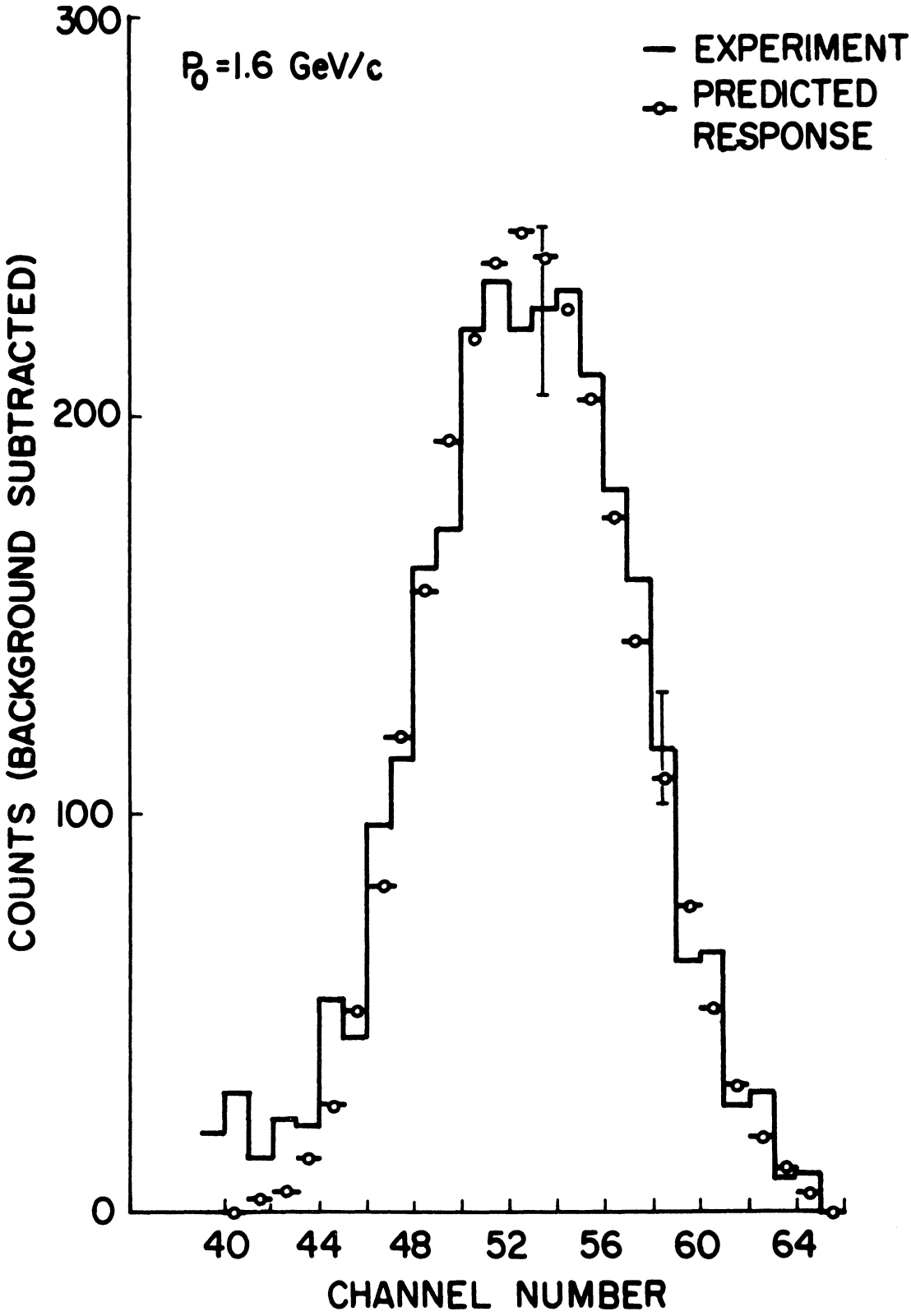

Fig. 14. Comparison of MCA spectrum with the predicted efficiency distribution. T_p=1.55 GeV, θd=11.55°.

the deuterons in the scintillation counters and air. The latter effect leads to a shift of the spectrum toward higher channels for small values of p_o. For example, the center would be shifted to channel 54 for p_o = 1.1 GeV/c, while at 2.2 GeV/c it would remain at channel 52. The effect of inaccurate timing is quite difficult to calculate, since it depends on the (unknown) errors made in the initial timing of the system on protons, as well as on the detailed operation of the electronic logic circuits, particularly the coincidence circuits. A computer program showed that the inaccurate timing could lead to erratic shifts of the spectrum of up to ± 2 channels for different momentum settings of the spectrometer in a series of runs at a given laboratory angle.

An empirical method was used to determine the proper centering for each spectrometer setting since the calculational approach did not seem to be sufficiently accurate. The effect of poor centering was generally to change the slope of the resulting cross section distribution, but to leave the cross section in the immediate neighborhood of p_o relatively constant. The centering was chosen to the nearest half-channel (.25 nsec.) for each value of p_o in a series of runs at a given angle and beam energy such that the wings of the distribution obtained for any given p_o agreed well with the centers of distributions taken at neighboring momentum settings. For example, the efficiency distribution was centered on channel 53 for the run at 1.6 GeV/c illustrated in Figs. 14 and 15 because this choice gave cross sections

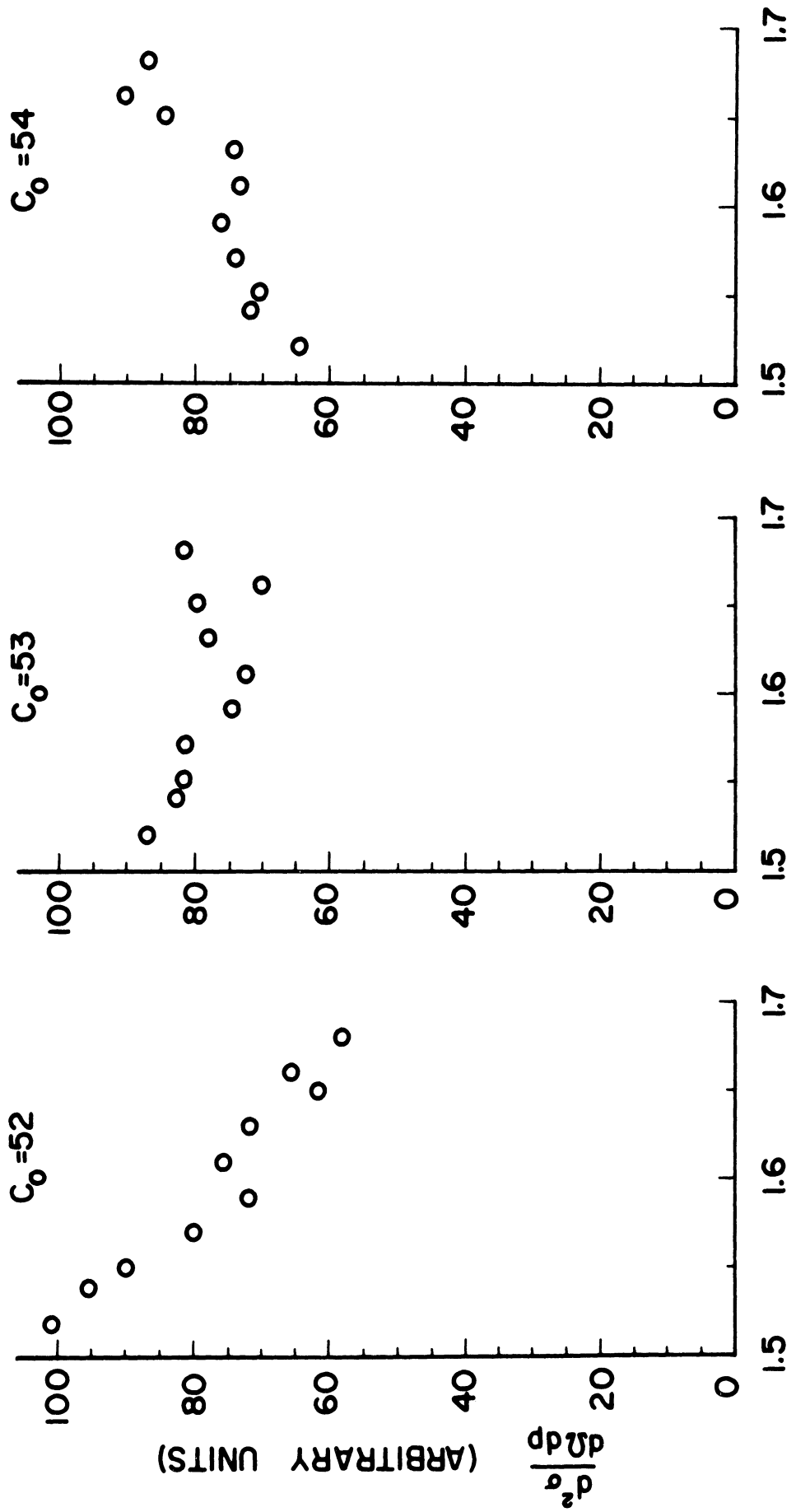

Fig. 15. Effect of improper centering of the efficiency distribution. The MCA spectrum is that of Fig. 14. C_0 is the MCA channel chosen to correspond to the center of the efficiency distribution for the cross section calculation.

most consistant with data obtained in other runs at 1.5 and 1.7 GeV/c.

E. Nuclear Absorption

The cross section was corrected for loss of deuterons in the target, air, and counters by nuclear interactions. The nuclear cross section, σ_{dA}, for deuterons on a nucleus of mass number A was approximated by a modified geometric cross section:

$$\sigma_{dA} = \sigma_{Nd} A^{2/3} .$$

σ_{Nd} is the average nucleon-deuteron cross section obtained from experiment.[28] A least squares fit was made to the combined neutron and proton total cross section data for nucleons of kinetic energy in the range .1 to 1.5 GeV incident on deuterons at rest. This corresponded to deuterons of momentum .9 to 4.5 GeV/c striking nucleons at rest. The resulting function in the region of interest for this experiment is shown in Fig. 16.

The deuteron was assumed lost if it interacted before entering counter B2. If it interacted in that counter or in the Čerenkov counter, it was assumed lost in 5% of the cases due to production of charged particles fast enough to trigger the Čerenkov counter and reject the event. The combined correction applied to the cross section was

$$\exp (2.47 \times 10^{-3} \sigma_{Nd})$$

with σ_{Nd} (in mb) chosen for the appropriate value of deuteron

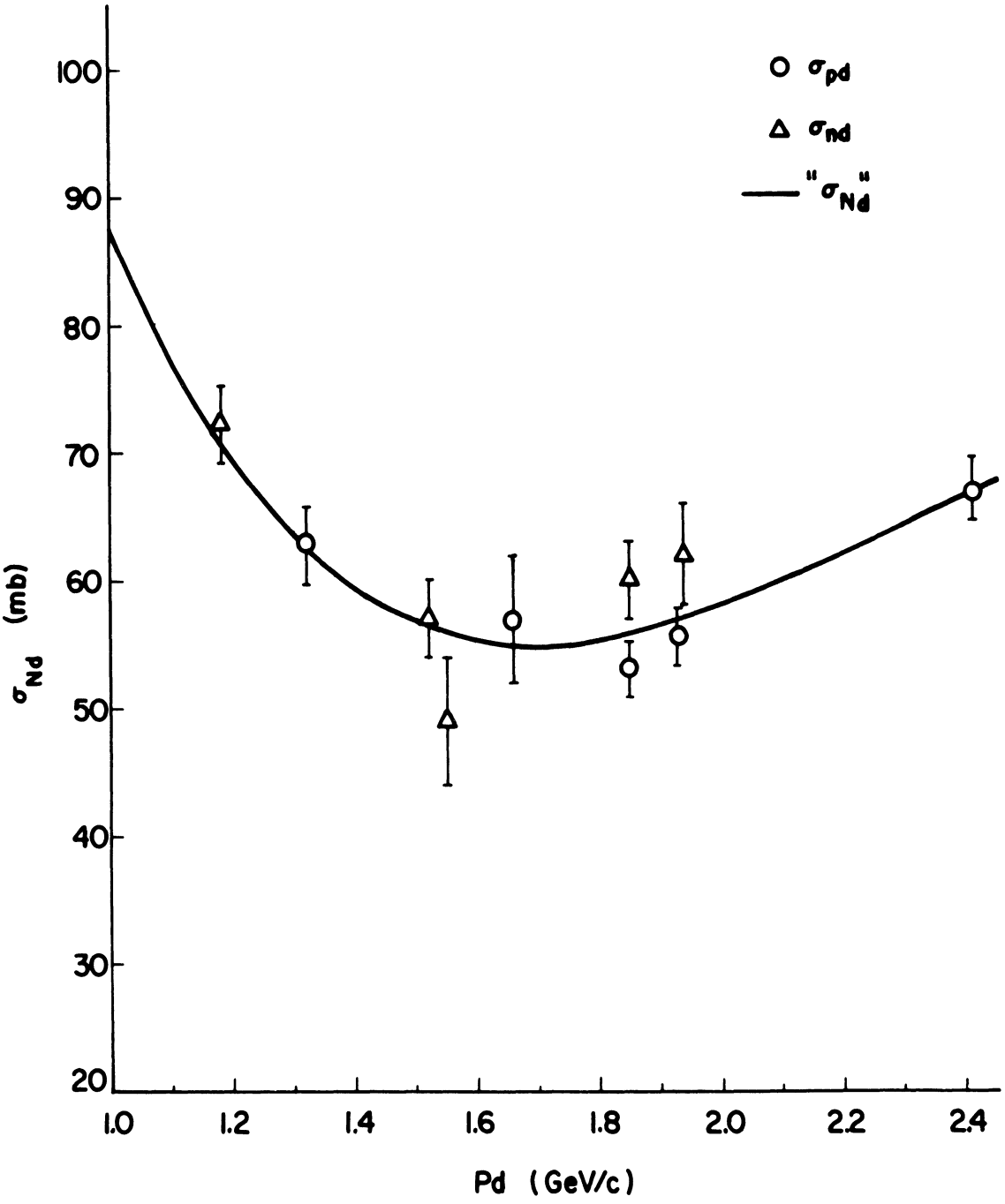

Fig. 16. Average deuteron-nucleon cross section as a function of the deuteron laboratory momentum. The data are taken from the compilation of Chen et al.[28]

momentum from the function shown in Fig. 16. The correction was typically 17.5%.

F. Electronic Dead Time

The operation of the limiter circuits is such that a dead time is introduced following each pulse during which additional pulses can not be produced. The dead time is equal to the length of the pulse from the photomultiplier, approximately 15 nsec. When the counting rate is high, the circuit may be insensitive for an appreciable fraction of the beam spill. Counters Al° and Al' were subjected to counting rates high enough to require correction for this effect.

Typically, the counting rate in Al° was 1.9×10^5 per burst of particles from the cosmotron. The associated dead time was 2.85 msec, the product of the number of pulses and the dead time per pulse. If the particles are distributed uniformly in a time interval of 125 msec, approximately 2.85/125, or 2.3%, will not be counted. The rate in Al' was essentially the same as in Al°. The counters were close together and most of their flux came from the target, so it was assumed that 60% of the particles passing through Al° passed through Al' as well, and introduced no further dead time. Thus, the loss predicted is 40% greater than that of Al° alone, or 3.2%. Other effects which can increase this loss are 1) bunching of the particles in the spill, and 2) operation with higher Al° rates in runs with the target full than in runs with it empty.

The dead time correction was difficult to make accurately. The length of the spill and the beam intensity fluctuated during the individual runs. Although the Al° counting rate was sampled and recorded several times in most runs, the length of the spill was not always noted. Also, the effect of nonuniformity of the beam spill was not known. The total dead time correction was taken to be $4 \pm 2\%$. A comparison of runs with the same spectrometer setting but vastly different beam intensities showed this estimate was reasonable.

The MCA was insensitive for an average period of 20 μsec during the analysis of each pulse recorded in its spectrum. But since the number of such pulses was generally fewer than 40 per burst, the dead time correction was less than one percent, and was disregarded.

G. Accidental Čerenkov Anticoincidences

The accidental anticoincidence rate of the Čerenkov counter was monitored during the experiment (see Chapter II, Sec. D). The average loss due to this effect was 1%.

H. Counter Inefficiency

The efficiencies of the scintillation counters used in the experiment were not measured, but previous experience indicated that the small counters (all except B1 and B2) should have been essentially 100% efficient. An efficiency of $99 \pm 1\%$ was assumed for counters B1 and B2. This was reasonable because the counters were thick, and the photo-

multipliers were operated at high gain. In addition, B2, the largest counter, was provided with a photomultiplier at each end.

I. Beam Attenuation

As the beam passes through the target, beam particles undergo nuclear interactions, reducing its intensity. The intensity as a function of ℓ, the distance (in inches) traveled by the beam in the target, is given by

$$I(\ell) = I_o \exp -(2.54\rho\sigma\ell)$$

where I_o is the intensity of the beam on entering the target, ρ is the number of protons per cm^3 in the liquid hydrogen, and σ is the total proton-proton cross section at the beam kinetic energy. Let us define an effective length, L_{eff}, for the target such that

$$I_o L_{eff} = \int_0^{L_T} I(\ell)\, d\ell$$

where L_T is the actual length of the target (3.03 in.). If we take σ = 44 mb[29], a good value for the three beam energies of the experiment, L_{eff} = 3.01 in. This quantity was used in place of L_T in the cross section calculation to correct for beam attenuation.

J. Results

The value of the differential cross section corresponding to N_i, the number of counts in the i^{th} channel of the MCA spectrum after background subtraction, was given by

$$\frac{d^2\sigma}{d\Omega dp} = \frac{N_i}{(\Delta\Omega)\ p_o\ \epsilon_i\ M\ R_M \rho L_{eff}}\ a\ b\ c\ d$$

where

$\Delta\Omega$ = solid angle subtended by counter A2 (1.056×10^{-4} sr);

p_o = momentum setting of the spectrometer (in GeV/c);

ϵ_i = predicted efficiency of the i^{th} channel for the momentum, angle, and beam distribution of the run;

M = number of counts registered by beam monitor M in the run with the target full (typically 10^5);

R_M = ratio of the beam flux to the number of counts registered by beam monitor M (typically 3×10^6);

ρ = density of liquid hydrogen (4.23×10^{22} protons/cm^3);

L_{eff} = effective length of the hydrogen target (7.65cm);

a = nuclear interaction correction (typically $1.175 \pm .05$);

b = electronic dead time correction ($1.04 \pm .02$);

c = accidental anticoincidence correction for the Čerenkov counter ($1.01 \pm .01$);

and d = counter inefficiency correction ($1.02 \pm .02$).

N_i was given by the following formula:

$$N_i = N_i^f - \frac{S^f}{S^e} N_i^e - \frac{1}{8} \sum_{j=71}^{78} (N_j^f - \frac{S^f}{S^e} N_j^e)$$

with an associated statistical error:

$$\Delta N_i = \left[N_i^f + (\frac{S^f}{S^e})^2 N_i^e + \frac{1}{64} \sum_{j=71}^{78} (N_j^f + (\frac{S^f}{S^e})^2 N_j^e) \right]^{\frac{1}{2}}$$

where

$N_k^{e(f)}$ = number of counts in MCA channel k in the run with the target empty (full), and

$S^{e(f)}$ = number of counts recorded by beam monitor S in the run with the target empty (full).

To the value of cross section thus obtained were associated an average momentum, $\overline{p}_i$ (see Sec. D of this chapter), and an error obtained by adding orthogonally the fractional error due to ΔN_i and the fractional error in ϵ_i (assumed to be 10%). Large systematic errors may occur in a cross section obtained from the wings of the deuteron spectrum. The number of counts in such a channel is small, and unsubtracted background, particularly in the proximity of the proton distribution, is magnified enormously by dividing by the small value of ϵ_i. Also, the ϵ_i themselves have large fractional errors in this region. Therefore, cross sections were not obtained from channels for which ϵ_i was less than half that predicted for the central channel of the deuteron spectrum.

In a series of runs at a given laboratory angle and beam energy, a large number of individual cross section measurements, each with its own average momentum, $\overline{p}_i$, is made from spectra taken at various spectrometer momentum (p_o) settings. These values are averaged over suitable momentum intervals to give the final cross sections listed in the tables and shown in the graphs that follow. For example, in the run at a beam kinetic energy of 1.55 GeV and a deuteron production angle of 11.55°, all of the

individual measurements with $1.60 \leq \bar{p}_i < 1.65$ GeV/c were averaged to give the final cross section and momentum for the interval. In the interval were points taken with p_o = 1.50, 1.60, and 1.70 GeV/c.

A comprehensive tabulation of the results of the experiment and graphs of the differential cross section for deuteron production in the c.m. system are given in Appendix II.

CHAPTER IV

DISCUSSION OF RESULTS

A. Differential Cross Section in the Laboratory System

Figs. 17-19 show the differential cross section for deuteron production in proton-proton collisions in the laboratory system as a function of momentum at angles of 5.9, 11.55, and 15.72° with respect to the beam direction. The proton kinetic energy was 1.55 GeV. Fig. 20 is the spectrum at 0° and 1.55 GeV obtained by Turkot, et al.[12]

The sharp peaks at the extremes of the continuous spectrum (see Fig. 19, for example) arise from the reaction $p + p \rightarrow d + \pi^+$. The region of these peaks was omitted in some spectra. The peaks at low momenta are sharper than those at high momenta because the time-of-flight technique yields finer momentum resolution for slower particles.

The laboratory spectra obtained at the other energies of this experiment are tabulated in Appendix II.

B. Differential Cross Section in the Center of Mass System

The cross section in the c.m. system for deuteron production in proton-proton collisions at a proton kinetic energy of 1.55 GeV is shown in Figs. 21-30. Fig. 21 is a plot showing the points where the differential cross section was measured as a function of p^*, the deuteron c.m. momentum, and $\cos\theta^*$, the cosine of the angle of the deuteron in the

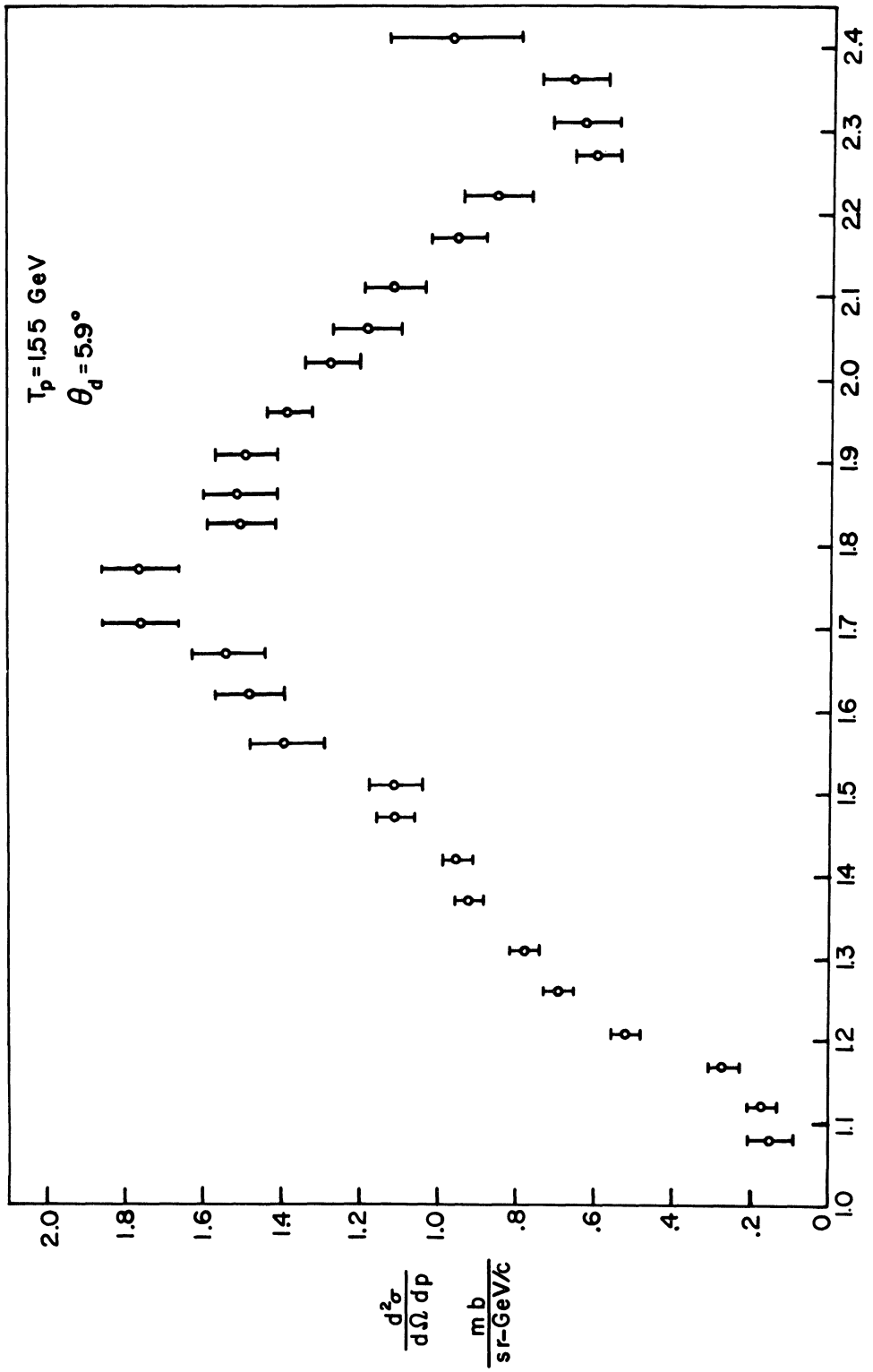

Fig. 17. Laboratory differential cross section for deuteron production in p-p collisions at 1.55 GeV. The deuteron production angle was 5.9°. The abcissa is the deuteron laboratory momentum.

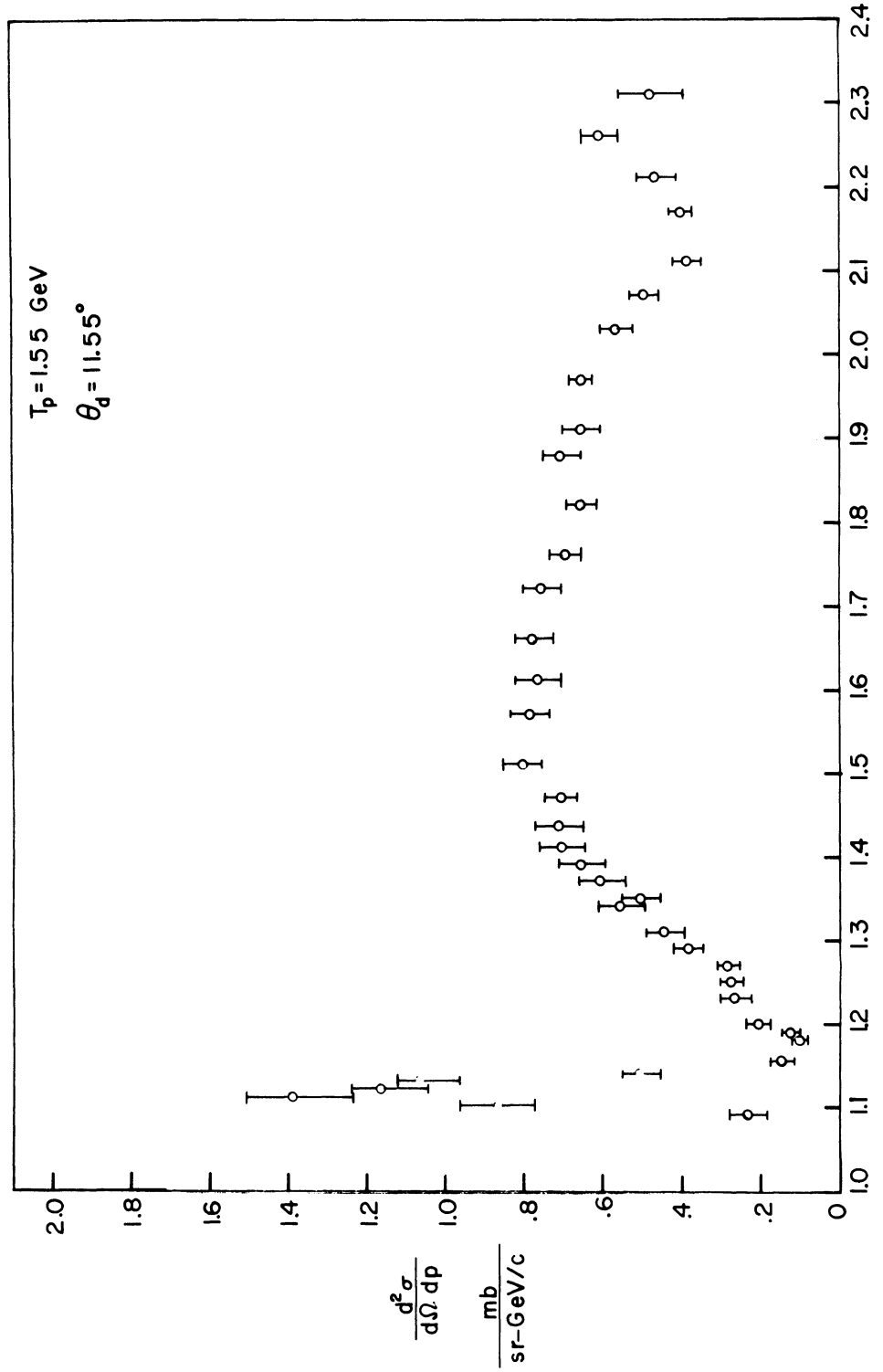

Fig. 18. Laboratory differential cross section for deuteron production in p-p collisions at 1.55 GeV. The deuteron production angle was 11.55°. The abcissa is the deuteron laboratory momentum.

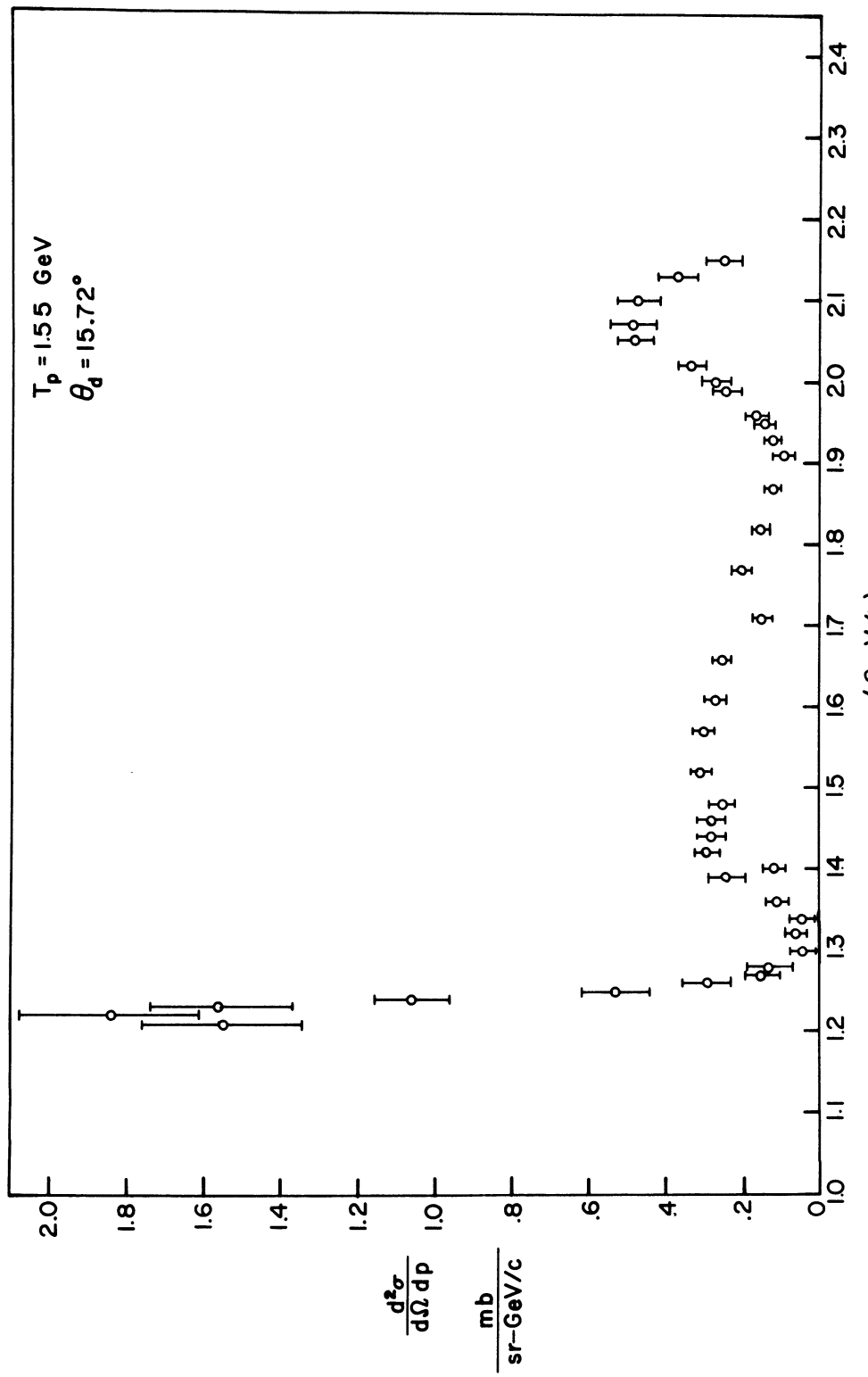

Fig. 19. Laboratory differential cross section for deuteron production in p-p collisions at 1.55 GeV. The deuteron production angle was 15.72°. The abcissa is the deuteron laboratory momentum.

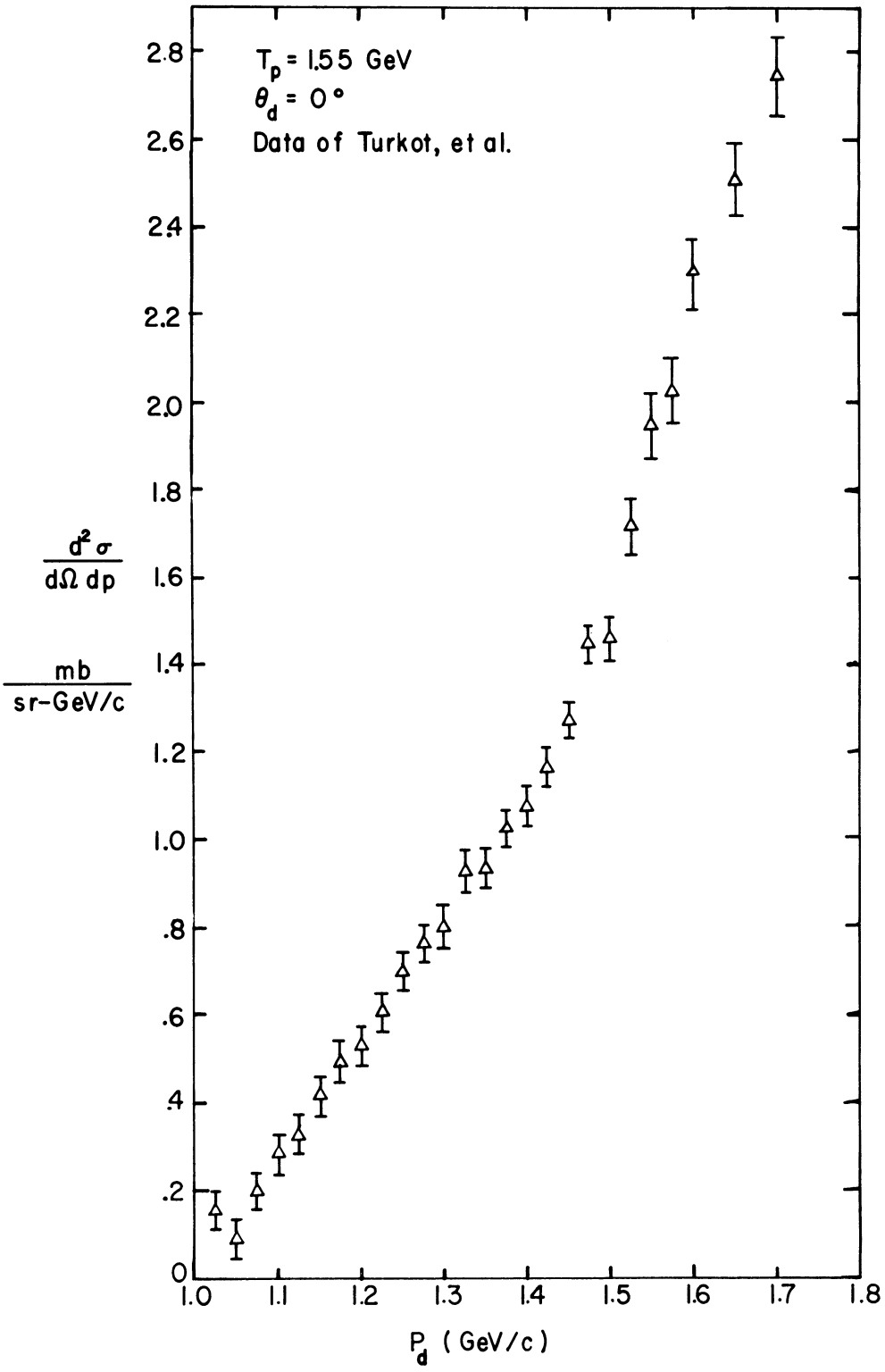

Fig. 20. Laboratory differential cross section for deuteron production in p-p collisions at 1.55 GeV from Turkot, et. al.[12] The deuteron production angle was 0°. The abcissa is the deuteron laboratory momentum.

Fig. 21. Plot of the points where the differential cross section for deuteron production in proton-proton collisions has been measured at 1.55 GeV as a function of the cosine of the deuteron c.m. production angle and c.m. momentum. The symbols have the following meanings:

● Point where a measurement was made in this experiment.

o Point indicating a measurement in this experiment at (p^*, $+\cos\theta^*$) plotted at (p^*, $-\cos\theta^*$) through use of the reflection symmetry of the differential cross section in the line $\cos\theta^*=0$ (see text).

▲ Point where a measurement was made by Turkot, et al.[12]

■ Point where an estimated cross section value was supplied to the least squares fitting routine.

The numbers next to the symbols are the values of the c.m. differential cross section,

$$\frac{d^2\sigma}{d\Omega^* dp^*} ,$$

in μb/(sr GeV/c). Estimated values have been placed in parentheses. The values quoted for this experiment are slightly in error. Corrections made to the data subsequent to the preparation of this plot resulted in a 5% increase in all the values. The corrected data have been used in the other graphs in this paper.

The line labeled P^*_{max} represents the maximum deuteron c.m. momentum possible in a final state containing two or more pions.

The measurements at a given fixed deuteron production angle in the laboratory, θ_L, fall on a curved trajectory in this plot.

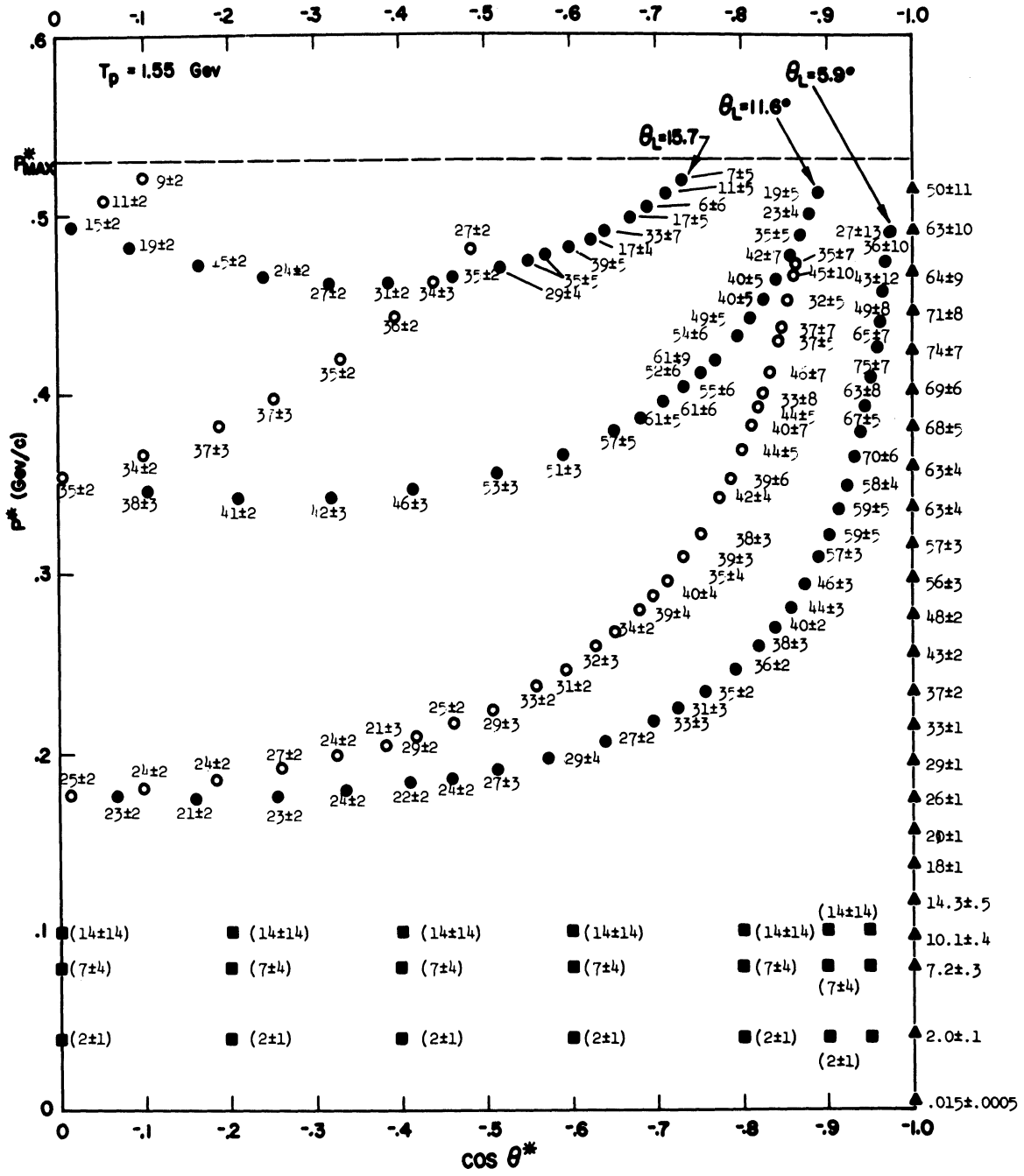
T_p = 1.55 Gev
θ_L=5.9°
θ_L=11.6°
θ_L=15.7°
P^*_{MAX}
P^* (Gev/c)
cos θ^*
(14±14)
(7±4)
(2±1)
.015±.0005

Fig. 21

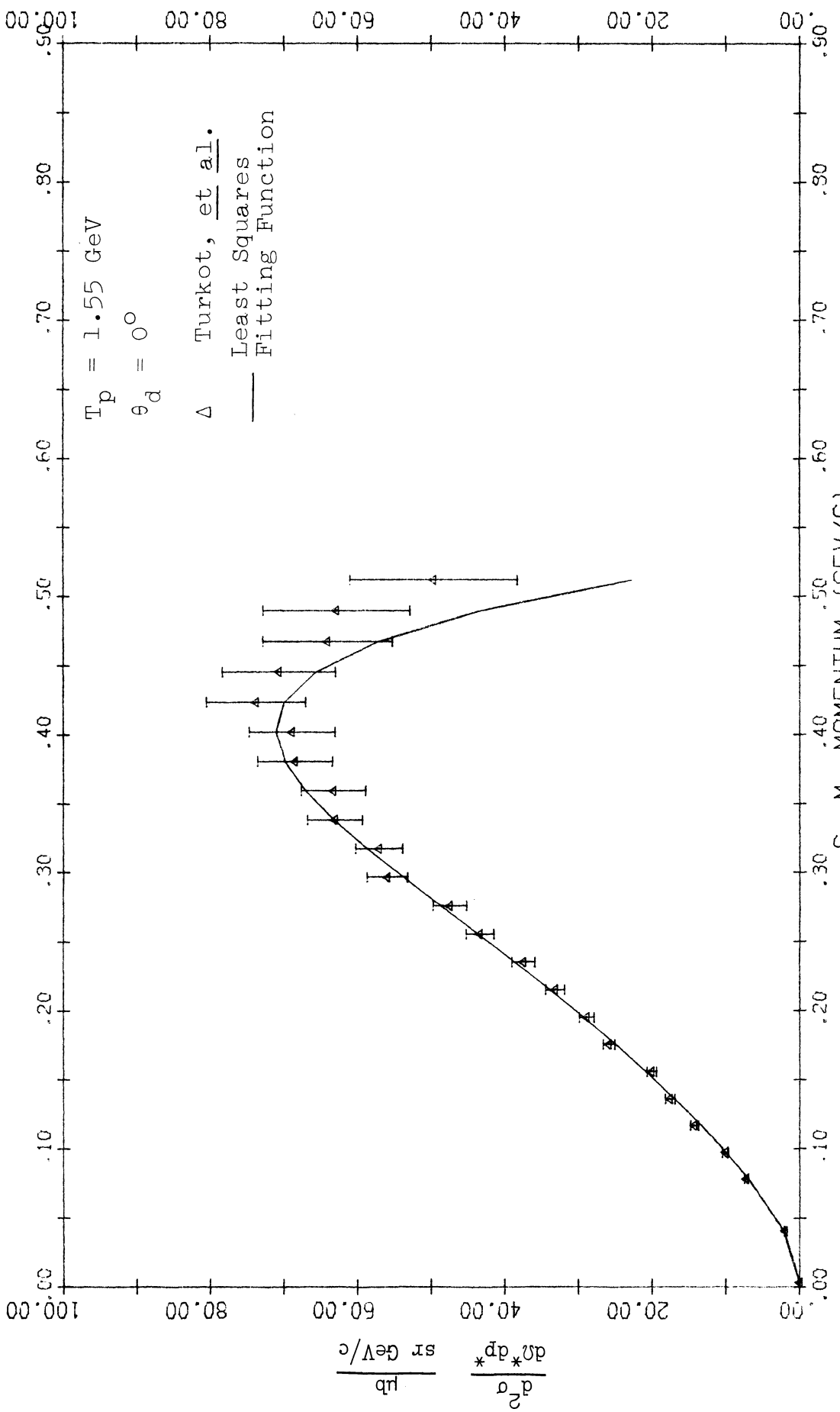

Fig. 22. C.m. differential cross section for deuteron production in p-p collisions vs. deuteron c.m. momentum from Turkot, et al.[12] T_p = 1.55 GeV, θ_d(lab) = 0°.

Fig. 23. C.m. differential cross section for deuteron production in p-p collisions vs. deuteron c.m. momentum. T_p = 1.55 GeV, θ_d(lab) = 5.9°, cos θ^* < 0.

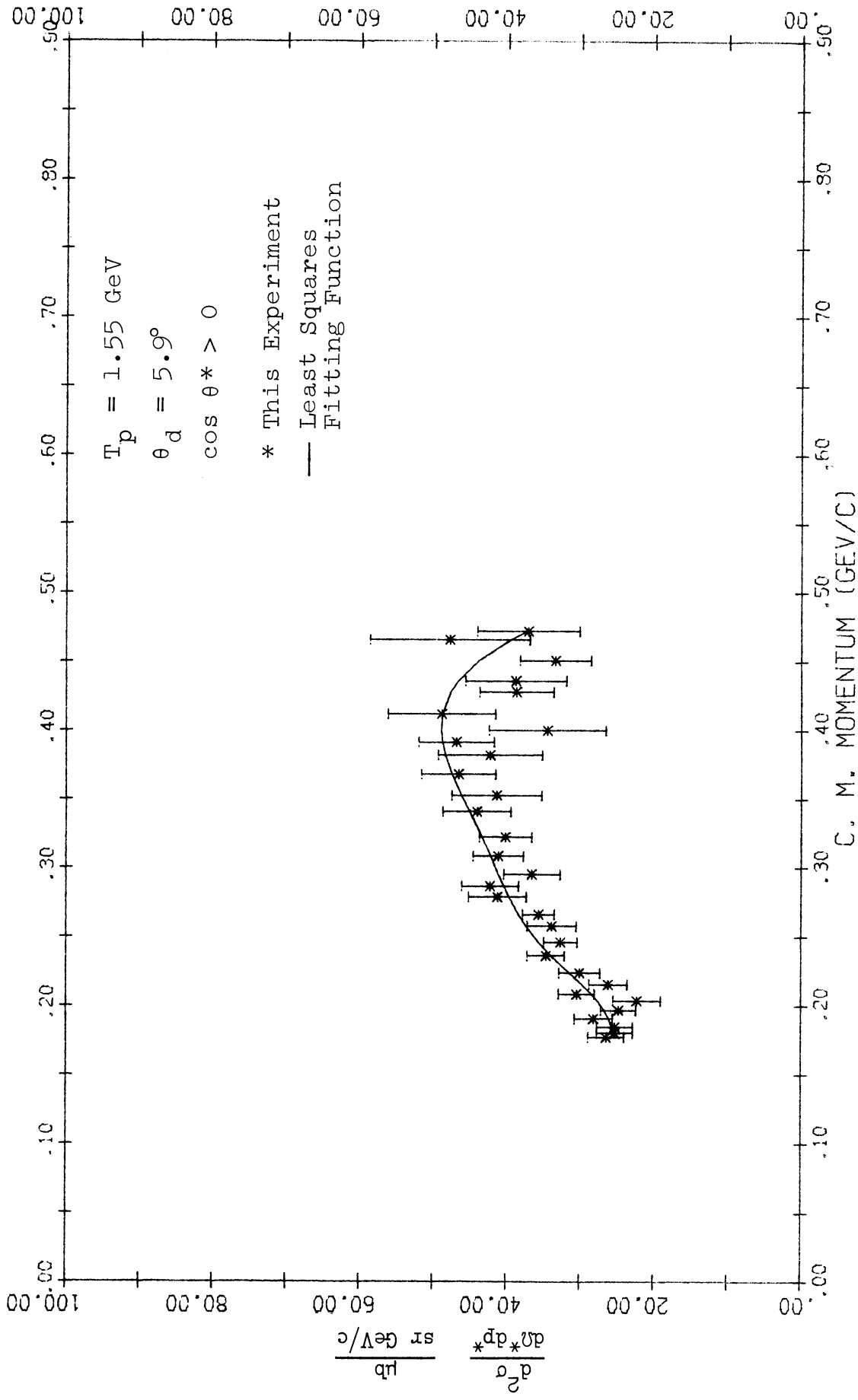

Fig. 24. C.m. differential cross section for deuteron production in p-p collisions vs. deuteron c.m. momentum. T_p = 1.55 GeV, θ_d(lab) = 5.9°, cos θ* > 0.

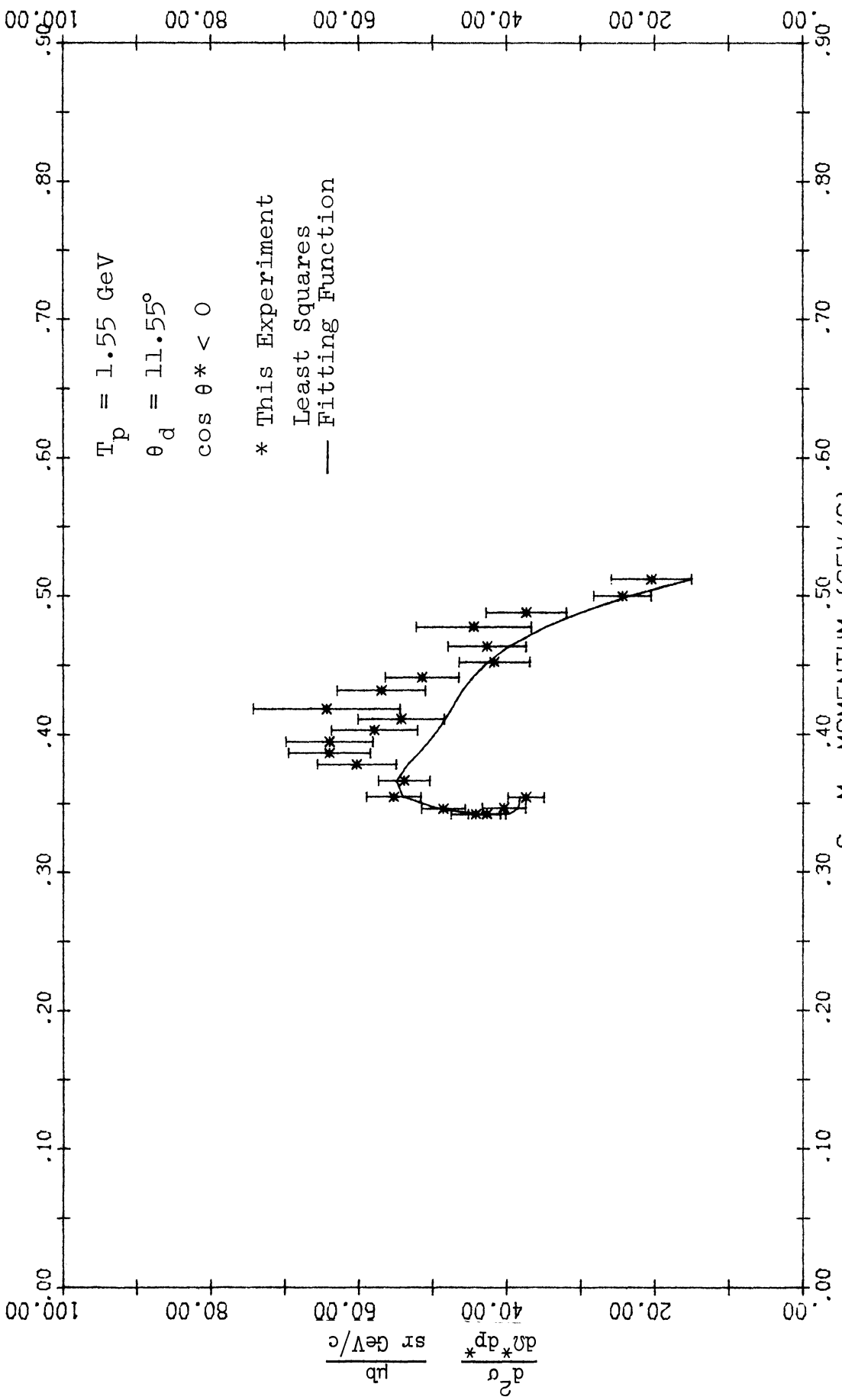

Fig. 25. C.m. differential cross section for deuteron production in p-p collisions vs. deuteron c.m. momentum. T_p = 1.55 GeV, θ_d(lab) = 11.55°, cos θ* < 0.

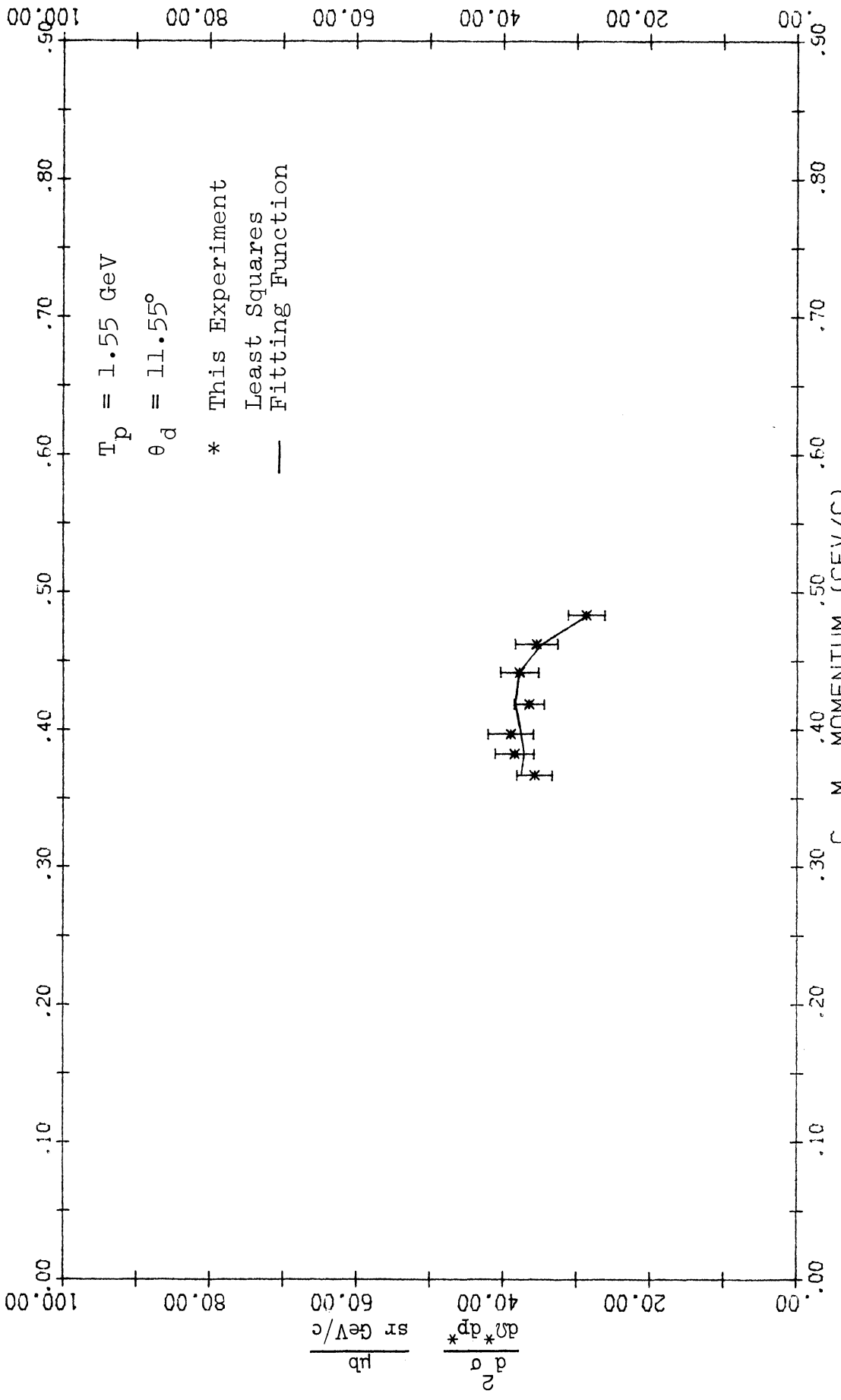

Fig. 26. C.m. differential cross section for deuteron production in p-p collisions vs. deuteron c.m. momentum. T_p = 1.55 GeV, θ_d(lab) = 11.55°, cos $\theta^* > 0$.

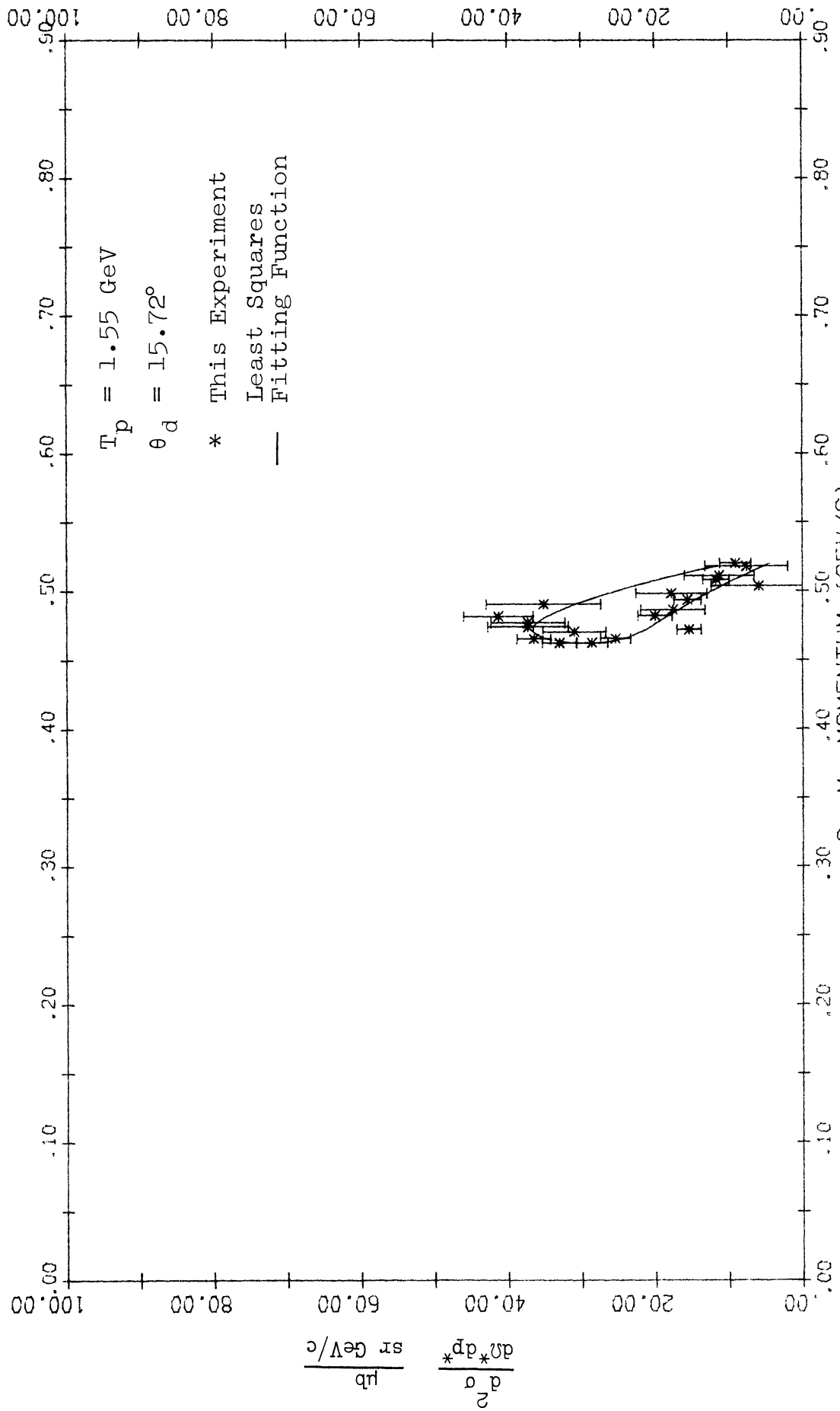

Fig. 27. C.m. differential cross section for deuteron production in p-p collisions vs. deuteron c.m. momentum. T_p = 1.55 GeV, θ_d = 15.72.

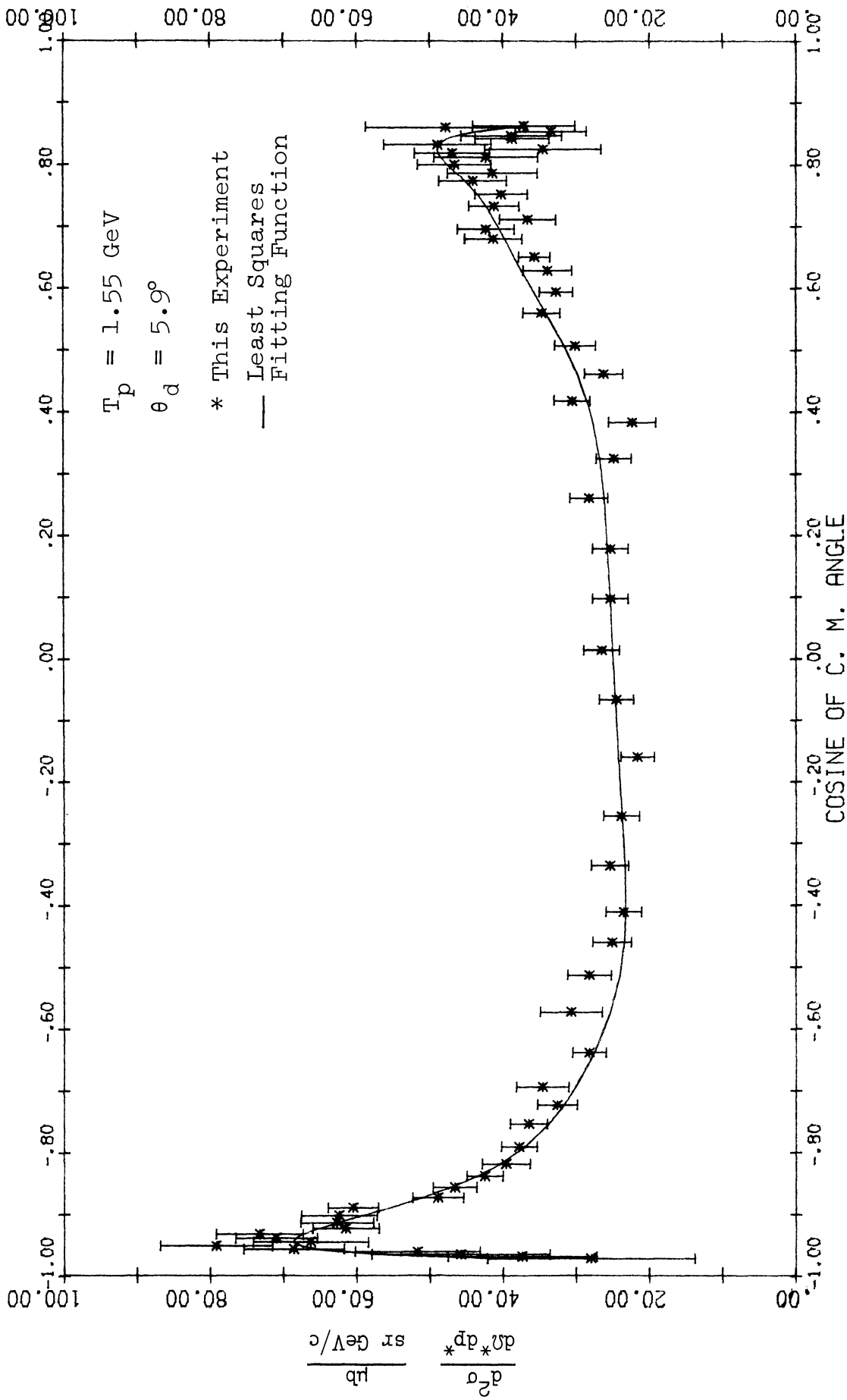

Fig. 28. C.m. differential cross section for deuteron production in p-p collisions vs. the cosine of the deuteron c.m. production angle. T_p = 1.55 GeV, θ_d(lab) = 5.9°.

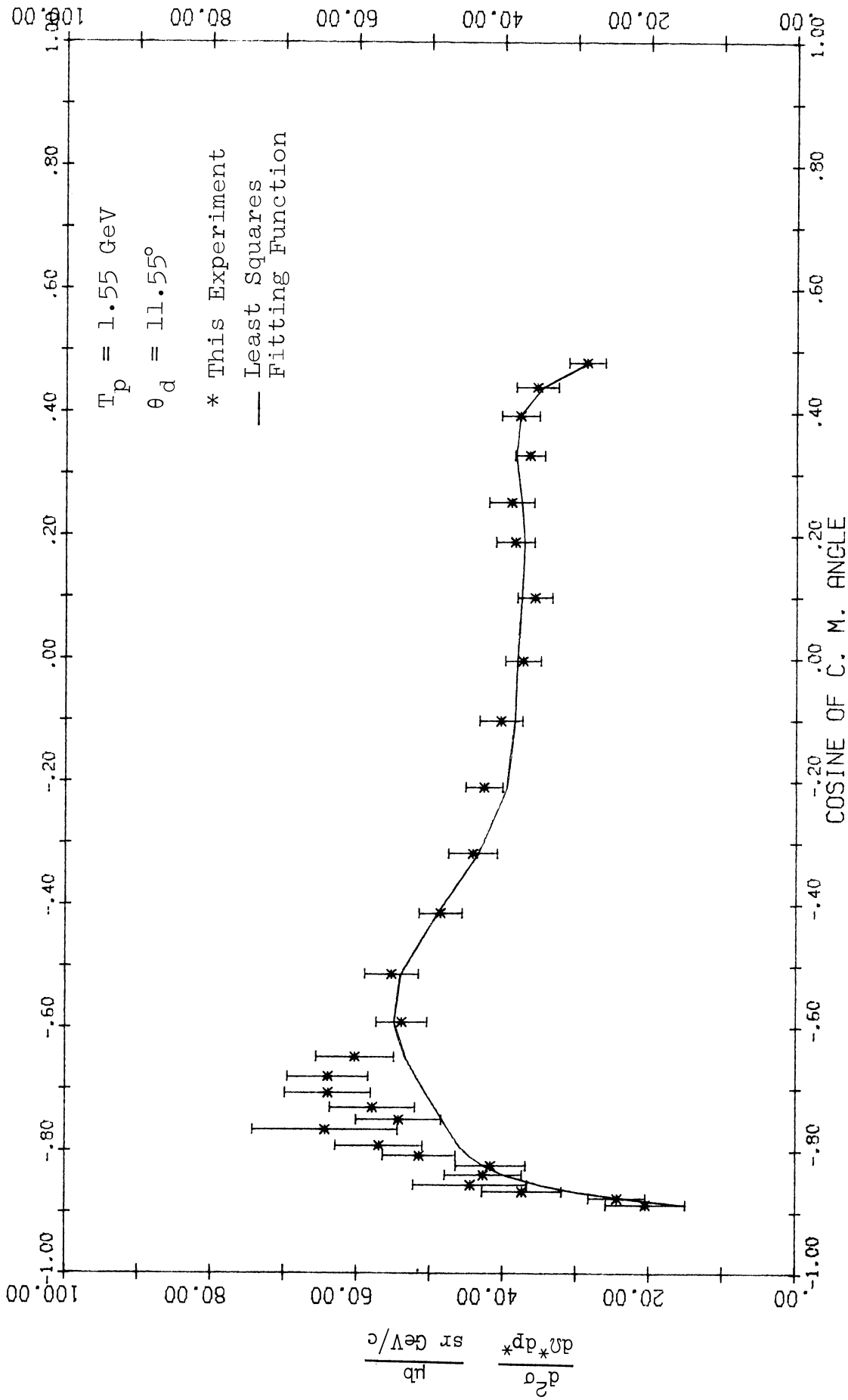

Fig. 29. C.m. differential cross section for deuteron production in p-p collisions vs. the cosine of the deuteron c.m. production angle. T_p = 1.55 GeV, θ_d(lab) = 15.72°.

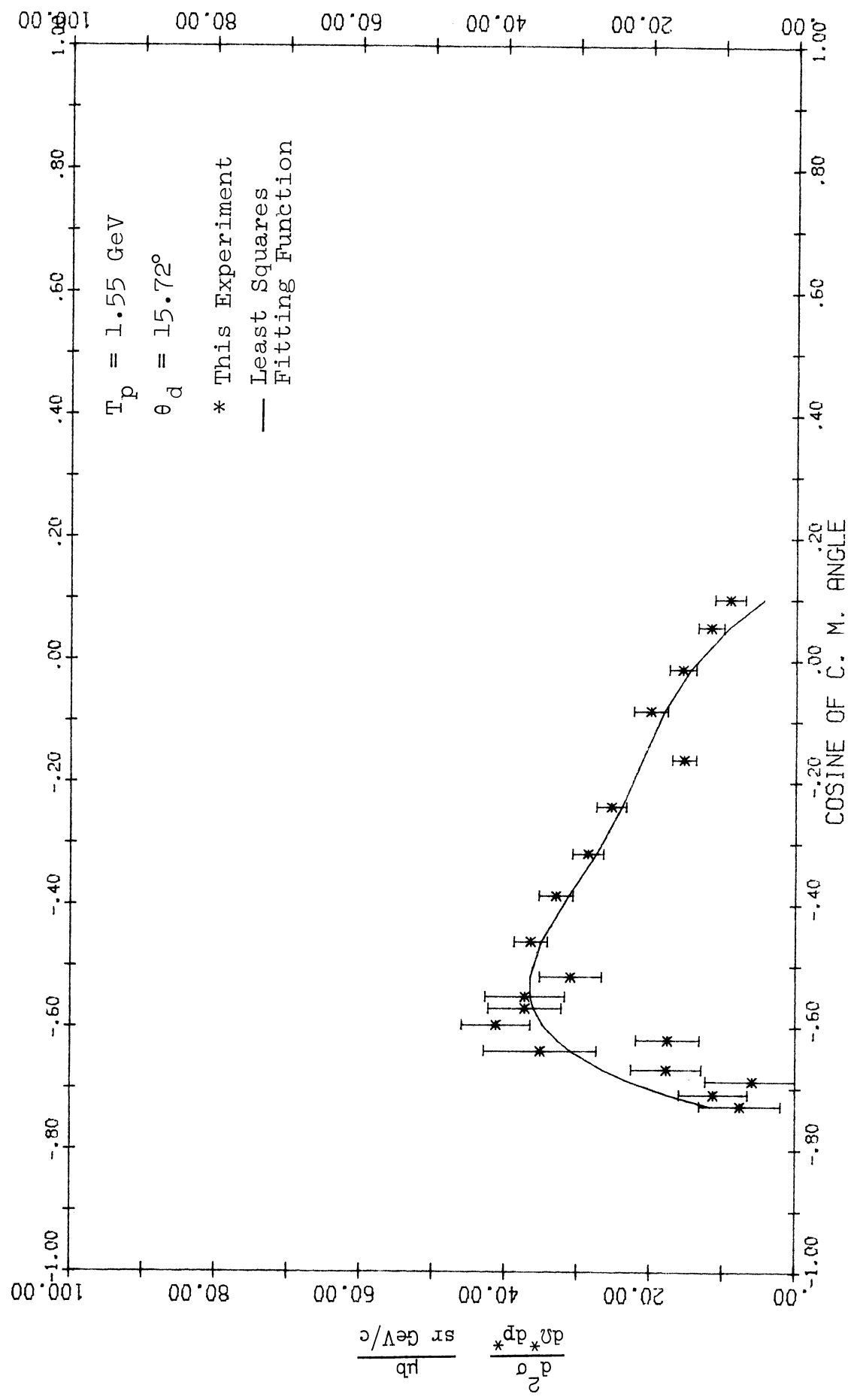

Fig. 30. C.m. differential cross section for deuteron production in p-p collisions vs. the cosine of the deuteron c.m. production angle. T_p = 1.55 GeV, θ_d(lab) = 15.72°.

c.m. relative to the direction of the incident proton. Points measured in this experiment for $\cos\theta^* < 0$ are plotted as solid circles. Since the initial state of the measured reaction consists of a pair of identical particles (assuming the proton beam was unpolarized), the cross section must be symmetric in the line $\cos\theta^* = 0$. The open circles represent points where data were obtained with $\cos\theta^* > 0$, but have been plotted at $-\cos\theta^*$ through the use of this symmetry. The triangles represent measurements of Turkot, et al.[12] The dashed line labeled p^*_{max} marks the maximum momentum at which the deuteron can be produced with two or more pions. The only contribution to the total deuteron production cross section above this line is from the reaction $p + p \rightarrow d + \pi^+$, which has been studied extensively elsewhere.[1,2] The points from this experiment at a given laboratory angle fall along a curved trajectory in the plot. Each point is labeled with the corresponding value of the c.m. differential cross section in μb/(sr GeV/c). Several corrections have been made to the data of this experiment since this chart was prepared, so the values quoted are 5% too low. The correct values, which are tabulated in Appendix II, have been used in all graphs presented in this paper and in the least squares fit to the data described below.

In order to obtain the total cross section for deuteron production at this energy, the data were fitted with a polynomial of the form

$$p^*(p^*_{max}-p^*) \sum_{j=0}^{B} \sum_{k=0}^{C} A_{jk} p^{*j} P_{2k}(\cos\theta^*).$$

The A_{jk} were determined by the method of least squares.[30] The total cross section (except for the reaction $p + p \rightarrow d + \pi^+$) was then given by the integral of this function over p^* between 0 and p^*_{max} and over all values of solid angle. The resulting expression is:

$$\sigma_{total}(d + \geq 2\pi) = 4\pi (p^*_{max})^3 \sum_{j=0}^{B} \frac{A_{jo}\, p^{*j}}{(j+2)(j+3)} .$$

The use of only even Legendre polynomials insured that the fitting function would have the desired symmetry about $\cos\theta^* = 0$. The cross section is zero when $p^* = 0$ and when $p^* = p^*_{max}$. The two leading terms guaranteed this behavior for the fitting function.

It was necessary to provide the least squares fitting routine with an estimate of the cross section in the region $0 < p^* \leq .1$ GeV/c where no measurements were made. Without such a constraint, the fitting function could assume large and unphysical positive or negative values in this region. This was done by supplying fictitious data at the locations indicated by the solid squares in Fig. 21. The values, shown in parentheses next to the squares, were chosen to be the same for all $\cos\theta^*$ at a given value of p^*, and to agree with the measured cross section at $\cos\theta^* = -1$. This seemed reasonable since the cross section data tend to become more

nearly isotropic as p* decreases, and are already nearly so when p* = .18 GeV/c. The fictitious values were given large errors so they would not be weighted heavily in the calculation of the A_{jk}.

The expansion coefficients for the best fit to the data at 1.55 GeV are given in Table IV. The total cross section was 187 $\pm$ 24 μb (not including the reaction $p + p \rightarrow d + \pi^+$). This value was insensitive to the order of the fit (i.e., the values of B and C chosen for the fitting polynomial), and hence to the detailed behavior of the fitting function.

Figs. 22-27 show the experimental values of the c.m. differential cross section plotted against p*. Note that this is a double valued function. The two branches have been plotted separately for the 5.9 and 11.55° data. The solid line is the least squares fitting function. The same data plotted against cosθ* are shown in Figs. 28-30.

The least squares function provides a useful representation of the general behavior of the c.m. cross section, although it tends to smooth the detailed structure of the data. It is shown in Fig. 31.

Fig. 32 is a plot of the points where the differential cross section for deuteron production in proton-proton collisions was measured for a proton kinetic energy of 2.5 GeV. The expansion coefficients for the least squares fitting function at this energy are given in Table V. The

TABLE IV

PARAMETERS FOR THE LEAST SQUARES FIT TO THE DATA AT 1.55 GeV

A_{jk}

j \ k	0	1	2	3	4	5
0	-.4146 ±33	-48.44 ±67	-39.00 ±76	152.5 ±92	-15.75 ±92	-50.56 ±78
1	2811. ±560	1418. ±1300	729.7 ±1400	-4765. ±1600	706.6 ±1700	2099. ±1600
2	-4732. ±2600	-6441. ±6100	476.1 ±6700	24 070. ±8100	-7918. ±8000	-13 365. ±8000
3	8555. ±3500	13 817. ±7900	-6091. ±9200	-28 023. ±11 000	16 088. ±11 000	18 050. ±12 000

B = 3, C = 5, p^*_{max} = .530 GeV/c; $\sigma_{total}(p + p \rightarrow d + \geq 2\pi)$ = 187 μb

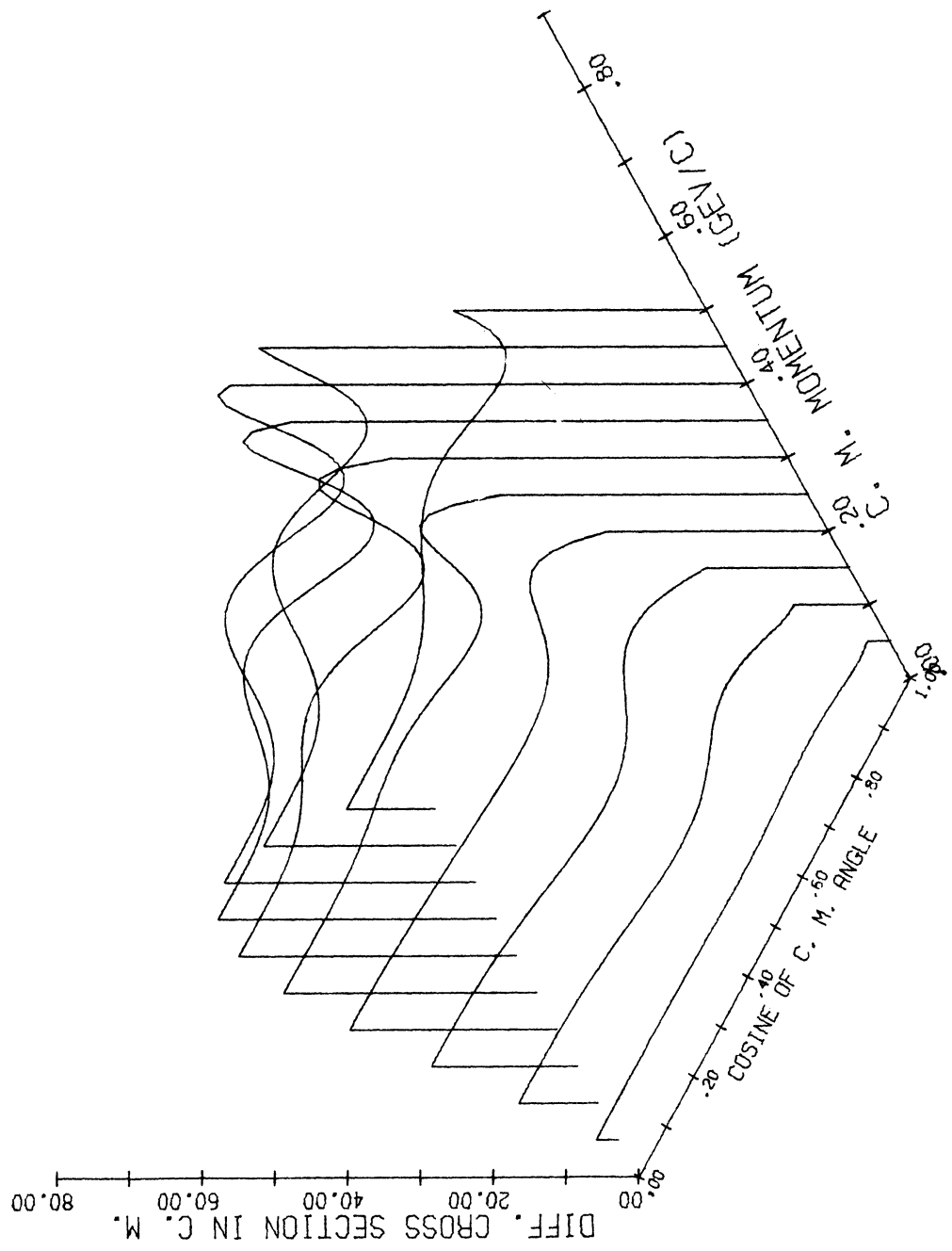

Fig. 31. Least squares fitting function for the data at 1.55 GeV. The function (in μb/(sr GeV/c)) is plotted vs. the cosine of the deuteron c.m. production angle and the deuteron c.m. momentum.

Fig. 32. Plot of the points where the differential cross section for deuteron production in proton-proton collisions has been measured at 2.5 GeV as a function of the cosine of the deuteron c.m. production angle and c.m. momentum. The symbols have the following meanings:

● Point where a measurement was made in this experiment.

o Point indicating a measurement in this experiment at (p*, + cosθ*) plotted at (p*, - cosθ*) through use of the reflection symmetry of the differential cross section in the line cosθ* = 0 (see text).

▲ Point where a measurement was made by Turkot, et al.[12]

■ Point where an estimated cross section value was supplied to the least squares fitting routine.

The numbers next to the symbols are the values of the c.m. differential cross section,

$$\frac{d^2\sigma}{d\Omega^* dp^*},$$

in μb/(sr GeV/c). Estimated values have been placed in parentheses. The values quoted for this experiment are slightly in error. Corrections made to the data subsequent to the preparation of this plot resulted in a 5% increase in all the values. The corrected data have been used in the other graphs in this paper.

The line labeled p^*_{max} represents the maximum deuteron c.m. momentum possible in a final state containing two or more pions.

The measurements at a given fixed deuteron production angle in the laboratory, θ_L, fall on a curved trajectory in this plot.

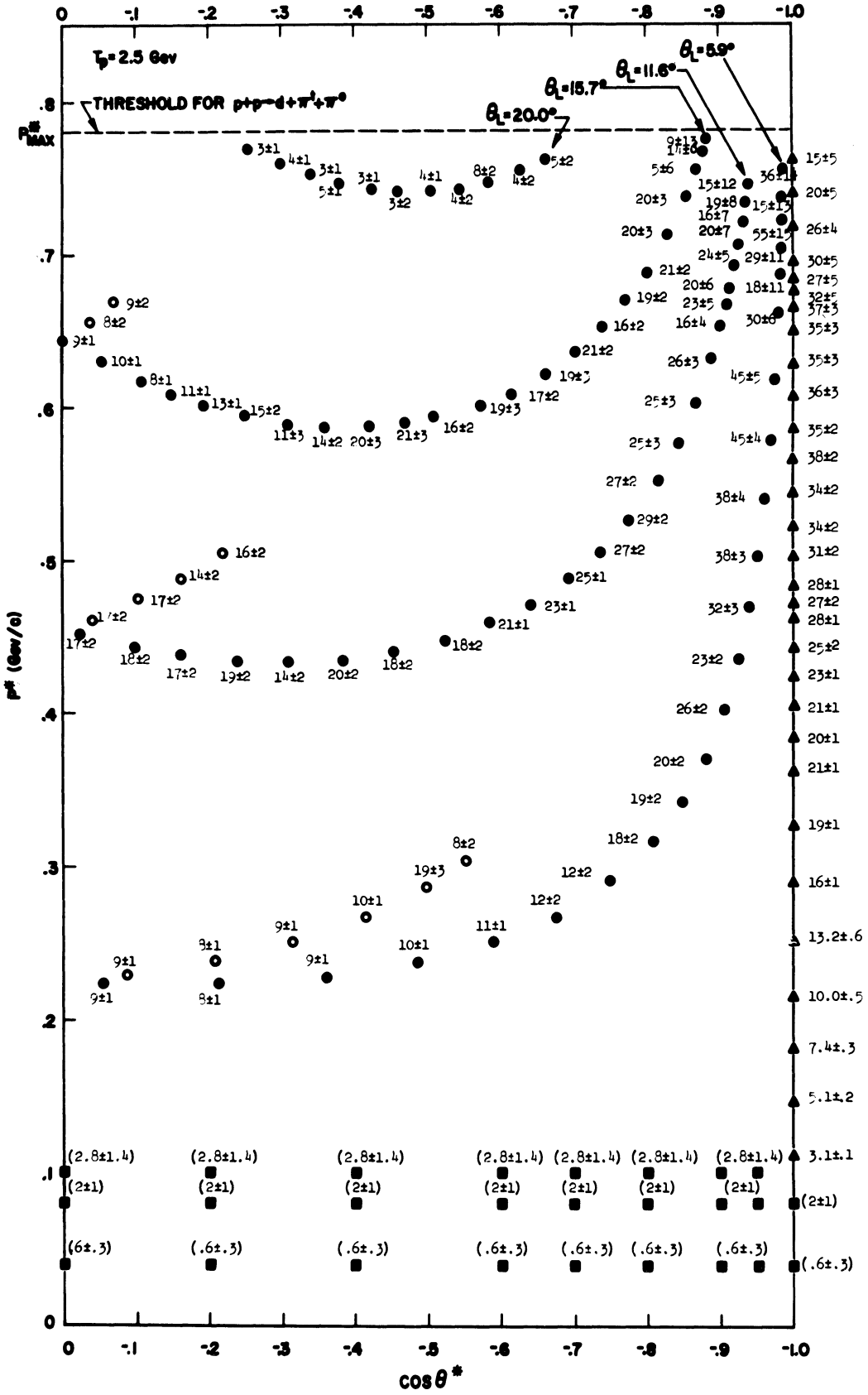
T_p = 2.5 Gev
THRESHOLD FOR p+p→d+π⁺+π°
θ_L=5.9°
θ_L=11.6°
θ_L=15.7°
θ_L=20.0°
P^{cm}_{MAX}
p^{cm} (Gev/c)
cos θ*
0
-.1
-.2
-.3
-.4
-.5
-.6
-.7
-.8
-.9
-1.0
.8
.7
.6
.5
.4
.3
.2
.1
(2.8±1.4)
(2±1)
(6±.3)
(.6±.3)
3.1±.1
(2±1)
(.6±.3)
13.2±.6
10.0±.5
7.4±.3
5.1±.2

Fig. 32

TABLE V

PARAMETERS FOR THE LEAST SQUARES FIT TO THE DATA AT 2.5 GeV

A_{jk}

j \ k	0	1	2	3	4	5
0	20.47 ±8	-21.23 ±16	-3.990 ±18	9.041 ±17	11.85 ±20	-10.59 ±19
1	-14.64 ±190	589.2 ±360	53.26 ±350	-164.5 ±200	-428.5 ±340	200.7 ±290
2	1895. ±1100	-3729. ±1900	-68.84 ±1800	508.0 ±240	3367. ±1600	-617.8 ±1200
3	-3904. ±2200	9054. ±3900	-670.3 ±3500	-888.9 ±1400	-8323. ±3100	-255.9 ±2000
4	2585. ±1500	-6035. ±2700	1167. ±2300	693.2 ±1000	6301. ±2200	1325. ±1500

$B = 4$, $C = 5$, $p^*_{max} = .780$ GeV/c; $\sigma_{total}(p + p \rightarrow d + \geq 2\pi) = 126$ μb.

function is shown in Fig. 33. Corresponding representations of the data at 2.9 GeV are given in Fig. 34, Table VI, and Fig. 35. Graphs of the c.m. differential cross section vs. $\cos\theta^*$ and p^* are given in Appendix II for these two energies.

The data shown here for a proton kinetic energy of 2.9 GeV were taken in the initial experimental run under poor beam conditions which produced a high background rate with the target empty. The observed cross section was then the small difference between two nearly equal numbers, and was subject to large statistical uncertainties. It was even possible to obtain negative experimental values for the cross section when by chance the run with the target empty yielded a proportionately larger number of counts than the run with the target full. Such measurements have not been discarded because to do so would bias the fitting function toward larger values of cross section. The negative values occurred when the differential cross section in the laboratory was very small. The values were magnified considerably by the Jacobian in the transformation to the c.m., but since they

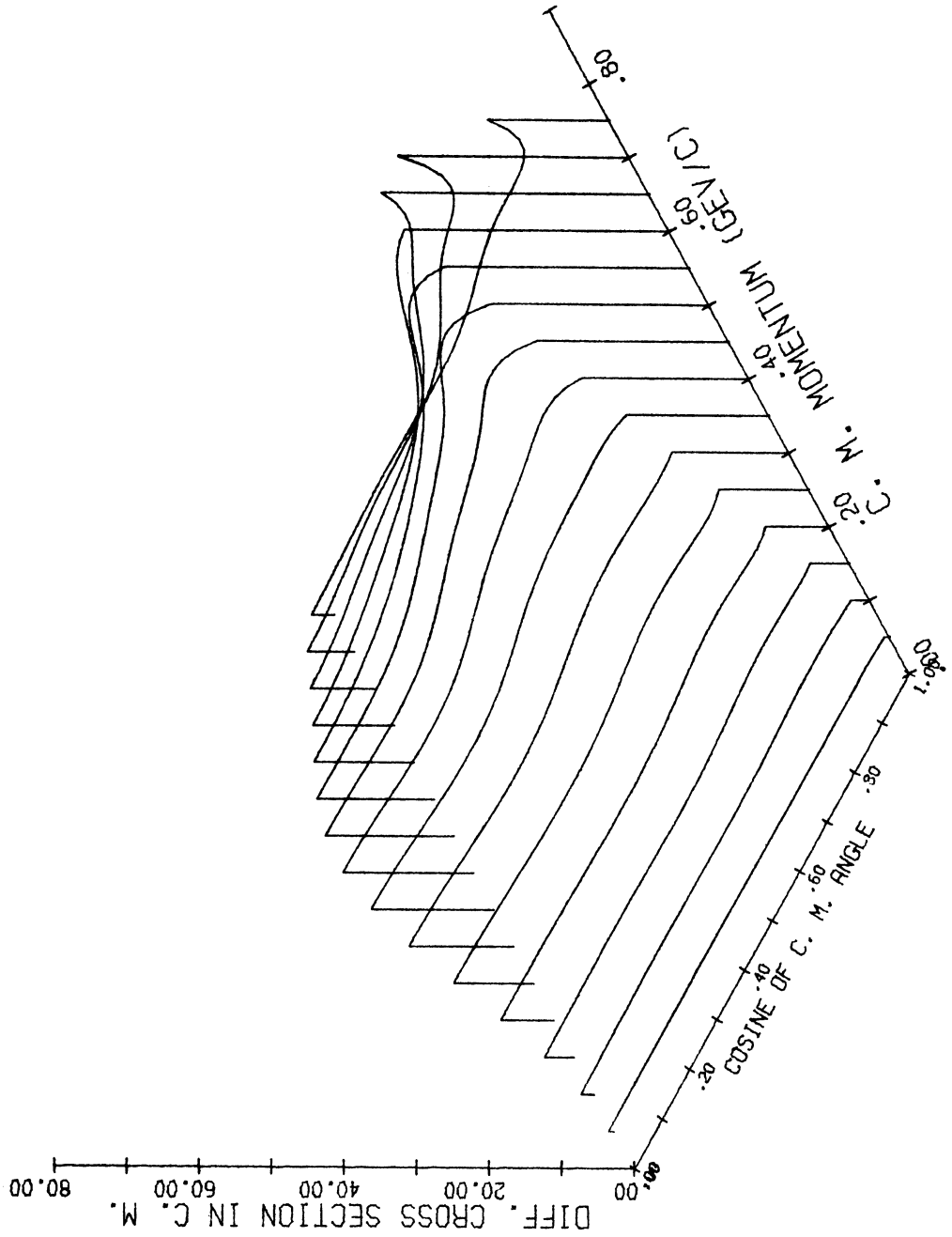

Fig. 33. Least squares fitting function for the data at 2.5 GeV. The function (in μb/(sr GeV/c)) is plotted vs. the cosine of the deuteron c.m. production angle and the deuteron c.m. momentum.

Fig. 34. Plot of the points where the differential cross section for deuteron production in p-p collisions has been measured at 2.9 GeV as a function of the cosine of the deuteron c.m. production angle and c.m. momentum.

The symbols have the following meanings:

● Point where a measurement was made in this experiment. The numbers next to these symbols, while representing the general trend of the differential cross section (in $\mu b/(sr\ GeV/c)$) at the points, do not correspond to the final data from the experiment. The correct data have been used elsewhere in this paper, and are tabulated in Appendix II.

■ Point where an estimated cross section value (shown in parentheses) was supplied to the least squares fitting routine.

The line labeled p^*_{max} represents the maximum deuteron c.m. momentum possible in a final state containing two or more pions.

The measurements at a given, fixed deuteron production angle in the laboratory, θ_L, fall on a curved trajectory in this plot.

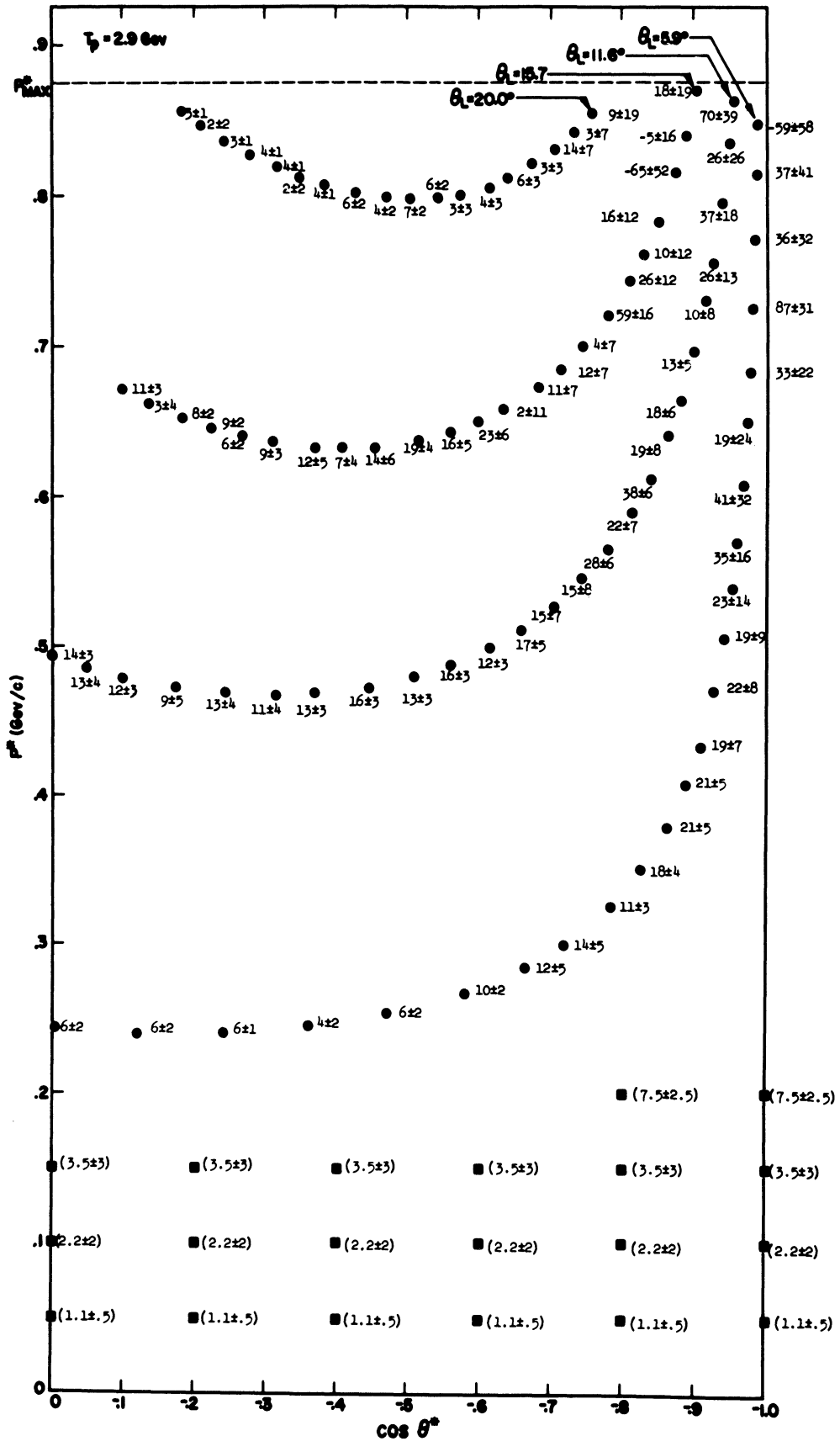
T_p = 2.9 Gev
θ_L=5.9°
θ_L=11.6°
θ_L=15.7°
θ_L=20.0°
P^*_{MAX}
P^* (Gev/c)
cos θ^*
0
.1
.2
.3
.4
.5
.6
.7
.8
.9
1.0

Fig. 34

TABLE VI

PARAMETERS FOR THE LEAST SQUARES FIT TO THE DATA AT 2.9 GeV

A_{jk}

j \ k	0	1	2	3	4
0	21.13 ±9	6.054 ±24	-.03354 ±29	-1.408 ±26	-.9677 ±41
1	61.03 ±110	-145.7 ±330	-38.02 ±360	28.50 ±370	87.06 ±500
2	317.4 ±350	999.9 ±1100	-16.39 ±1200	-346.2 ±1400	-228.6 ±1600
3	-330.3 ±310	-860.5 ±950	195.4 ±1200	542.3 ±1400	273.4 ±1400

$B = 3$, $C = 4$, $p^*_{max} = .875$ GeV/c; $\sigma_{total}(p+p \rightarrow d + \geq 2\pi) = 107$ μb

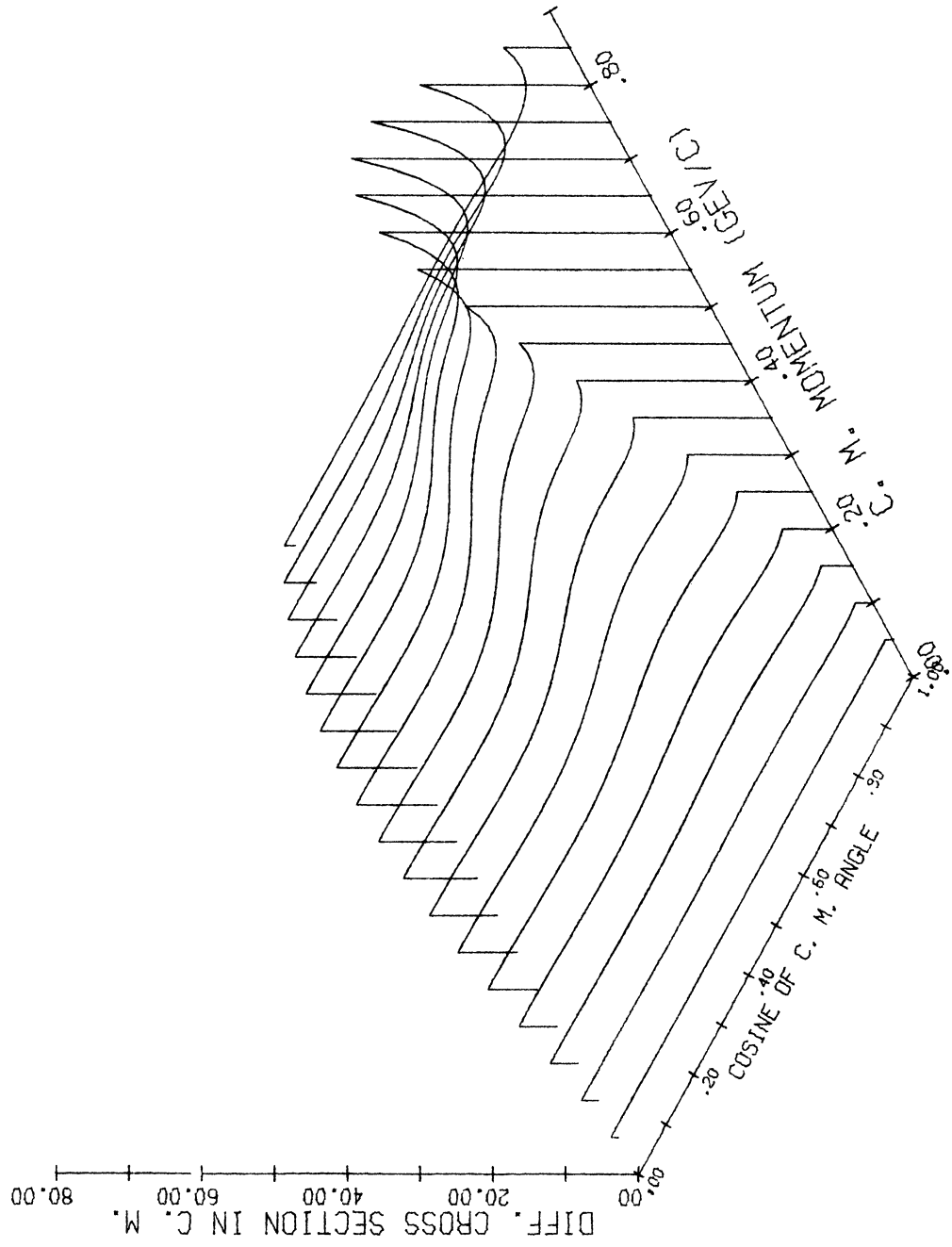

Fig. 35. Least squares fitting function for the data at 2.9 GeV. The function (in μb/(sr GeV/c)) is plotted vs. the cosine of the deuteron c.m. production angle and the deuteron c.m. momentum.

Since no data were available for values of $p^* < .23$ GeV/c at 2.9 GeV, fictitious c.m. cross section values for the fitting routine were chosen in this region so that the resulting function would decrease smoothly to zero as p^* went to zero.

C. Energy Dependence of the Total Cross Section

The total cross section for the reaction $p + p \rightarrow d + \geq 2\pi$ obtained from the least squares fitting function is shown for the three proton kinetic energies of this experiment in Fig. 36. The errors indicated include the 8% uncertainty in the calibration of the beam intensity monitors. Also shown is the total deuteron production cross section in proton-proton collisions at these energies. The cross section for the reaction $p + p \rightarrow d + \pi^+$ was obtained from Heinz, et al.[1,2] and added to the results of this experiment to get these data. The data are compared with total cross section measurements at 2.05 GeV by Sechi Zorn,[7] at 970 MeV by Bugg, et al.,[11] and at 380 MeV by Holt, et al.[31]

D. Differential Cross Section vs. Invariant Mass of the Pion System

A system of two or more pions in a state of unit isotopic spin and a net charge of +1 was formed along with the deuteron in this experiment. At a fixed beam energy, a measurement of the magnitude of the deuteron c.m. momentum was sufficient to determine the invariant mass, M_x, of the pion system. In Figs. 37-45, the differential cross section

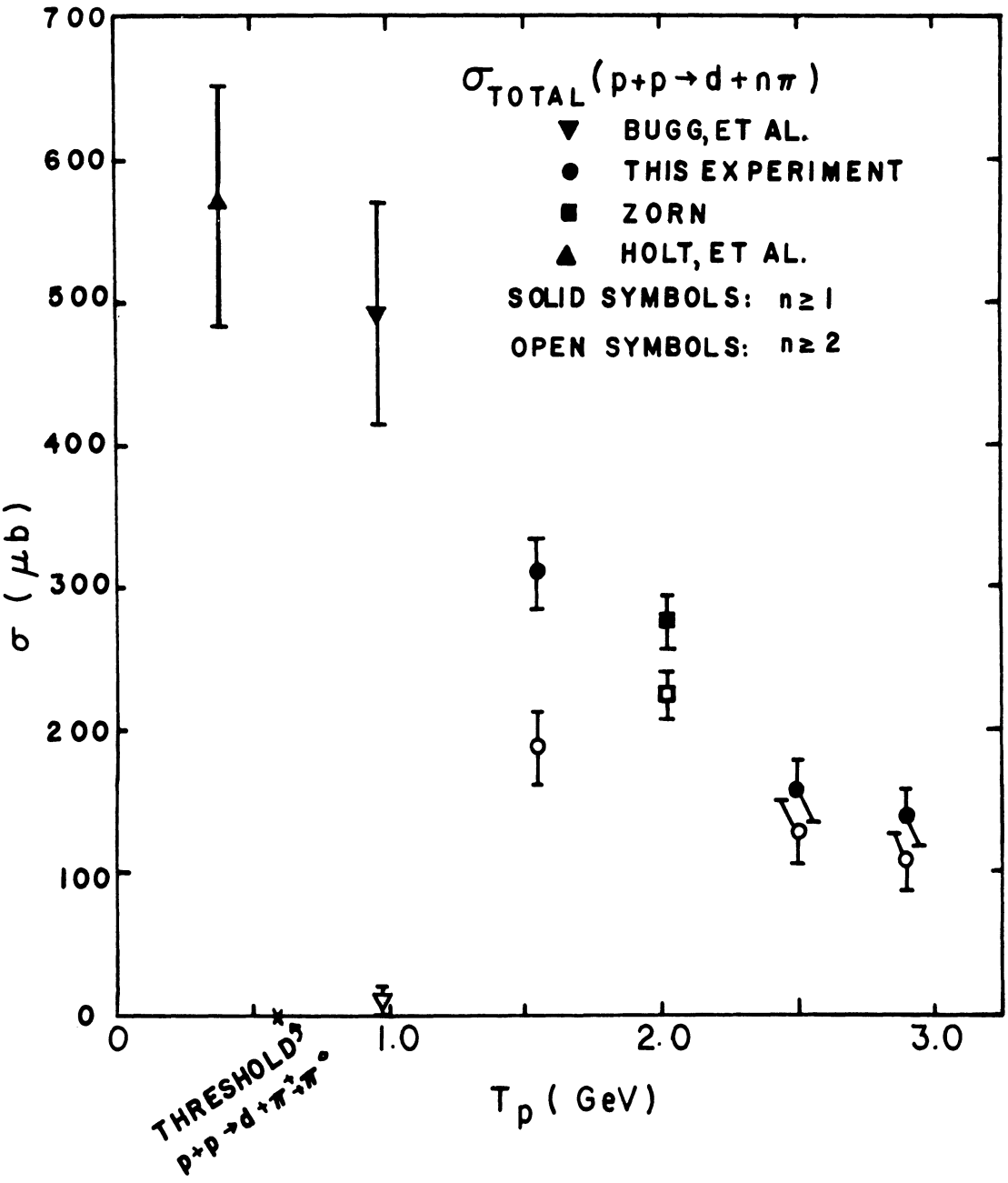

Fig. 36. Total cross section for deuteron production in p-p collisions vs. the kinetic energy of the incident proton. The values plotted with open symbols do not include the cross section for the reaction $p + p \rightarrow d + \pi^+$.

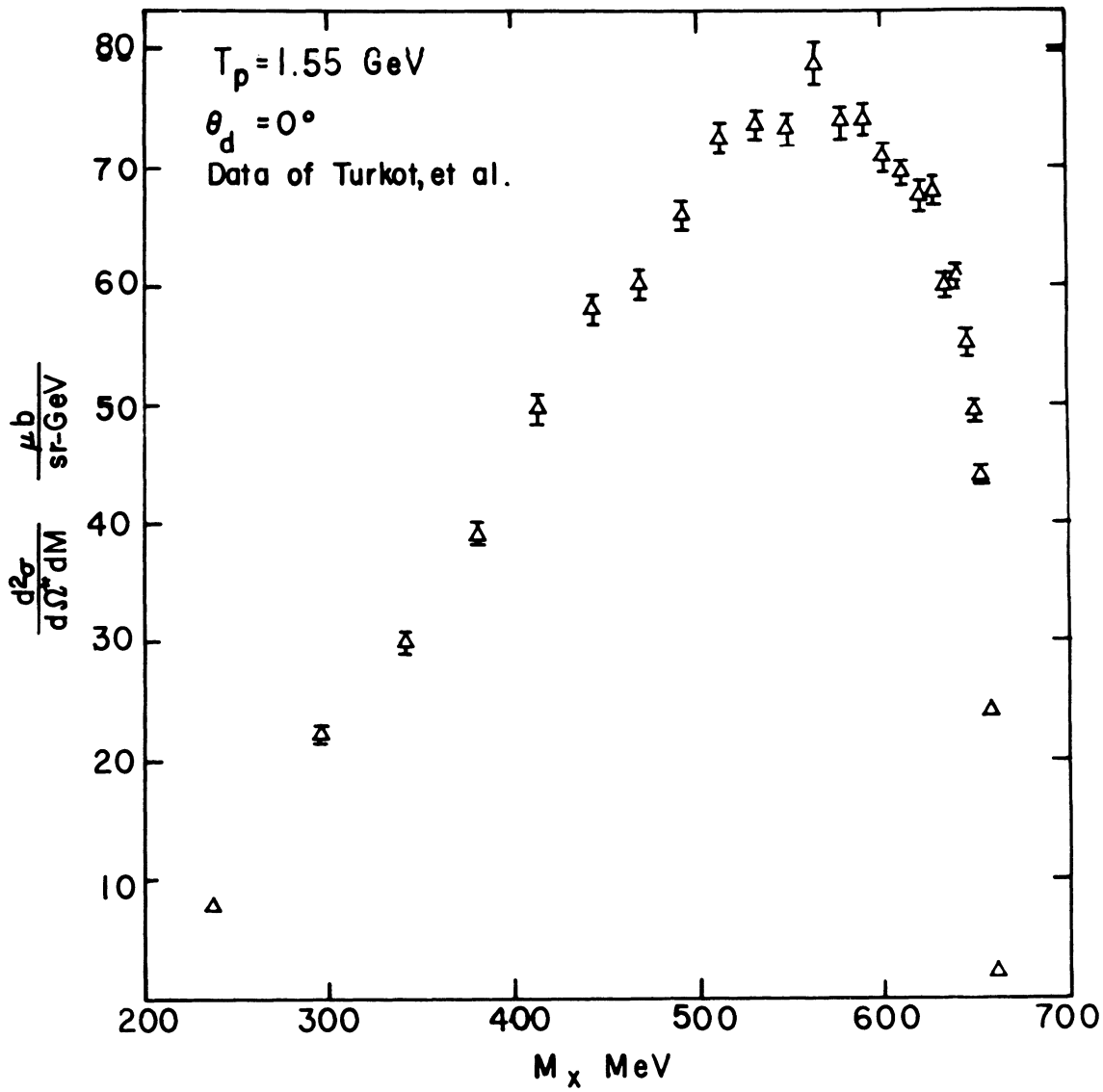

Fig. 37. Differential cross section for deuteron production in p-p collisions at 1.55 GeV vs. the invariant mass of the system of particles formed along with the deuteron from Turkot, et al.[12] The laboratory deuteron production angle was 0°.

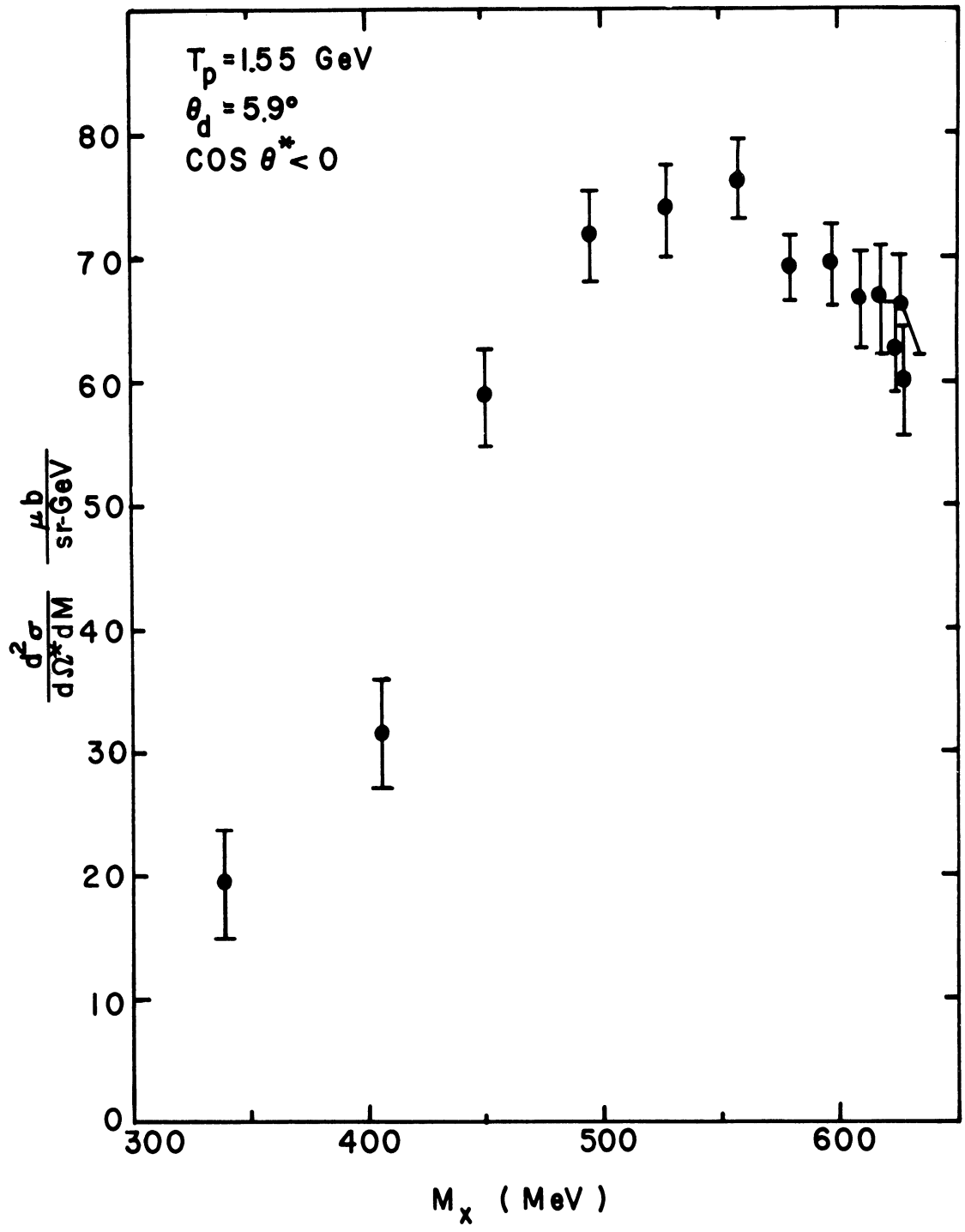

Fig. 38. Differential cross section for deuteron production in p-p collisions at 1.55 GeV vs. the invariant mass of the system of particles formed along with the deuteron. The deuterons were produced at a laboratory angle of 5.9° and a c.m. angle > 90°.

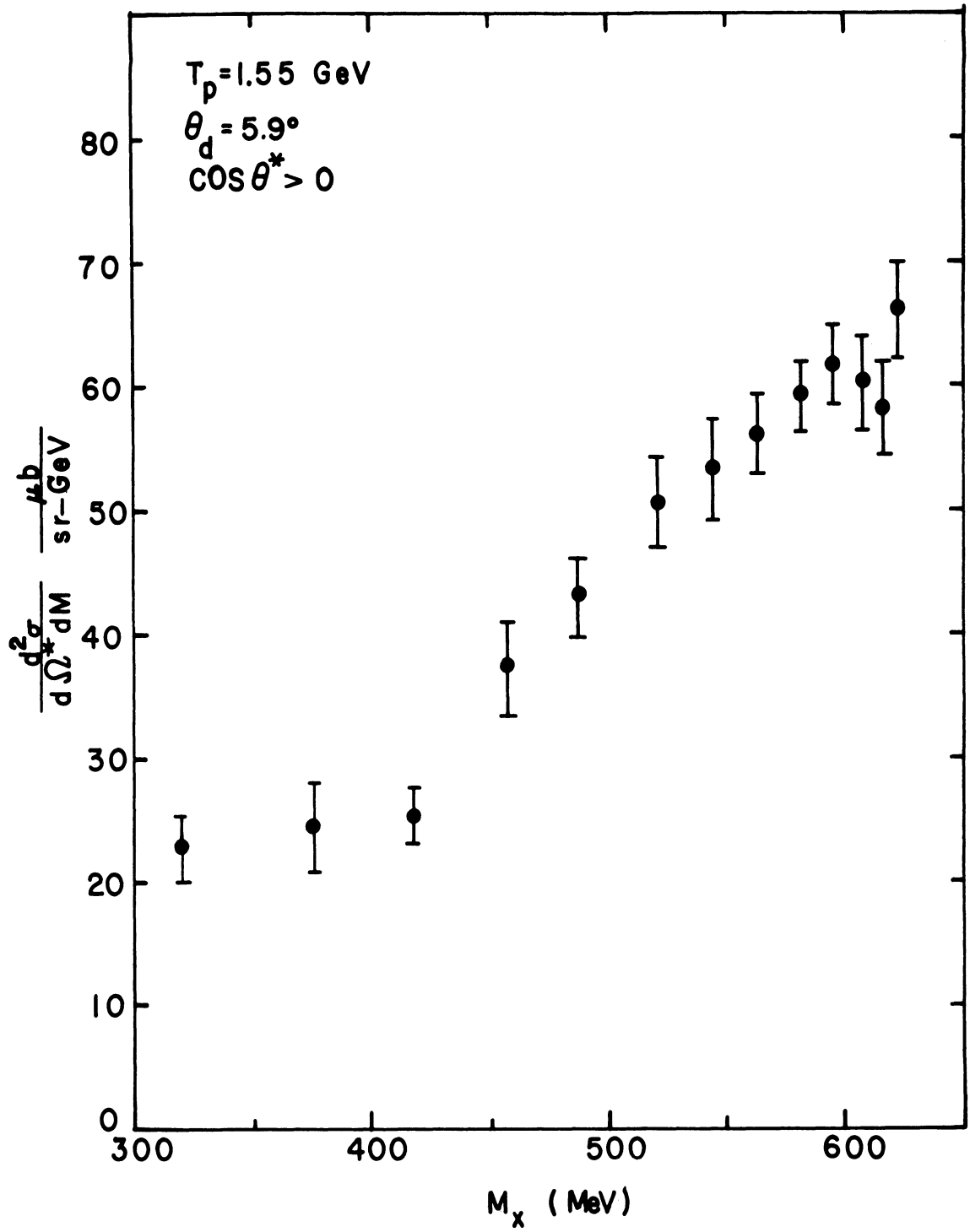

Fig. 39. Differential cross section for deuteron production in p-p collisions at 1.55 GeV vs. the invariant mass of the system of particles formed along with the deuteron. The deuterons were produced at a laboratory angle of 5.9° and a c.m. angle < 90°.

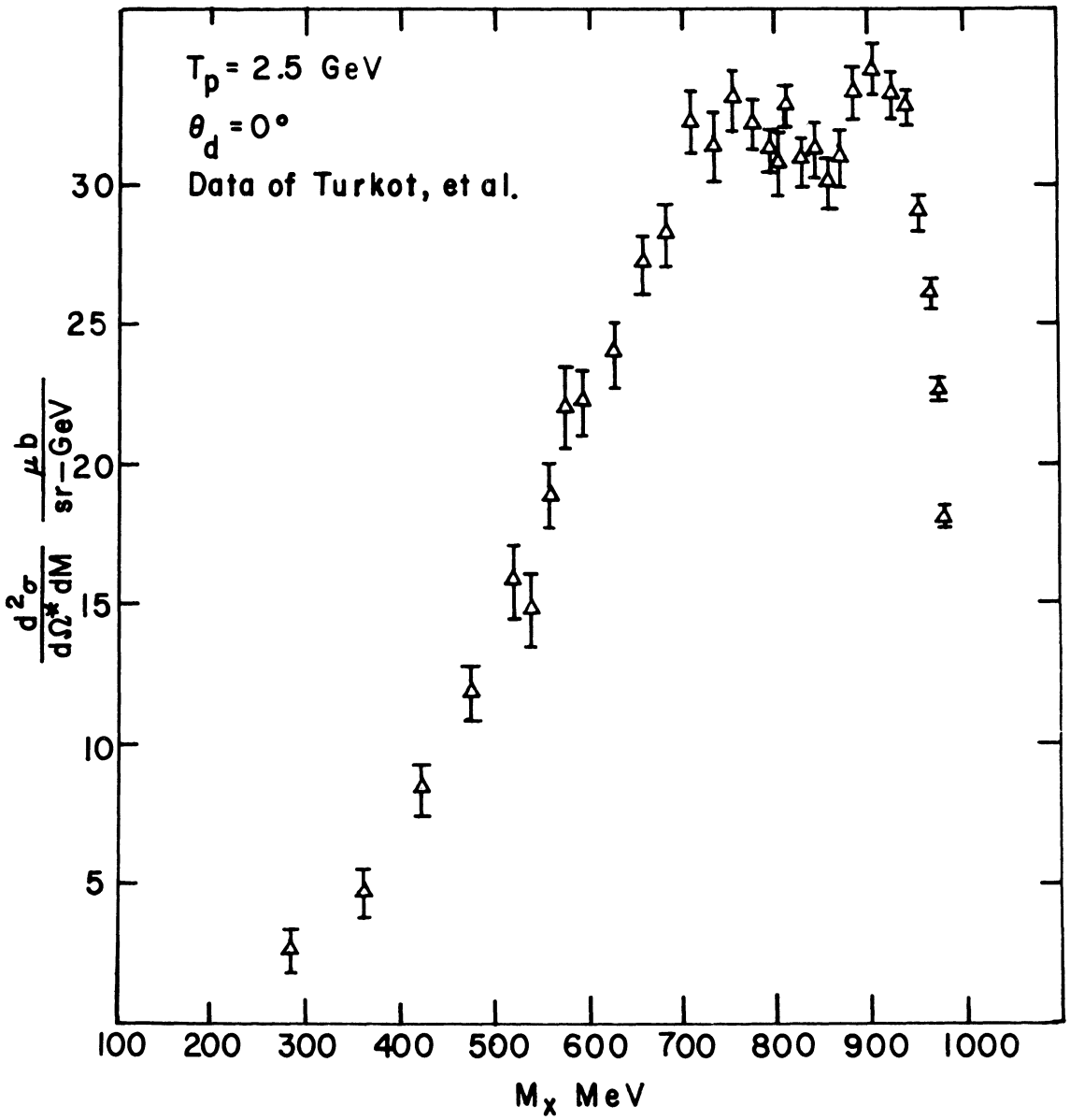

Fig. 40. Differential cross section for deuteron production in p-p collisions at 2.5 GeV vs. the invariant mass of the system of particles formed along with the deuteron from Turkot, et al.[12] The laboratory production angle of the deuterons was 0°.

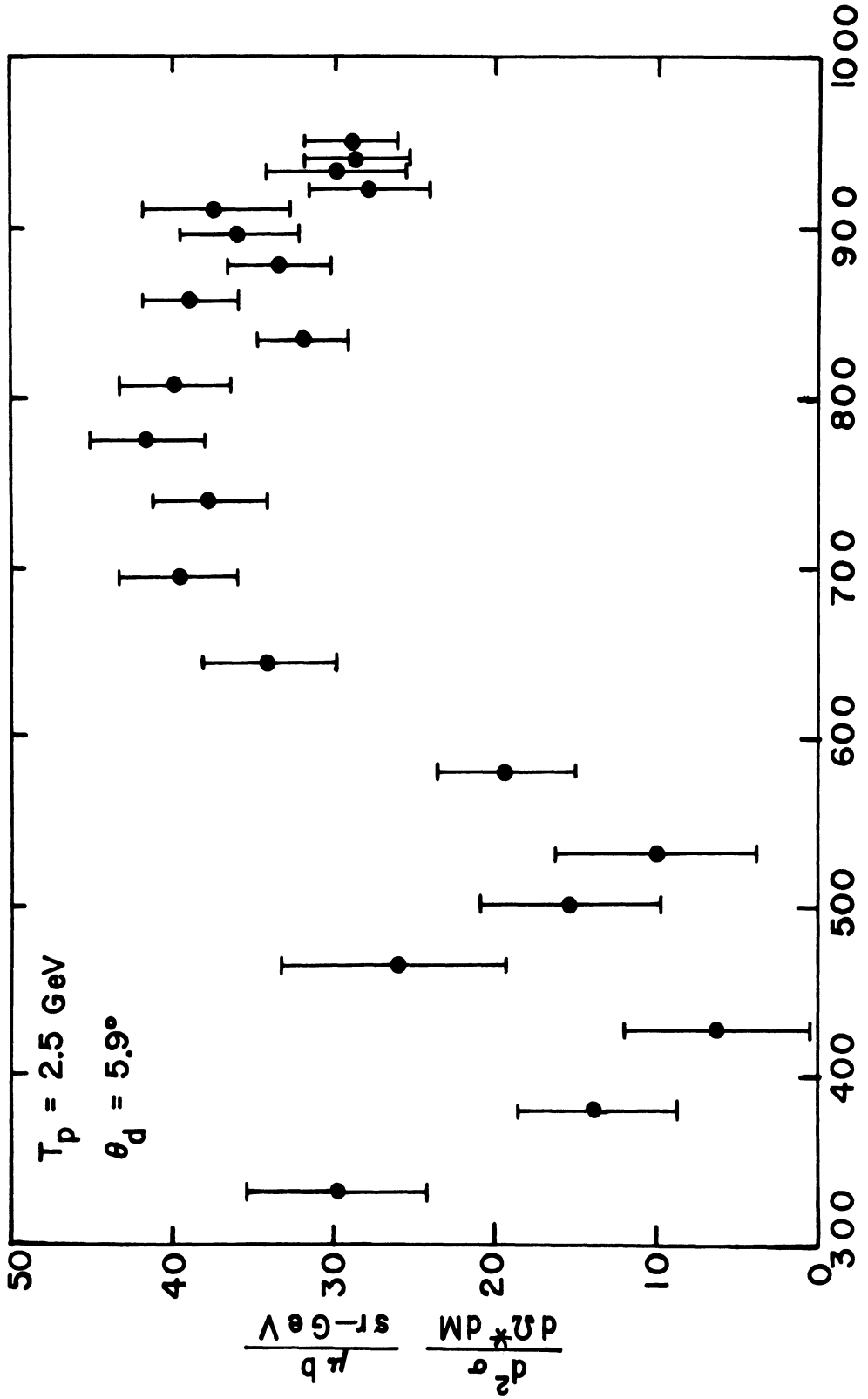

Fig. 41. Differential cross section for deuteron production in p-p collisions at 2.5 GeV vs. the invariant mass of the system of particles formed along with the deuteron. The laboratory production angle of the deuterons was 5.9°.

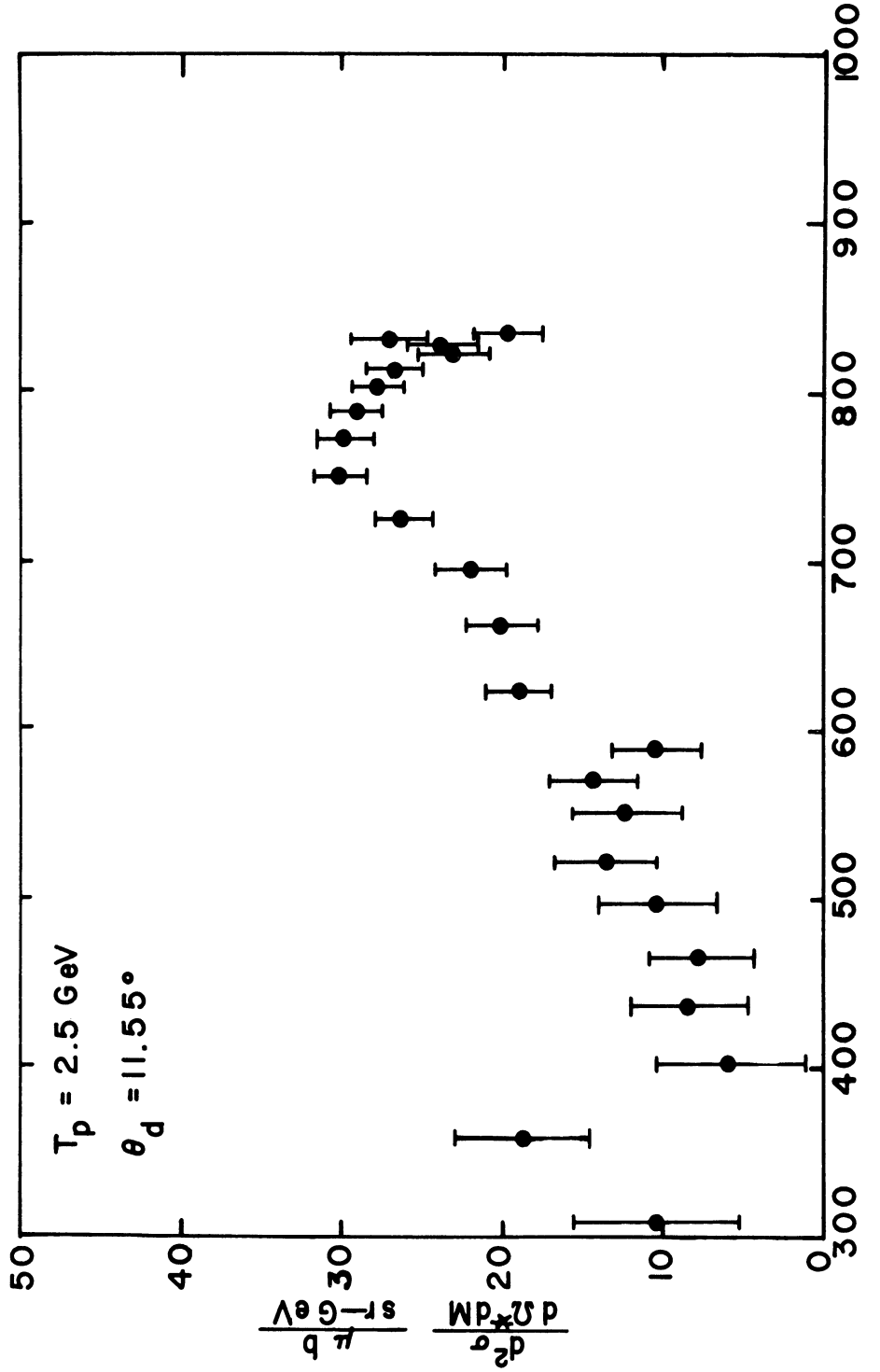

Fig. 42. Differential cross section for deuteron production in p-p collisions at 2.5 GeV vs. the invariant mass of the system of particles formed along with the deuteron. The laboratory production angle of the deuterons was 11.55°.

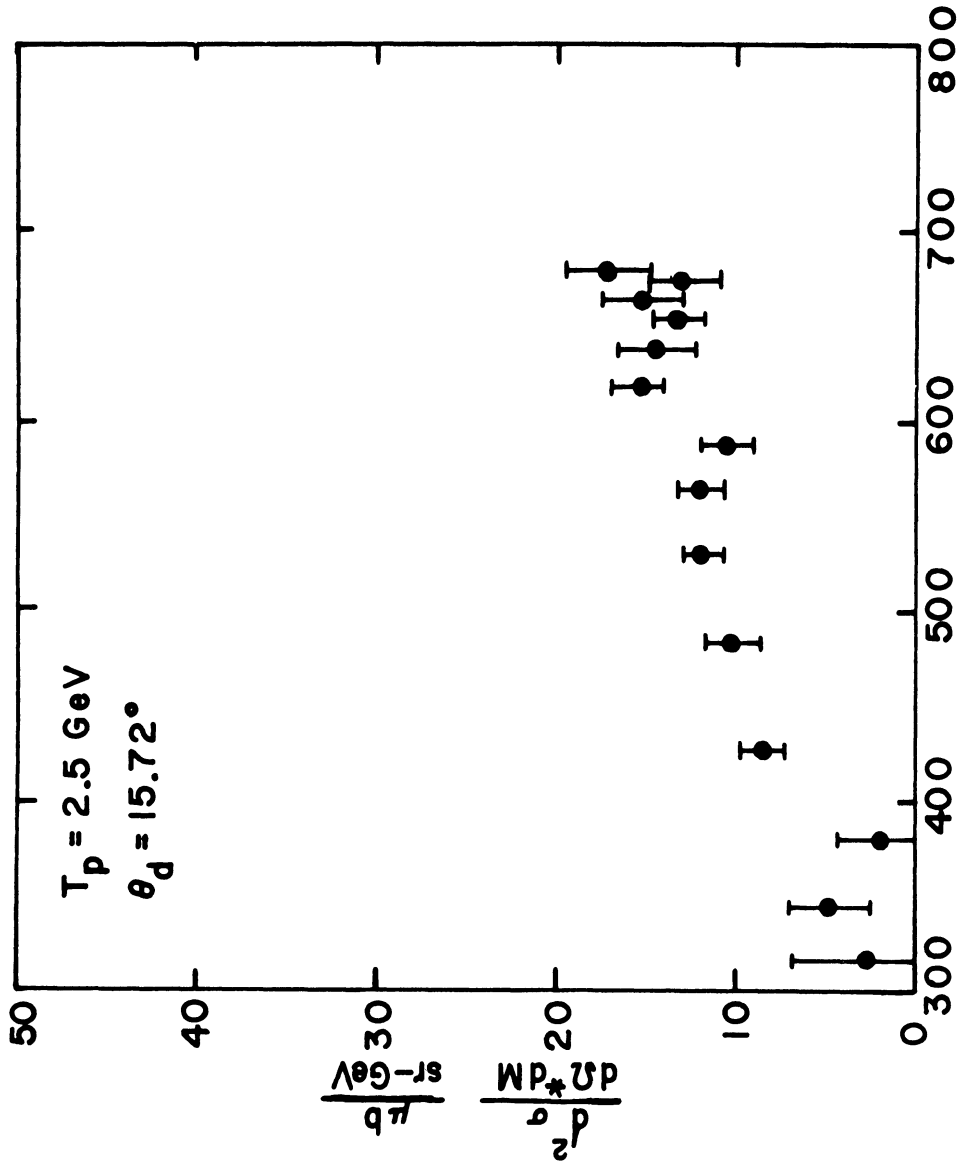

Fig. 43. Differential cross section for deuteron production in p-p collisions at 2.5 GeV vs. the invariant mass of the system of particles formed along with the deuteron. The laboratory production angle of the deuterons was 15.72°.

Fig. 44. Differential cross section for deuteron production in p-p collisions at 2.9 GeV vs. the invariant mass of the system of particles formed along with the deuteron. The laboratory production angle of the deuterons was 5.9°. The raw data were averaged in laboratory momentum steps of .02 GeV/c (see Chapter III, Section J).

Fig. 45. Differential cross section for deuteron production in p-p collisions at 2.9 GeV vs. the invariant mass of the system of particles formed along with the deuteron. The laboratory production angle of the deuterons was 5.9°. The raw data were averaged in laboratory momentum steps of .04 GeV/c (see Chapter III, Section J).

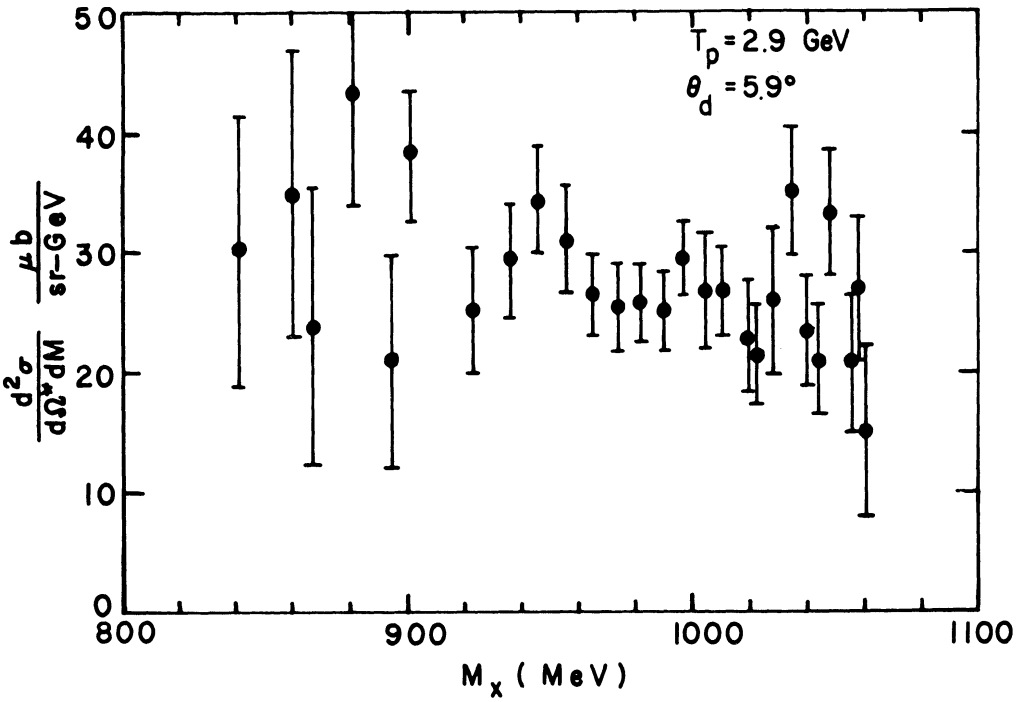
T_p = 2.9 GeV
θ_d = 5.9°
$\frac{d^2\sigma}{d\Omega^* dM}$ $\frac{\mu b}{sr-GeV}$
0
10
20
30
40
50
800
900
1000
1100
M_x (MeV)

Fig. 44

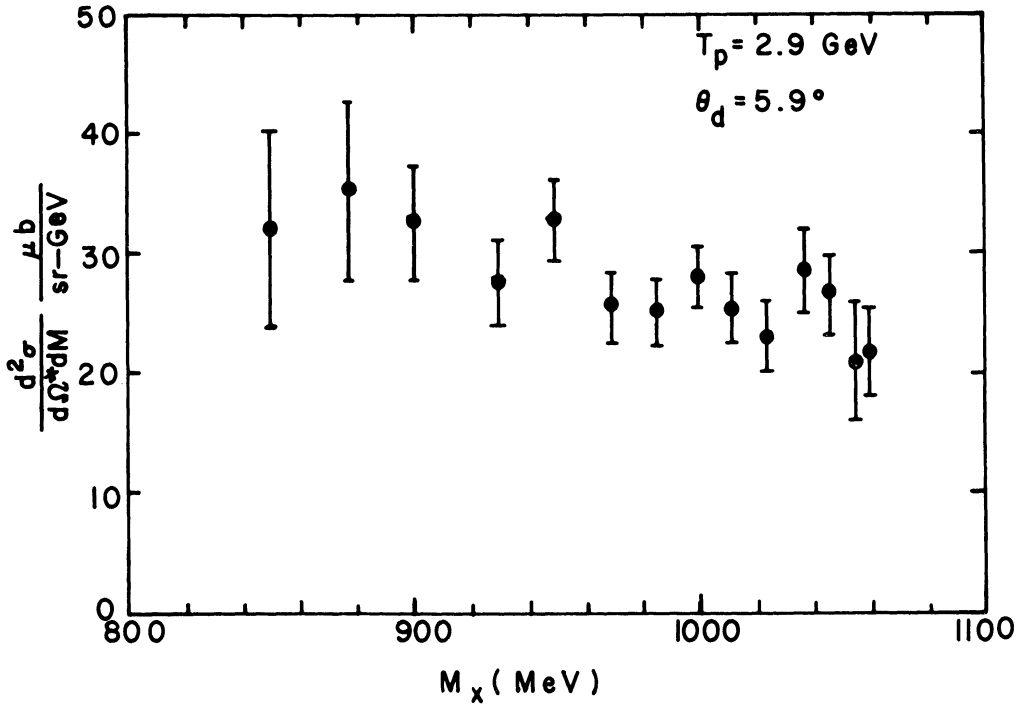
T_p = 2.9 GeV
θ_d = 5.9°
$\frac{d^2\sigma}{d\Omega^* dM}$ $\frac{\mu b}{sr-GeV}$
0
10
20
30
40
50
800
900
1000
1100
M_x (MeV)

Fig. 45

for deuteron production is plotted against this variable. The formation of a resonant state in the pion system would produce an enhancement in the cross section at a value of M_X corresponding to the mass of the resonance.

Statistical errors in the data from the first experimental run at 2.9 GeV are so large that detailed structure is obscured. Figs. 44 and 45 show the data from the second run at this energy, which was performed under improved beam conditions. The cross section was averaged in deuteron laboratory momentum steps of .02 GeV/c for Fig. 44. Fig. 45 shows the same data averaged in steps of .04 GeV/c.

CHAPTER V

CONCLUSIONS

A. General Features of the Cross Section

The laboratory angular distributions of the deuterons produced in proton-proton collisions from 1.5 to 3 GeV are peaked in the forward direction. No deuterons have angles greater than 23° relative to the beam direction due to the kinematics of the process. All deuterons are formed with large momenta (> 1.0 GeV/c).

The c.m. differential cross section distributions obtained at the three energies of this experiment show a general similarity to one another. The cross section is peaked in the forward and backward directions for large deuteron c.m. momenta. The maximum becomes more broad as the momentum decreases until the cross section is almost isotropic at small momenta. There is evidence of structure in the broad maximum at intermediate momenta.

The cross section at 1.55 GeV seems to possess a valley and second maximum at intermediate values of momentum. All the measurements in the valley come from the experimental run at a laboratory production angle of 5.9° with deuteron momenta greater than 1.7 GeV/c. The two neighboring peaks come from points taken at momenta less than this value. A systematic error resulting in a loss of counting efficiency

at high momenta could cause this effect. An argument against such an error is the fact that the cross sections agree within statistics in the neighborhood of the two points where measurements were made at both high and low momenta: ($p^*= .48$, $\cos\theta^*= -.87$) and ($p^*= .47$, $\cos\theta^*= -.45$). There is another possible source of error. The measurements in the valley come from data taken with $\cos\theta^*>0$ and reflected in the line $\cos\theta^*= 0$. The cross section need not be symmetric in this line if the proton beam were polarized. However, a recent polarization experiment[32] performed in Beam III of the Brookhaven cosmotron showed no evidence of this, and Beam II, where this experiment was performed, is very similar in all respects. Another possible interpretation of these data, which follows from neglecting the high momentum half of the 5.9° run, is that there is a broad maximum in the cross section extending from $\cos\theta^*= -1$ to $\cos\theta^*= -.5$ for c.m. momenta near .35 GeV/c.

The sharp peak at $\cos\theta^*= -1$ disappears for c.m. momenta less than .4 GeV/c. The cross section is almost isotropic for momenta less than .2 GeV/c. The peak seen in the fitting function (Fig. 31) between $\cos\theta^*= -.9$ and $\cos\theta^*= -1$ is of little significance since no data were taken in that region.

The 2.5 GeV data show evidence of suppression of deuteron production in the extreme backward direction for c.m. momenta between .4 and .6 GeV/c. Of course, the observed behavior of the cross section at 180° depends on the

normalization of the data of this experiment relative to that of Turkot et al. Errors in normalization arise from the various errors in the analysis technique summarized in Chapter III, Section J and indirectly from the error in the beam energy determination, which leads to errors in the Jacobians used to transform the cross section from the laboratory to c.m. system. The combination of these effects leads to an error of ± 15% in the absolute normalization of this experiment if we assume a 10% systematic error in the determination of the ϵ_i (see Chapter III, Section J). Since an error of 8% is quoted for the data of Turkot et al., the normalizations of the two experiments should agree to within ± 17%. The observed decrease in the cross section at 180° is typically 24%, and so appears to be significant.

No conclusions can be made concerning the detailed structure of the cross section at 2.9 GeV because the statistical errors are so large and because no measurements were made at $\cos\theta^* = -1$. The general trend of the data is similar to that observed at the other two energies.

The total deuteron production cross section seems to decrease monotonically with energy (see Fig. 36). A maximum appears in the cross section for multiple pion production near 2 GeV. A listing of the partial cross sections from this experiment, the experiment of Heinz et al.,[1,2] and various bubble chamber experiments is shown in Table VII. The data appear to be consistent except for the measurement of the cross section for the reaction $p + p \rightarrow d + \pi^+ + \pi^\circ$ at

TABLE VII

PARTIAL CROSS SECTIONS FOR DEUTERON PRODUCTION
IN PROTON-PROTON COLLISIONS FROM 1 TO 3 GeV

σ(partial), μb

Final State	Approximate Kinetic Energy: 1.0	1.5	2.0	2.5	2.9(GeV)
$d\pi^+$ (Refs.1,2)	452 ± 21	123 ± 27	53 ± 3	33 ± 3	30 ± 3
$d\pi^+\pi^o$	10 ± 10 (one event)	430 ± 80	126 ± 13		...
$d\pi^+\pi^+\pi^-$	0	...	68 ± 9		64 ± 20 (10 events)
$d\pi^+\pi^o\pi^o$	0	...	29 ± 6		...
$d\pi^+\pi^+\pi^-\pi^o$	0 (Refs.11,29)	... (Ref.3)	1 ± 1 (Ref.7)		... (Ref.5)
d, $\geq 2\pi$ (this experiment)	...	187 ± 24	...	126 ± 22	107 ± 21

1.48 GeV by Eisner et al.,[3] which is based on 26 events. It seems probable that the measurement is erroneous since the results of our experiment seem consistent with those of Turkot et al. at 1.55 GeV and the bubble chamber measurements at neighboring energies give relatively small values for this partial cross section. Perhaps some other final states containing one neutral and two charged particles, for example $pn\pi^+$ (of which 1048 were observed), or $pp\pi^\circ$ (of which 242 were observed) were mistaken for $d\pi^+\pi^\circ$.

It is interesting to note that the total multi-pion cross section deduced from the measurement at 0° of Turkot et al.[12] assuming an isotropic angular distribution would be 230 μb at 1.55 GeV, 150 μb at 1.93 GeV, 190 μb at 2.11 GeV, and 190 μb at 2.50 GeV. The values measured in this experiment are smaller at 1.55 and 2.5 GeV since the c.m. differential cross section is smaller on the average for nonzero production angles than for 0°. At 2 GeV, however, Sechi Zorn reports a total cross section of 224 ±18 μb, significantly larger than that obtained from the results of Turkot et al. If the measurements are correct, the differential cross section for deuteron production must be larger on the average for nonzero production angles at 2 GeV. Such behavior is seen, for example, in the reaction $p + p \rightarrow d + \pi^+$ at 1.5 GeV.[1,2]

B. Comparison with General Proton-Proton Inelastic Scattering

Bubble chamber experiments [4,5] studying proton-proton inelastic scattering in the energy range 2-3 GeV have reported

angular distributions of nucleons produced in final states containing two and three pions. It is interesting to compare them with the results of this experiment.

At 2 GeV,[4] the distributions of nucleons produced with two pions show sharp peaking in the forward and backward directions. For example, in the reaction $p + p \rightarrow p + n + \pi^+ + \pi^\circ$, approximately four times as many nucleons are formed with a c.m. angle whose cosine lies between .8 and 1.0 as between 0 and .2. In the final states containing three pions, the nucleons emerge almost isotropically. At 2.85 GeV,[5] the distributions of nucleons from both two and three pion final states are more sharply peaked forward and backward than they are at 2 GeV.

A similarity exists in the results from this experiment. Sharp peaking is observed in the c.m. differential cross section at large deuteron c.m. momenta where phase space arguments indicate that final states containing two pions are dominant. At lower momenta, as the final states containing three pions become increasingly important, the differential cross section becomes more nearly isotropic. But even at high momenta, the peaking does not appear to be as sharp as that observed in the distributions of unbound nucleons produced with two pions.

Triple pion final states play a more important role in deuteron production than in general proton-proton inelastic scattering. For example, at 2 GeV, the ratio of the number of $pn\pi^+\pi^\circ$ to $pn\pi^+\pi^+\pi^-$ final states is $\sim$10:1, whereas the

ratio of $d\pi^+\pi^\circ$ to $d\pi^+\pi^+\pi^-$ is only ~2:1.[7]

The experiments on proton-proton inelastic scattering gave no indication of structure, such as suppression of nucleon production in the extreme forward or backward direction, at either 2 or 2.85 GeV. The number of events in most of the angular distributions was small, however, and the data were averaged in intervals too broad to reveal fine details.

C. Comparison with Statistical Model

A prediction can be made on the basis of the statistical model for the ratio of the total deuteron production cross section to the total proton-proton inelastic cross section at a given energy. Hagedorn[17] has calculated this ratio for an incident proton kinetic energy of 2.3 GeV. If we take the total proton-proton inelastic cross section to be 27 mb[29] at this energy, the total deuteron production cross section should lie between 160 and 340 μb depending on the value chosen for Ω_d, the integral of the normalized deuteron wave function over the interaction volume. The interpolated value at 2.3 GeV from the data of Fig. 36 is 190 ± 30 μb, which is within the predicted range. A prediction was also made for the ratio of the cross section for the reaction $p + p \rightarrow d + \pi^+$ to the total proton-proton inelastic cross section. At 2.3 GeV, the cross section for the reaction should fall between 10 and 20 μb. The interpolated experimental value from Heinz *et al.*[1,2] is 40 ± 2 μb, in definite disagreement with the theory. It is encouraging, however, that the proper order of magnitude was

predicted for the cross section. No calculation was made for the deuteron momentum distribution at this energy.

D. Pion Resonances

A search for pion resonances of unit isotopic spin in the mass range 400 - 1000 MeV yielded evidence for ρ production. Upper limits were set for the production of the ζ(560) and X^+(960) in this reaction. The results are given in Table VIII.

The conclusions were drawn from the graphs of the differential cross section plotted against the invariant mass, M_X, of the system of pions formed with the deuteron (Figs. 37-45). Phase space distributions for $d\pi^+\pi^\circ$ and $d\pi^+\pi^+\pi^\circ$ final states are given in Fig. 46 for a beam energy of 2.5 GeV and in Fig. 47 for 1.55 GeV. A discussion of the results concerning each resonance follows.

1) The ρ

An enhancement centered at 760 MeV appears in the three spectra where that mass value was covered at 2.5 GeV (see Figs. 40-42). For example, in Fig. 41, the cross section is ≈36 μb/sr at M_X = 650 MeV and also in the neighborhood of 875 MeV, while between 700 and 800 MeV, the average is ≈40 μb/sr. The fact that the enhancement occurs in all spectra with a position and width consistent with the accepted values for the ρ meson led to the conclusion that the effect was caused by that particle. The spectrum of Fig. 42 is particularly convincing, since the background seems to be slowly

TABLE VIII

RESONANCE DATA

Resonance	Beam Energy GeV	Deuteron Production Angle (lab)	Approximate Mass Resolution	$\cos\theta^*$	$\frac{d\sigma}{d\Omega^*}$
$\rho(760)$	2.5	0°	20 MeV	-1.00	$.36 \pm .16 \frac{\mu b}{sr}$ †
$\rho(760)$	2.5	5.9	40	- .95	$.7 \pm .4$
$\rho(760)$	2.5	11.55	40	- .75	$.6 \pm .4$
$\zeta(560)$	1.55	0°	20	-1.00	$< .15$†
$\zeta(560)$	1.55	5.9	30	- .88	$< .3$
$\zeta(560)$	2.5	11.55	70	- .91	$< .5$
$\chi^+(960)$	2.9	5.9	50	- .9	$< .7$

† Deduced from the data of Turkot, et al.[12]

Fig. 46. Lorentz invariant momentum space distributions[33] for $d\pi^+\pi^\circ$ and $d\pi^+\pi^+\pi^-$ final states formed in proton-proton collisions at 2.5 GeV. The abcissa is the invariant mass of the pion system. The relative normalization of the two distributions is arbitrary. The $d\pi^+\pi^\circ\pi^\circ$ distribution differs only slightly from that of $d\pi^+\pi^+\pi^-$.

Fig. 47. Lorentz invariant momentum space distributions[33] for $d\pi^+\pi^\circ$ and $d\pi^+\pi^+\pi^-$ final states formed in proton-proton collisions at 1.55 GeV. The abcissa is the invariant mass of the pion system. The relative normalization of the two distributions is arbitrary. The $d\pi^+\pi^\circ\pi^\circ$ distribution differs only slightly from that of $d\pi^+\pi^+\pi^-$.

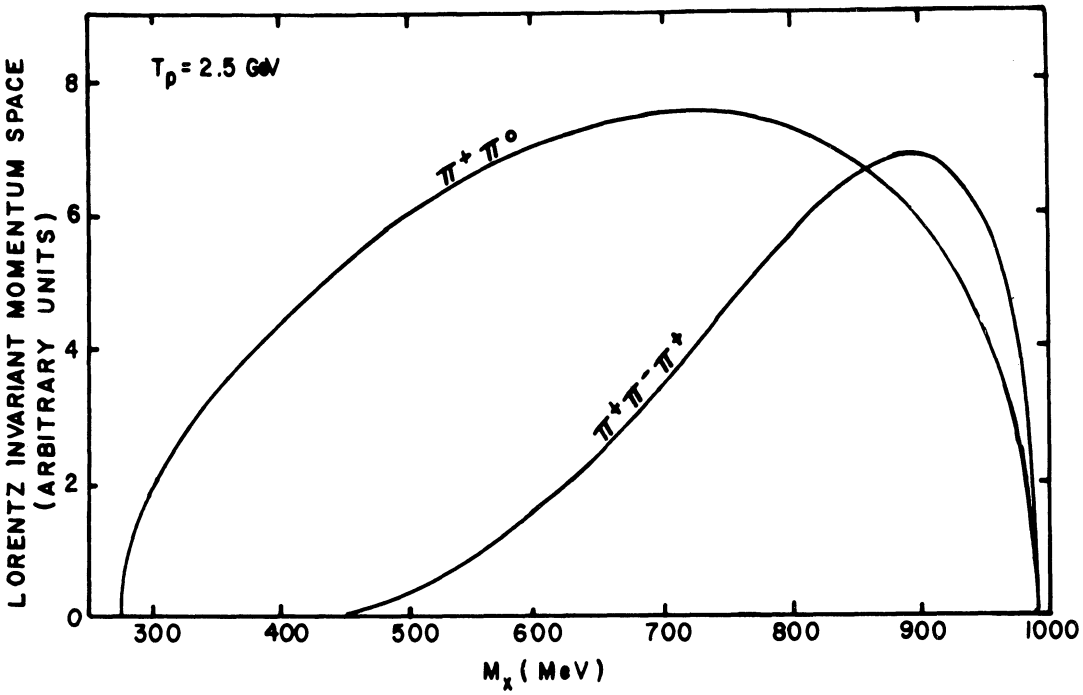
T_p = 2.5 GeV
$\pi^+\pi^0$
$\pi^+\pi^-\pi^+$
LORENTZ INVARIANT MOMENTUM SPACE (ARBITRARY UNITS)
0
2
4
6
8
300
400
500
600
700
800
900
1000
M_x (MeV)

Fig. 46

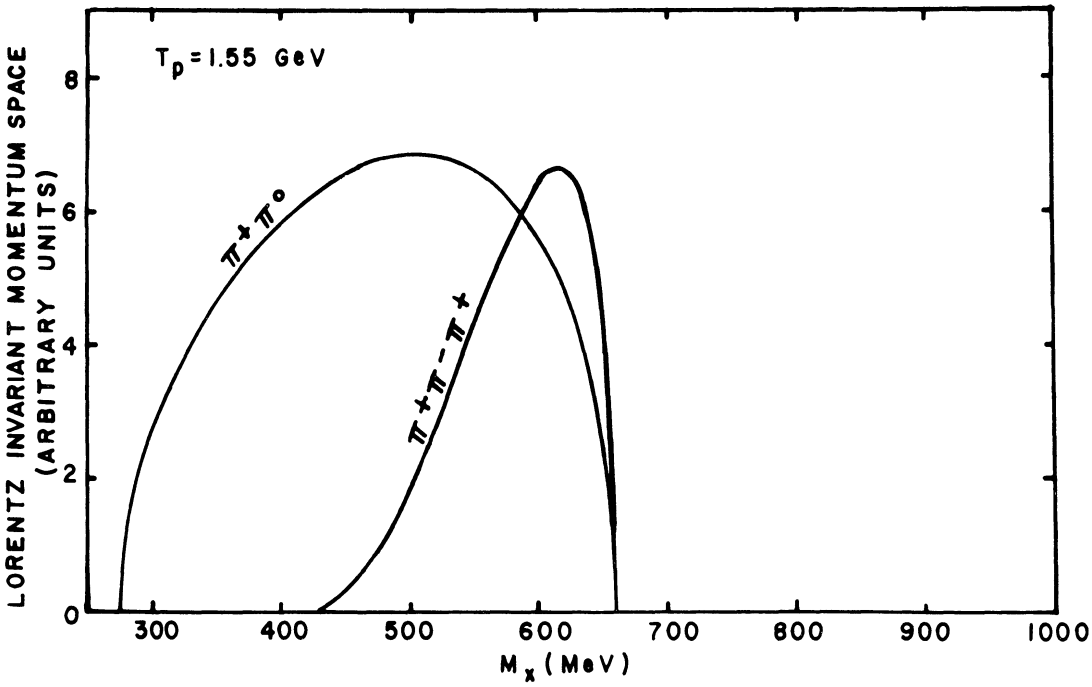
T_p = 1.55 GeV
$\pi^+\pi^0$
$\pi^+\pi^-\pi^+$
LORENTZ INVARIANT MOMENTUM SPACE (ARBITRARY UNITS)
0
2
4
6
8
300
400
500
600
700
800
900
1000
M_x (MeV)

Fig. 47

varying in the region of the ρ. The fact that the enhancement is so small is not unusual in proton-proton scattering. For example, Hart et al.[5] report no evidence of the ρ in 414 events of the type $p + p \rightarrow p + p + \pi^+ + \pi^-$ at 2.85 GeV.

The differential cross section for ρ production is difficult to determine from these spectra because the size and shape of the nonresonant background is unknown. Both two and three pion final states would be expected to contribute significantly to it at this energy. Also, the c.m. production angle varies with M_X in the spectra taken in this experiment, so the general angular dependence of the differential cross section will contribute to the variation. The resonance contribution was estimated by finding a function consisting of a Breit-Wigner distribution of 120 MeV width plus a smoothly varying background which was consistent with the data. The differential cross section for ρ production found in this manner was .7 ± .4 μb/sr at $\cos\theta^* = -.95$ and .6 ± .4 μb/sr at $\cos\theta^* = -.75$. The result at $\cos\theta^* = -1.0$ from Turkot et al.[12] was .36 ± .16 μb/sr. Although the errors are large, the data indicate that the differential cross section for the reaction $p + p \rightarrow d + \rho^+$ is not sharply peaked in the forward direction at 2.5 GeV.

No data were obtained with sufficiently small statistical errors in the region of the ρ to allow an estimate for the production cross section to be made at 2.9 GeV.

2) The ζ

The experiment of Sechi Zorn[6,7] at 2.05 GeV showed evidence for the reaction $p + p \rightarrow d + \zeta^+$, where ζ is a narrow two pion resonance with isotopic spin equal to one and a mass of 560 MeV. (see Chapter I, Section B). The total cross section, based on 10 events, was 8 ± 3 μb. Subsequently, Turkot *et al.*[13] found no convincing evidence for ζ production in spectra of deuterons produced at 0° in proton-proton collisions at 1.55, 1.93, 2.11, and 2.50 GeV, although total cross sections ~ 1 μb could not be excluded.

Some reactions[2] involving deuterons seem to be suppressed at 0° in this energy range, so it was of interest to search for the ζ at nonzero production angles, as was done in this experiment. No evidence for ζ formation was seen. Upper bounds on the total cross section at a 90% level of confidence are 4 μb at 1.55 GeV and 6 μb at 2.5 GeV if we assume the particles are produced isotropically.

3) The X^+

A neutral $\eta\pi\pi$ resonance of narrow width has been seen at a mass of 960 MeV.[34] It is called the X°, and is generally believed to have isotopic spin zero, although its quantum numbers have not been determined conclusively, and an assignment with an isotopic spin of one is possible. For this reason, we decided to look for a charged particle with a mass near 960 MeV. A special run at 2.9 GeV with improved statistics was made in the mass region 900-1000 MeV. The results (Figs. 44 and 45) show a small peak at a mass of 940 MeV, but it is not statistically significant. An upper

limit at a 90% level of confidence for the production of the hypothetical X^+ is .7 μb/sr.

A recent experiment of Kienzle et al.[35] reports evidence of the formation of a narrow multipion resonance with a mass of 962 ± 5 MeV and an isotopic spin of one or two. The particle, X^-, was produced in pion-proton collisions with incident pion momenta in the range 3-5 GeV/c. The total production cross section was very small: 15 ± 5 μb. Since the ρ, which is produced with a large cross section in pion-proton collisions,[36] is barely seen in our experiment, the fact that we do not observe an X^+ does not indicate disagreement with the experiment of Kienzle et al.

E. Comparison with Deuteron Production in Proton-Nucleus Collisions

Deuteron production by 2.9 GeV protons incident on beryllium and platinum has been studied in a recent experiment by Piroué and Smith.[15] The deuteron yield was measured as a function of momentum at angles of 13°, 30°, 60°, and 93° with respect to the beam direction in the laboratory. The results at 13° for beryllium are compared with those from this experiment at 11.55° and 2.9 GeV in Table IX.

The elementary interaction may make an important contribution to high momentum (>2 GeV/c) deuteron emission. Here, the differential cross section for deuteron production in proton-proton collisions at 11.55° approaches that observed per nucleon in the 13° proton-beryllium data. Also, the high momentum deuteron yield from proton-nucleus

TABLE IX

COMPARISON OF MOMENTUM DISTRIBUTIONS OF DEUTERONS PRODUCED IN PROTON - PROTON AND PROTON - NUCLEUS COLLISIONS

Deuteron Laboratory Momentum (GeV/c)	$\frac{d^2\sigma}{d\Omega\, dp}\left[\frac{mb}{sr\ GeV/c}\right]$	
	p - p [a]	p - Be^9 (per nucleon) [b]
.7	0	.29
1.0	0	.47
1.5	.06 ± .02	.38
1.7	.15 ± .05	.32
2.0	.15 ± .04	.27
2.1	.23 ± .04	.23
2.2	.18 ± .06	.19[c]
2.3	.21 ± .06	...
2.4	.22 ± .07	...

[a] Data from this experiment at 2.9 GeV, 11.55°

[b] Approximate values from Piroué and Smith[15] at 2.9 GeV, 13°. The values shown are 1/9 x the Be^9 cross sections.

[c] Extrapolated value.

collisions falls off rapidly with increasing angle, as is observed for proton-proton collisions. The low momentum deuterons from proton-nucleon collisions do not display this marked an angular dependence.

The most striking feature of the data of Piroué and Smith is the large number of deuterons produced at momenta too low or angles too great to be kinematically allowed in elementary proton-proton collisions. Moreover, the total deuteron production cross section per nucleon in proton-beryllium collisions was found to be $\sim$1 mb, compared with .14 mb in proton-proton collisions at 2.9 GeV (see Fig. 36). The dominant role in deuteron emission from proton-nucleus reactions must therefore be played by specifically nuclear processes.

APPENDIX I

BEAM MONITOR CALIBRATION

The beam monitor telescopes (see p. 19) recorded a number of counts proportional to the total number of protons passing through the target in each experimental run. The radioactive foil technique was used to determine the constant of proportionality between the number of monitor counts and the actual proton flux.

At some point during the series of experimental runs at each energy, a thin polyethylene foil 10 cm square was exposed in the beam for one minute at a flux of $2\text{-}5 \times 10^9$ protons per burst. The radioactive isotope C^{11} was produced in the foil through the reaction $C^{12}(p,pn)C^{11}$. C^{11} decays through positron emission with a half-life of 20.5 min. The number of C^{11} nuclei produced by the beam was determined by measuring the activity of the foil at a known time after the activation. Since the cross section for the reaction $C^{12}(p,pn)C^{11}$ is known,[37] the number of protons which passed through the foil could be determined. The ratio of the proton flux to the number of counts recorded by the beam monitors during the foil activation was then calculated and used to determine the absolute proton flux in the experimental runs at the same beam energy.

The following formula was used to determine the proton flux, F, by the radioactive foil technique:

$$F = \frac{10^{30}\, M}{\mathcal{N}_o\,(1-\eta)\,\sigma(E)\,s\,\epsilon}\;\frac{t_o}{1-e^{-\lambda t_o}}\;\frac{dN}{dt}\Big|_{t=t_o}$$

where M = gram molecular weight of the foil (14.03 gm for polyethylene)

$\mathcal{N}_o$ = Avogadro's number (6.02×10^{23})

$\sigma(E)$ = cross section for $C^{12}(p,pn)C^{11}$ at the energy of the activation ($\approx$ 26 mb in the energy range 1-3 GeV [37])

s = thickness of the foil in mg/cm^2 determined by carefully measuring the area and mass of the individual foils (typically 9 mg/cm^2)

ϵ = fractional efficiency of the NaI well counter used in measuring the activation of the foil (.90)

t_o = time at the end of the activation period (in minutes; t = 0 at the beginning of the activation)

$\frac{dN}{dt}$ = C^{11} decay rate in counts per minute

λ = decay constant for C^{11} (3.39×10^{-2} min^{-1})

η = fraction of C^{11} atoms lost due to formation with sufficient kinetic energy to escape from the foil (.142 for a polyethylene foil of thickness .004 in.[38]).

The decay rate at $t = t_o$ was given by

$$\frac{dN}{dt}\Big|_{t=t_o} = \frac{\lambda\, N_c\, e^{\lambda(t_1-t_o)}}{1-e^{-\lambda(t_2-t_1)}}$$

where t_1 = time at beginning of counting period to determine the C^{11} activity (t = 0 at the beginning of the foil activation)

t_2 = time at end of counting period

N_C = number of counts (background subtracted).

$t_2 - t_1$ was typically 10 min.

The derivation of the formula for F is described in detail in references 2 and 39. Analysis of the errors involved shows that the flux is determined to an accuracy of ±8% in this manner.[2]

APPENDIX II

TABLES AND GRAPHS OF THE DIFFERENTIAL CROSS SECTION

In the tables that follow (Tables X-XX), differential cross section distributions for deuteron production in proton-proton collisions are given for all incident proton kinetic energies and deuteron laboratory production angles covered in this experiment. The symbols used have the following meanings:

p = deuteron laboratory momentum

p^* = deuteron c.m. momentum

M_X = invariant mass of the system of particles produced with the deuteron

$\cos\theta^*$ = cosine of the deuteron c.m. production angle

$\frac{d^2\sigma}{d\Omega\, dp}$ = differential cross section for deuteron production in the laboratory system

$\frac{d^2\sigma}{d\Omega^* dp^*}$ = differential cross section for deuteron production in the c.m. system

$\frac{d^2\sigma}{d\Omega^* dM}$ = spectrum of differential cross section vs. M_X.

The power of ten multiplying the values listed for the differential cross sections are given following the E. That is, .327E-02 means .327 x 10^{-2}.

Graphs of the differential cross section in the c.m. are given in Figs. 48-64 for incident proton kinetic energies of 2.5 and 2.9 GeV. The graphs at 1.55 GeV are given in Chapter IV, Section B. In the captions of these figures,

T_p is the incident proton kinetic energy and θ_d is the deuteron laboratory production angle.

TABLE X

DIFFERENTIAL CROSS SECTIONS AT 1.55 GeV, 5.9°

p	$\frac{d^2\sigma}{d\Omega\, dp}$		p*	$\frac{d^2\sigma}{d\Omega^* dp^*}$		M_x	$\frac{d^2\sigma}{d\Omega^* dM}$		cosθ*
GeV/c	mb/(sr GeV/c)		GeV/c	mb/(sr GeV/c)		GeV	mb/(sr GeV)		
1.084	.151E 00	± .550E-01	.524	.392E-01	± .143E-01	.268	.154E-01	± .561E-02	-.9771
1.123	.171E 00	.385E-01	.491	.367E-01	.827E-02	.340	.194E-01	.438E-02	-.9719
1.172	.271E 00	.381E-01	.451	.461E-01	.647E-02	.406	.315E-01	.443E-02	-.9636
1.215	.522E 00	.352E-01	.417	.714E-01	.483E-02	.451	.586E-01	.396E-02	-.9541
1.269	.693E 00	.364E-01	.376	.721E-01	.378E-02	.496	.718E-01	.377E-02	-.9380
1.316	.784E 00	.385E-01	.341	.632E-01	.310E-02	.529	.737E-01	.362E-02	-.9179
1.371	.925E 00	.391E-01	.303	.553E-01	.234E-02	.559	.764E-01	.323E-02	-.8855
1.420	.954E 00	.378E-01	.272	.434E-01	.172E-02	.580	.692E-01	.274E-02	-.8434
1.472	.111E 01	.510E-01	.242	.377E-01	.173E-02	.598	.695E-01	.320E-02	-.7802
1.517	.121E 01	.692E-01	.218	.320E-01	.183E-02	.609	.666E-01	.381E-02	-.7001
1.568	.139E 01	.951E-01	.197	.286E-01	.195E-02	.619	.666E-01	.455E-02	-.5771
1.621	.148E 01	.880E-01	.182	.246E-01	.146E-02	.625	.627E-01	.373E-02	-.4058
1.672	.154E 01	.114E 00	.176	.226E-01	.167E-02	.628	.601E-01	.444E-02	-.2061
1.719	.176E 01	.108E 00	.177	.252E-01	.154E-02	.627	.664E-01	.406E-02	-.0073
1.772	.176E 01	.105E 00	.186	.265E-01	.158E-02	.624	.660E-01	.393E-02	.1992
1.825	.150E 01	.943E-01	.202	.256E-01	.160E-02	.617	.581E-01	.364E-02	.3709
1.867	.151E 01	.925E-01	.219	.289E-01	.178E-02	.609	.601E-01	.369E-02	.4786
1.919	.149E 01	.756E-01	.242	.336E-01	.171E-02	.597	.618E-01	.314E-02	.5802
1.968	.138E 01	.625E-01	.267	.364E-01	.165E-02	.583	.594E-01	.269E-02	.6525
2.022	.127E 01	.736E-01	.296	.395E-01	.230E-02	.564	.562E-01	.327E-02	.7127
2.063	.118E 01	.879E-01	.320	.414E-01	.309E-02	.546	.531E-01	.397E-02	.7482
2.114	.111E 01	.841E-01	.349	.449E-01	.339E-02	.522	.506E-01	.382E-02	.7826
2.172	.957E 00	.749E-01	.383	.447E-01	.350E-02	.489	.430E-01	.337E-02	.8129
2.220	.853E 00	.888E-01	.412	.444E-01	.462E-02	.458	.374E-01	.389E-02	.8323
2.270	.602E 00	.576E-01	.442	.348E-01	.333E-02	.419	.251E-01	.240E-02	.8490
2.317	.633E 00	.928E-01	.470	.402E-01	.589E-02	.376	.245E-01	.359E-02	.8621
2.367	.665E 00	.824E-01	.500	.462E-01	.572E-02	.321	.227E-01	.281E-02	.8737
2.410	.967E 00	.179E 00	.526	.722E-01	.134E-01	.262	.277E-01	.513E-02	.8821

TABLE XI

DIFFERENTIAL CROSS SECTIONS AT 1.55 GeV, 11.55°

p	$\frac{d^2\sigma}{d\Omega\, dp}$		p*	$\frac{d^2\sigma}{d\Omega^* dp^*}$		M_x	$\frac{d^2\sigma}{d\Omega^* dM}$		cosθ*
GeV/c	mb/(sr GeV/c)		GeV/c	mb/(sr GeV/c)		GeV	mb/(sr GeV)		
1.090	.226E 00 ±	.507E-01	.572	.689E-01 ±	.154E-01	.060	.564E-02 ±	.126E-02	-.9243
1.100	.858E 00	.117E 00	.565	.251E 00	.342E-01	.119	.410E-01	.559E-02	-.9208
1.110	.139E 01	.165E 00	.557	.391E 00	.464E-01	.157	.849E-01	.101E-01	-.9171
1.120	.116E 01	.123E 00	.550	.312E 00	.332E-01	.186	.815E-01	.868E-02	-.9132
1.130	.106E 01	.109E 00	.543	.274E 00	.281E-01	.211	.820E-01	.843E-02	-.9092
1.140	.505E 00	.514E-01	.536	.126E 00	.128E-01	.233	.421E-01	.429E-02	-.9050
1.156	.141E 00	.320E-01	.526	.330E-01	.750E-02	.263	.127E-01	.288E-02	-.8979
1.176	.951E-01	.253E-01	.512	.205E-01	.545E-02	.296	.909E-02	.242E-02	-.8880
1.196	.122E 00	.195E-01	.500	.244E-01	.390E-02	.323	.120E-01	.193E-02	-.8778
1.214	.201E 00	.294E-01	.488	.374E-01	.547E-02	.345	.202E-01	.296E-02	-.8670
1.231	.256E 00	.447E-01	.477	.445E-01	.779E-02	.364	.259E-01	.453E-02	-.8563
1.255	.268E 00	.332E-01	.463	.427E-01	.529E-02	.387	.272E-01	.336E-02	-.8402
1.275	.282E 00	.326E-01	.452	.417E-01	.481E-02	.404	.284E-01	.328E-02	-.8253
1.295	.375E 00	.365E-01	.441	.515E-01	.501E-02	.420	.372E-01	.362E-02	-.8090
1.313	.444E 00	.467E-01	.432	.570E-01	.600E-02	.433	.434E-01	.456E-02	-.7929
1.340	.551E 00	.853E-01	.418	.644E-01	.996E-02	.450	.525E-01	.812E-02	-.7671
1.356	.490E 00	.529E-01	.411	.543E-01	.586E-02	.458	.459E-01	.495E-02	-.7508
1.373	.555E 00	.560E-01	.403	.579E-01	.585E-02	.468	.508E-01	.513E-02	-.7311
1.393	.654E 00	.606E-01	.395	.640E-01	.592E-02	.477	.584E-01	.541E-02	-.7075
1.413	.698E 00	.607E-01	.386	.640E-01	.556E-02	.486	.608E-01	.528E-02	-.6810
1.436	.705E 00	.625E-01	.378	.603E-01	.535E-02	.494	.595E-01	.528E-02	-.6493
1.474	.699E 00	.454E-01	.366	.539E-01	.350E-02	.506	.562E-01	.365E-02	-.5923
1.519	.803E 00	.535E-01	.355	.553E-01	.369E-02	.517	.607E-01	.405E-02	-.5141
1.571	.783E 00	.477E-01	.346	.486E-01	.296E-02	.525	.555E-01	.338E-02	-.4154
1.618	.762E 00	.581E-01	.342	.442E-01	.337E-02	.528	.513E-01	.392E-02	-.3183
1.669	.773E 00	.458E-01	.342	.427E-01	.253E-02	.528	.496E-01	.294E-02	-.2104
1.721	.748E 00	.547E-01	.346	.404E-01	.296E-02	.524	.460E-01	.337E-02	-.1019
1.769	.690E 00	.454E-01	.354	.374E-01	.246E-02	.517	.411E-01	.270E-02	-.0041
1.823	.647E 00	.432E-01	.367	.358E-01	.239E-02	.506	.372E-01	.249E-02	.0987
1.875	.669E 00	.462E-01	.382	.385E-01	.266E-02	.490	.373E-01	.258E-02	.1887
1.917	.650E 00	.514E-01	.397	.390E-01	.308E-02	.475	.352E-01	.279E-02	.2535
1.973	.573E 00	.324E-01	.419	.365E-01	.207E-02	.449	.297E-01	.168E-02	.3301
2.027	.555E 00	.383E-01	.442	.378E-01	.260E-02	.419	.272E-01	.188E-02	.3940
2.073	.493E 00	.402E-01	.462	.355E-01	.289E-02	.389	.227E-01	.185E-02	.4403
2.117	.377E 00	.330E-01	.483	.287E-01	.251E-02	.354	.160E-01	.141E-02	.4803
2.170	.396E 00	.293E-01	.510	.322E-01	.239E-02	.302	.146E-01	.108E-02	.5225
2.211	.462E 00	.467E-01	.530	.395E-01	.400E-02	.251	.144E-01	.146E-02	.5506
2.263	.559E 00	.542E-01	.558	.510E-01	.494E-02	.155	.110E-01	.106E-02	.5829

TABLE XII

DIFFERENTIAL CROSS SECTIONS AT 1.55 GeV, 15.72°

p	$\frac{d^2\sigma}{d\Omega\, dp}$		p*	$\frac{d^2\sigma}{d\Omega^* dp^*}$		M_x	$\frac{d^2\sigma}{d\Omega^* dM}$		cosθ*
GeV/c	mb/(sr GeV/c)		GeV/c	mb/(sr GeV/c)		GeV	mb/(sr GeV)		
1.210	.155E 01	± .213E 00	.560	.379E 00	± .522E-01	.142	.741E-01	± .102E-01	-.8111
1.220	.184E 01	.233E 00	.556	.438E 00	.553E-01	.165	.100E 00	.127E-01	-.8038
1.230	.156E 01	.198E 00	.551	.359E 00	.454E-01	.185	.928E-01	.118E-01	-.7962
1.240	.106E 01	.145E 00	.546	.238E 00	.325E-01	.202	.677E-01	.925E-02	-.7883
1.250	.530E 00	.940E-01	.541	.115E 00	.204E-01	.217	.355E-01	.630E-02	-.7803
1.260	.286E 00	.660E-01	.537	.601E-01	.139E-01	.231	.199E-01	.460E-02	-.7720
1.270	.150E 00	.504E-01	.533	.306E-01	.103E-01	.244	.108E-01	.363E-02	-.7634
1.280	.134E 00	.558E-01	.528	.266E-01	.111E-01	.256	.989E-02	.412E-02	-.7545
1.307	.413E-01	.306E-01	.518	.762E-02	.564E-02	.283	.319E-02	.236E-02	-.7298
1.325	.644E-01	.270E-01	.511	.113E-01	.475E-02	.299	.507E-02	.213E-02	-.7112
1.346	.355E-01	.391E-01	.503	.591E-02	.650E-02	.315	.283E-02	.311E-02	-.6892
1.364	.112E 00	.304E-01	.498	.178E-01	.484E-02	.326	.892E-02	.243E-02	-.6703
1.390	.235E 00	.522E-01	.490	.352E-01	.781E-02	.341	.187E-01	.416E-02	-.6399
1.405	.121E 00	.305E-01	.486	.176E-01	.442E-02	.349	.964E-02	.242E-02	-.6219
1.425	.297E 00	.344E-01	.481	.413E-01	.477E-02	.357	.234E-01	.270E-02	-.5973
1.446	.280E 00	.380E-01	.477	.373E-01	.505E-02	.365	.218E-01	.295E-02	-.5700
1.460	.288E 00	.424E-01	.474	.373E-01	.548E-02	.370	.222E-01	.326E-02	-.5508
1.484	.250E 00	.347E-01	.470	.310E-01	.431E-02	.376	.189E-01	.263E-02	-.5183
1.523	.313E 00	.199E-01	.465	.365E-01	.232E-02	.384	.230E-01	.146E-02	-.4612
1.573	.302E 00	.217E-01	.462	.330E-01	.237E-02	.389	.212E-01	.152E-02	-.3859
1.618	.273E 00	.208E-01	.462	.286E-01	.217E-02	.389	.183E-01	.139E-02	-.3173
1.668	.251E 00	.204E-01	.465	.254E-01	.206E-02	.384	.160E-01	.129E-02	-.2401
1.718	.155E 00	.169E-01	.472	.154E-01	.167E-02	.373	.927E-02	.101E-02	-.1630
1.772	.203E 00	.237E-01	.482	.200E-01	.233E-02	.356	.113E-01	.132E-02	-.0836
1.821	.158E 00	.186E-01	.493	.156E-01	.184E-02	.335	.811E-02	.956E-03	-.0152
1.872	.117E 00	.179E-01	.508	.118E-01	.180E-02	.305	.541E-02	.828E-03	.0530
1.910	.890E-01	.207E-01	.520	.907E-02	.211E-02	.277	.371E-02	.863E-03	.0991
1.930	.116E 00	.239E-01	.527	.120E-01	.246E-02	.260	.455E-02	.931E-03	.1225
1.950	.144E 00	.315E-01	.534	.150E-01	.328E-02	.240	.520E-02	.114E-02	.1452
1.966	.159E 00	.212E-01	.540	.167E-01	.223E-02	.223	.532E-02	.708E-03	.1623
1.990	.241E 00	.447E-01	.549	.257E-01	.476E-02	.192	.692E-02	.128E-02	.1880
2.000	.274E 00	.408E-01	.553	.294E-01	.437E-02	.177	.723E-02	.108E-02	.1983
2.020	.332E 00	.351E-01	.561	.360E-01	.381E-02	.140	.696E-02	.735E-03	.2181
2.050	.483E 00	.456E-01	.573	.534E-01	.505E-02	.040	.291E-02	.274E-03	.2465

TABLE XIII

DIFFERENTIAL CROSS SECTIONS AT 2.5 GeV, 5.9°

p	$\frac{d^2\sigma}{d\Omega\ dp}$	p*	$\frac{d^2\sigma}{d\Omega^* dp^*}$	M_x	$\frac{d^2\sigma}{d\Omega^* dM}$	cosθ*
GeV/c	mb/(sr GeV/c)	GeV/c	mb/(sr GeV/c)	GeV	mb/(sr GeV)	
1.145	.336E 00 ± .810E-01	.806	.179E 00 ± .432E-01	.173	.274E-01 ± .661E-02	-.9893
1.165	.605E 00 .935E-01	.788	.300E 00 .464E-01	.266	.719E-01 .111E-01	-.9884
1.186	.211E 00 .411E-01	.770	.975E-01 .190E-01	.332	.297E-01 .579E-02	-.9874
1.204	.887E-01 .330E-01	.754	.384E-01 .143E-01	.380	.136E-01 .508E-02	-.9864
1.225	.384E-01 .353E-01	.736	.154E-01 .141E-01	.428	.629E-02 .578E-02	-.9853
1.244	.154E 00 .417E-01	.720	.578E-01 .156E-01	.465	.262E-01 .708E-02	-.9841
1.265	.874E-01 .319E-01	.702	.304E-01 .111E-01	.502	.152E-01 .555E-02	-.9827
1.284	.568E-01 .363E-01	.686	.185E-01 .118E-01	.532	1.000E-02 .638E-02	-.9813
1.317	.110E 00 .230E-01	.659	.317E-01 .664E-02	.580	.193E-01 .405E-02	-.9787
1.370	.198E 00 .243E-01	.616	.471E-01 .578E-02	.644	.340E-01 .416E-02	-.9735
1.420	.242E 00 .220E-01	.577	.479E-01 .436E-02	.695	.395E-01 .360E-02	-.9675
1.470	.246E 00 .238E-01	.539	.403E-01 .390E-02	.739	.376E-01 .364E-02	-.9599
1.521	.294E 00 .249E-01	.501	.397E-01 .336E-02	.776	.416E-01 .353E-02	-.9501
1.569	.304E 00 .265E-01	.468	.342E-01 .298E-02	.807	.398E-01 .347E-02	-.9387
1.618	.266E 00 .235E-01	.434	.246E-01 .218E-02	.835	.318E-01 .281E-02	-.9236
1.667	.357E 00 .274E-01	.402	.272E-01 .209E-02	.858	.388E-01 .298E-02	-.9048
1.718	.340E 00 .314E-01	.371	.211E-01 .194E-02	.879	.333E-01 .308E-02	-.8791
1.768	.407E 00 .421E-01	.342	.205E-01 .213E-02	.896	.359E-01 .371E-02	-.8469
1.816	.468E 00 .573E-01	.316	.194E-01 .238E-02	.911	.372E-01 .455E-02	-.8065
1.869	.393E 00 .550E-01	.290	.132E-01 .184E-02	.924	.278E-01 .389E-02	-.7483
1.921	.468E 00 .684E-01	.267	.129E-01 .188E-02	.934	.297E-01 .433E-02	-.6743
1.969	.496E 00 .562E-01	.250	.115E-01 .131E-02	.941	.286E-01 .324E-02	-.5892
2.018	.526E 00 .643E-01	.237	.106E-01 .129E-02	.946	.279E-01 .340E-02	-.4841
2.066	.533E 00 .592E-01	.228	.957E-02 .106E-02	.949	.263E-01 .292E-02	-.3604
2.119	.537E 00 .746E-01	.223	.891E-02 .124E-02	.951	.251E-01 .348E-02	-.2132
2.174	.585E 00 .628E-01	.224	.941E-02 .101E-02	.951	.264E-01 .283E-02	-.0526
2.223	.554E 00 .796E-01	.229	.908E-02 .130E-02	.949	.248E-01 .356E-02	.0862
2.270	.472E 00 .628E-01	.238	.812E-02 .108E-02	.945	.212E-01 .282E-02	.2072
2.317	.508E 00 .817E-01	.251	.937E-02 .151E-02	.941	.232E-01 .373E-02	.3141
2.368	.532E 00 .636E-01	.267	.108E-01 .129E-02	.934	.249E-01 .298E-02	.4142
2.420	.870E 00 .148E 00	.287	.197E-01 .336E-02	.925	.421E-01 .717E-02	.4964
2.461	.354E 00 .911E-01	.303	.875E-02 .225E-02	.917	.175E-01 .452E-02	.5514

TABLE XIV

DIFFERENTIAL CROSS SECTIONS AT 2.5 GeV, 11.55°

p	$\frac{d^2\sigma}{d\Omega\, dp}$	p*	$\frac{d^2\sigma}{d\Omega^* dp^*}$	M_x	$\frac{d^2\sigma}{d\Omega^* dM}$	cosθ*
GeV/c	mb/(sr GeV/c)	GeV/c	mb/(sr GeV/c)	GeV	mb/(sr GeV)	
1.210	.399E 00 ± .121E 00	.803	.193E 00 ± .581E-01	.190	.325E-01 ± .981E-02	-.9534
1.226	.263E 00 .575E-01	.791	.120E 00 .263E-01	.253	.274E-01 .599E-02	-.9506
1.245	.855E-01 .417E-01	.777	.369E-01 .180E-01	.309	.104E-01 .507E-02	-.9471
1.266	.140E 00 .318E-01	.761	.567E-01 .129E-01	.359	.189E-01 .428E-02	-.9430
1.288	.405E-01 .323E-01	.745	.153E-01 .122E-01	.403	.583E-02 .464E-02	-.9383
1.306	.557E-01 .244E-01	.732	.199E-01 .870E-02	.437	.833E-02 .365E-02	-.9340
1.324	.491E-01 .218E-01	.719	.166E-01 .736E-02	.466	.751E-02 .334E-02	-.9296
1.346	.665E-01 .231E-01	.704	.210E-01 .728E-02	.498	.104E-01 .360E-02	-.9238
1.365	.859E-01 .193E-01	.691	.256E-01 .575E-02	.523	.135E-01 .304E-02	-.9185
1.388	.771E-01 .219E-01	.676	.214E-01 .610E-02	.551	.121E-01 .345E-02	-.9117
1.406	.908E-01 .183E-01	.665	.239E-01 .482E-02	.571	.143E-01 .287E-02	-.9059
1.425	.665E-01 .173E-01	.652	.165E-01 .430E-02	.590	.104E-01 .270E-02	-.8993
1.461	.124E 00 .134E-01	.630	.278E-01 .300E-02	.624	.190E-01 .205E-02	-.8857
1.509	.136E 00 .160E-01	.602	.264E-01 .312E-02	.663	.200E-01 .236E-02	-.8650
1.557	.156E 00 .158E-01	.576	.265E-01 .270E-02	.696	.219E-01 .223E-02	-.8409
1.609	.196E 00 .141E-01	.549	.290E-01 .208E-02	.727	.261E-01 .188E-02	-.8101
1.660	.240E 00 .127E-01	.526	.310E-01 .164E-02	.752	.301E-01 .159E-02	-.7749
1.710	.252E 00 .139E-01	.505	.287E-01 .159E-02	.773	.298E-01 .165E-02	-.7349
1.757	.260E 00 .138E-01	.487	.265E-01 .141E-02	.790	.290E-01 .154E-02	-.6921
1.809	.263E 00 .143E-01	.471	.240E-01 .131E-02	.804	.276E-01 .151E-02	-.6395
1.859	.268E 00 .174E-01	.458	.222E-01 .144E-02	.815	.266E-01 .173E-02	-.5822
1.906	.243E 00 .247E-01	.448	.186E-01 .189E-02	.823	.230E-01 .234E-02	-.5233
1.959	.264E 00 .236E-01	.440	.187E-01 .168E-02	.830	.237E-01 .213E-02	-.4522
2.008	.314E 00 .287E-01	.435	.210E-01 .192E-02	.833	.271E-01 .247E-02	-.3829
2.059	.237E 00 .253E-01	.433	.152E-01 .162E-02	.835	.196E-01 .210E-02	-.3097
2.106	.321E 00 .316E-01	.434	.200E-01 .197E-02	.834	.258E-01 .254E-02	-.2394
2.159	.291E 00 .269E-01	.438	.178E-01 .165E-02	.831	.227E-01 .210E-02	-.1618
2.203	.309E 00 .320E-01	.443	.188E-01 .195E-02	.827	.236E-01 .244E-02	-.0976
2.257	.295E 00 .261E-01	.452	.180E-01 .159E-02	.820	.220E-01 .195E-02	-.0225
2.303	.289E 00 .294E-01	.461	.179E-01 .182E-02	.812	.212E-01 .216E-02	.0383
2.356	.281E 00 .264E-01	.474	.178E-01 .167E-02	.801	.203E-01 .190E-02	.1036
2.405	.234E 00 .310E-01	.488	.151E-01 .201E-02	.789	.166E-01 .219E-02	.1607
2.459	.258E 00 .353E-01	.504	.173E-01 .237E-02	.774	.180E-01 .246E-02	.2173

TABLE XV

DIFFERENTIAL CROSS SECTIONS AT 2.5 GeV, 15.72°

p	$\frac{d^2\sigma}{d\Omega\, dp}$		p*	$\frac{d^2\sigma}{d\Omega^* dp^*}$		M_x	$\frac{d^2\sigma}{d\Omega^* dM}$		cosθ*
GeV/c	mb/(sr GeV/c)		GeV/c	mb/(sr GeV/c)		GeV	mb/(sr GeV)		
1.310	.297E 00	± .652E-01	.798	.124E 00	± .272E-01	.218	.241E-01	± .529E-02	-.8957
1.326	.107E 00	.306E-01	.788	.426E-01	.122E-01	.264	.101E-01	.290E-02	-.8900
1.350	.245E-01	.364E-01	.775	.917E-02	.137E-01	.316	.265E-02	.395E-02	-.8815
1.365	.421E-01	.186E-01	.766	.152E-01	.670E-02	.344	.482E-02	.213E-02	-.8757
1.387	.157E-01	.199E-01	.754	.536E-02	.680E-02	.380	.191E-02	.242E-02	-.8669
1.421	.663E-01	.942E-02	.736	.208E-01	.295E-02	.427	.848E-02	.120E-02	-.8523
1.471	.777E-01	.102E-01	.711	.216E-01	.283E-02	.484	.103E-01	.134E-02	-.8282
1.523	.886E-01	.955E-02	.687	.218E-01	.235E-02	.530	.117E-01	.127E-02	-.7997
1.571	.906E-01	.118E-01	.668	.201E-01	.262E-02	.565	.118E-01	.154E-02	-.7704
1.616	.833E-01	.123E-01	.651	.169E-01	.249E-02	.592	.106E-01	.157E-02	-.7404
1.669	.124E 00	.133E-01	.634	.226E-01	.243E-02	.619	.153E-01	.164E-02	-.7009
1.718	.121E 00	.189E-01	.620	.203E-01	.317E-02	.638	.144E-01	.225E-02	-.6614
1.770	.116E 00	.137E-01	.608	.179E-01	.212E-02	.655	.132E-01	.157E-02	-.6152
1.817	.137E 00	.210E-01	.600	.199E-01	.304E-02	.666	.152E-01	.232E-02	-.5720
1.873	.123E 00	.194E-01	.593	.166E-01	.262E-02	.676	.130E-01	.205E-02	-.5160
1.920	.169E 00	.239E-01	.589	.216E-01	.306E-02	.681	.172E-01	.243E-02	-.4676
1.965	.173E 00	.219E-01	.587	.213E-01	.269E-02	.683	.170E-01	.215E-02	-.4207
2.022	.122E 00	.149E-01	.587	.145E-01	.176E-02	.683	.115E-01	.140E-02	-.3590
2.070	.972E-01	.276E-01	.589	.112E-01	.318E-02	.680	.886E-02	.251E-02	-.3073
2.123	.136E 00	.148E-01	.594	.154E-01	.167E-02	.674	.120E-01	.130E-02	-.2502
2.176	.119E 00	.105E-01	.601	.133E-01	.116E-02	.665	.101E-01	.884E-03	-.1944
2.220	.106E 00	.130E-01	.608	.117E-01	.144E-02	.655	.870E-02	.107E-02	-.1492
2.263	.749E-01	.868E-02	.617	.828E-02	.960E-03	.644	.596E-02	.690E-03	-.1065
2.322	.977E-01	.114E-01	.630	.109E-01	.127E-02	.625	.743E-02	.870E-03	-.0507
2.378	.879E-01	.110E-01	.644	.986E-02	.123E-02	.603	.638E-02	.798E-03	.0002
2.420	.721E-01	.180E-01	.656	.817E-02	.203E-02	.585	.504E-02	.126E-02	.0360
2.462	.866E-01	.146E-01	.669	.993E-02	.168E-02	.564	.582E-02	.982E-03	.0701

TABLE XVI

DIFFERENTIAL CROSS SECTIONS AT 2.5 GeV, 20°

p	$\frac{d^2\sigma}{d\Omega\, dp}$		p*	$\frac{d^2\sigma}{d\Omega^* dp^*}$		M_x	$\frac{d^2\sigma}{d\Omega^* dM}$		cosθ*
GeV/c	mb/(sr GeV/c)		GeV/c	mb/(sr GeV/c)		GeV	mb/(sr GeV)		
1.460	.934E-01	± .326E-01	.818	.341E-01	± .119E-01	.045	.133E-02	± .464E-03	-.7922
1.484	.223E 00	.283E-01	.810	.777E-01	.987E-02	.147	.101E-01	.128E-02	-.7790
1.510	.278E 00	.436E-01	.801	.924E-01	.145E-01	.203	.167E-01	.261E-02	-.7644
1.530	.245E 00	.411E-01	.795	.784E-01	.132E-01	.235	.165E-01	.277E-02	-.7526
1.540	.140E 00	.223E-01	.792	.440E-01	.702E-02	.249	.984E-02	.157E-02	-.7466
1.565	.690E-01	.130E-01	.785	.208E-01	.393E-02	.279	.525E-02	.990E-03	-.7314
1.588	.452E-01	.133E-01	.778	.134E-01	.386E-02	.302	.370E-02	.106E-02	-.7162
1.621	.230E-01	.973E-02	.770	.635E-02	.269E-02	.330	.192E-02	.814E-03	-.6943
1.669	.196E-01	.755E-02	.761	.534E-02	.195E-02	.360	.169E-02	.651E-03	-.6611
1.717	.193E-01	.102E-01	.753	.466E-02	.248E-02	.383	.167E-02	.889E-03	-.6257
1.771	.358E-01	.792E-02	.746	.812E-02	.180E-02	.401	.307E-02	.681E-03	-.5843
1.822	.194E-01	.891E-02	.742	.417E-02	.192E-02	.411	.163E-02	.748E-03	-.5435
1.869	.197E-01	.725E-02	.741	.406E-02	.150E-02	.416	.160E-02	.590E-03	-.5053
1.925	.141E-01	.805E-02	.741	.279E-02	.159E-02	.415	.110E-02	.627E-03	-.4586
1.966	.190E-01	.565E-02	.742	.365E-02	.109E-02	.411	.142E-02	.423E-03	-.4240
2.019	.264E-01	.553E-02	.746	.493E-02	.103E-02	.400	.186E-02	.390E-03	-.3794
2.067	.172E-01	.542E-02	.752	.315E-02	.990E-03	.387	.114E-02	.359E-03	-.3400
2.117	.220E-01	.520E-02	.759	.394E-02	.934E-03	.367	.135E-02	.319E-03	-.2988
2.174	.167E-01	.447E-02	.768	.296E-02	.791E-03	.336	.918E-03	.245E-03	-.2530
2.226	.205E-01	.551E-02	.779	.361E-02	.967E-03	.300	.985E-03	.264E-03	-.2125
2.270	.138E-01	.419E-02	.789	.241E-02	.733E-03	.260	.564E-03	.172E-03	-.1788
2.316	.122E-01	.608E-02	.801	.212E-02	.106E-02	.205	.387E-03	.193E-03	-.1450
2.364	.270E-01	.668E-02	.814	.471E-02	.117E-02	.113	.466E-03	.115E-03	-.1114

TABLE XVII

DIFFERENTIAL CROSS SECTIONS AT 2.9 GeV, 5.9°

p	$\frac{d^2\sigma}{d\Omega\, dp}$		p*	$\frac{d^2\sigma}{d\Omega^* dp^*}$		M_x	$\frac{d^2\sigma}{d\Omega^* dM}$		cosθ*
GeV/c	mb/(sr GeV/c)		GeV/c	mb/(sr GeV/c)		GeV	mb/(sr GeV)		
1.210	-.189E 00	± .253E 00	.863	-.104E 00	± .139E 00	.343	-.285E-01	± .381E-01	-.9896
1.243	-.816E-01	.900E-01	.834	-.403E-01	.445E-01	.435	-.144E-01	.159E-01	-.9882
1.291	.777E-01	.910E-01	.793	.327E-01	.383E-01	.538	.151E-01	.177E-01	-.9859
1.338	.458E-01	.102E 00	.754	.166E-01	.368E-01	.614	.913E-02	.203E-01	-.9832
1.388	.261E 00	.921E-01	.712	.800E-01	.282E-01	.684	.515E-01	.182E-01	-.9797
1.437	.197E 00	.858E-01	.673	.512E-01	.223E-01	.741	.375E-01	.164E-01	-.9756
1.480	.732E-01	.126E 00	.640	.165E-01	.284E-01	.784	.134E-01	.230E-01	-.9713
1.551	.266E 00	.136E 00	.587	.471E-01	.241E-01	.845	.446E-01	.228E-01	-.9624
1.590	.209E 00	.907E-01	.558	.323E-01	.140E-01	.875	.331E-01	.144E-01	-.9560
1.638	.172E 00	.107E 00	.524	.225E-01	.139E-01	.906	.253E-01	.157E-01	-.9470
1.683	.220E 00	.816E-01	.493	.245E-01	.910E-02	.932	.300E-01	.111E-01	-.9364
1.742	.275E 00	.815E-01	.454	.248E-01	.735E-02	.962	.338E-01	.100E-01	-.9190
1.790	.219E 00	.904E-01	.424	.166E-01	.685E-02	.983	.247E-01	.102E-01	-.9012
1.842	.340E 00	.765E-01	.394	.213E-01	.479E-02	1.003	.347E-01	.781E-02	-.8767
1.896	.336E 00	.102E 00	.363	.172E-01	.520E-02	1.021	.309E-01	.933E-02	-.8437
1.946	.409E 00	.100E 00	.337	.174E-01	.427E-02	1.035	.340E-01	.835E-02	-.8048
1.979	.357E 00	.129E 00	.321	.135E-01	.487E-02	1.042	.278E-01	.100E-01	-.7742
2.029	.466E 00	.162E 00	.299	.148E-01	.514E-02	1.053	.330E-01	.115E-01	-.7173
2.092	.439E 00	.115E 00	.276	.113E-01	.296E-02	1.063	.276E-01	.722E-02	-.6265
2.135	.409E 00	.993E-01	.263	.931E-02	.226E-02	1.068	.239E-01	.580E-02	-.5503
2.183	.311E 00	.877E-01	.252	.628E-02	.177E-02	1.072	.169E-01	.477E-02	-.4519
2.241	.271E 00	.722E-01	.243	.491E-02	.131E-02	1.076	.137E-01	.366E-02	-.3149
2.290	.425E 00	.954E-01	.240	.729E-02	.164E-02	1.077	.207E-01	.464E-02	-.1887
2.334	.301E 00	.102E 00	.241	.506E-02	.172E-02	1.076	.143E-01	.485E-02	-.0766
2.380	.339E 00	.177E 00	.245	.575E-02	.300E-02	1.075	.160E-01	.833E-02	.0410

TABLE XVIII

DIFFERENTIAL CROSS SECTIONS AT 2.9 GeV, 11.55°

p	$\frac{d^2\sigma}{d\Omega\, dp}$	p*	$\frac{d^2\sigma}{d\Omega^* dp^*}$	M_x	$\frac{d^2\sigma}{d\Omega^* dM}$	cosθ*
GeV/c	mb/(sr GeV/c)	GeV/c	mb/(sr GeV/c)	GeV	mb/(sr GeV)	
1.279	.147E 00 ± .830E-01	.862	.733E-01 ± .415E-01	.348	.204E-01 ± .115E-01	-.9549
1.317	.613E-01 .603E-01	.833	.274E-01 .269E-01	.439	.988E-02 .972E-02	-.9486
1.370	-.101E-01 .482E-01	.794	-.388E-02 .185E-01	.533	-.177E-02 .844E-02	-.9385
1.428	.851E-01 .418E-01	.754	.277E-01 .136E-01	.613	.152E-01 .747E-02	-.9254
1.467	.344E-01 .272E-01	.729	.101E-01 .795E-02	.658	.610E-02 .482E-02	-.9152
1.520	.546E-01 .225E-01	.695	.138E-01 .569E-02	.710	.941E-02 .388E-02	-.8992
1.575	.860E-01 .279E-01	.663	.187E-01 .608E-02	.755	.142E-01 .460E-02	-.8796
1.618	.101E 00 .458E-01	.639	.197E-01 .892E-02	.786	.160E-01 .726E-02	-.8619
1.670	.238E 00 .395E-01	.611	.405E-01 .673E-02	.818	.357E-01 .593E-02	-.8372
1.718	.154E 00 .509E-01	.588	.234E-01 .771E-02	.844	.220E-01 .727E-02	-.8108
1.770	.223E 00 .480E-01	.564	.298E-01 .642E-02	.868	.300E-01 .646E-02	-.7780
1.819	.134E 00 .669E-01	.545	.161E-01 .802E-02	.887	.171E-01 .852E-02	-.7434
1.870	.149E 00 .699E-01	.526	.161E-01 .753E-02	.904	.180E-01 .841E-02	-.7024
1.921	.185E 00 .520E-01	.510	.180E-01 .506E-02	.918	.211E-01 .591E-02	-.6563
1.965	.145E 00 .403E-01	.498	.130E-01 .362E-02	.928	.158E-01 .437E-02	-.6134
2.015	.198E 00 .329E-01	.487	.164E-01 .273E-02	.937	.205E-01 .340E-02	-.5597
2.062	.178E 00 .350E-01	.479	.138E-01 .272E-02	.944	.176E-01 .347E-02	-.5059
2.112	.226E 00 .390E-01	.472	.165E-01 .285E-02	.949	.214E-01 .370E-02	-.4442
2.172	.196E 00 .384E-01	.468	.135E-01 .264E-02	.952	.177E-01 .347E-02	-.3682
2.214	.175E 00 .575E-01	.467	.117E-01 .384E-02	.953	.154E-01 .506E-02	-.3138
2.267	.206E 00 .594E-01	.468	.133E-01 .385E-02	.952	.175E-01 .506E-02	-.2438
2.320	.143E 00 .809E-01	.472	.915E-02 .516E-02	.949	.119E-01 .671E-02	-.1742
2.379	.203E 00 .472E-01	.479	.129E-01 .299E-02	.944	.164E-01 .381E-02	-.0987
2.420	.215E 00 .709E-01	.485	.137E-01 .450E-02	.939	.171E-01 .564E-02	-.0482
2.461	.233E 00 .533E-01	.493	.149E-01 .341E-02	.932	.183E-01 .418E-02	.0006

TABLE XIX

DIFFERENTIAL CROSS SECTIONS AT 2.9 GeV, 15.72

p	$\frac{d^2\sigma}{d\Omega\ dp}$		p*	$\frac{d^2\sigma}{d\Omega^* dp^*}$		M_x	$\frac{d^2\sigma}{d\Omega^* dM}$		cosθ*
GeV/c	mb/(sr GeV/c)		GeV/c	mb/(sr GeV/c)		GeV	mb/(sr GeV)		
1.321	-.122E 00	± .666E-01	.897	-.620E-01	± .339E-01	.178	-.854E-02	± .466E-02	-.9169
1.369	.427E-01	.438E-01	.868	.193E-01	.198E-01	.328	.502E-02	.515E-02	-.9040
1.416	-.132E-01	.426E-01	.839	-.529E-02	.171E-01	.421	-.182E-02	.589E-02	-.8894
1.460	-.190E 00	.151E 00	.815	-.687E-01	.546E-01	.486	-.280E-01	.223E-01	-.8743
1.523	.549E-01	.408E-01	.782	.172E-01	.128E-01	.559	.836E-02	.621E-02	-.8496
1.569	.357E-01	.514E-01	.760	.101E-01	.146E-01	.603	.543E-02	.781E-02	-.8289
1.611	.104E 00	.467E-01	.742	.270E-01	.121E-01	.636	.156E-01	.701E-02	-.8086
1.666	.268E 00	.726E-01	.719	.623E-01	.169E-01	.673	.391E-01	.106E-01	-.7784
1.723	.198E-01	.376E-01	.699	.414E-02	.786E-02	.705	.279E-02	.530E-02	-.7441
1.771	.630E-01	.409E-01	.683	.121E-01	.787E-02	.727	.860E-02	.558E-02	-.7119
1.815	.659E-01	.398E-01	.672	.118E-01	.715E-02	.743	.871E-02	.526E-02	-.6911
1.878	.132E-01	.688E-01	.657	.216E-02	.112E-01	.763	.166E-02	.866E-02	-.6323
1.921	.154E 00	.414E-01	.649	.238E-01	.639E-02	.773	.188E-01	.505E-02	-.5974
1.965	.116E 00	.367E-01	.642	.170E-01	.536E-02	.781	.137E-01	.432E-02	-.5593
2.017	.147E 00	.330E-01	.636	.204E-01	.456E-02	.788	.167E-01	.374E-02	-.5126
2.082	.115E 00	.465E-01	.632	.150E-01	.608E-02	.793	.125E-01	.504E-02	-.4520
2.130	.562E-01	.331E-01	.632	.709E-02	.417E-02	.794	.589E-02	.346E-02	-.4064
2.179	.104E 00	.423E-01	.632	.129E-01	.521E-02	.793	.107E-01	.432E-02	-.3684
2.231	.788E-01	.233E-01	.636	.942E-02	.278E-02	.789	.774E-02	.228E-02	-.3101
2.275	.528E-01	.149E-01	.640	.621E-02	.175E-02	.784	.504E-02	.142E-02	-.2677
2.322	.774E-01	.197E-01	.645	.901E-02	.229E-02	.777	.719E-02	.182E-02	-.2243
2.367	.757E-01	.153E-01	.652	.874E-02	.177E-02	.769	.683E-02	.138E-02	-.1830
2.420	.245E-01	.337E-01	.662	.281E-02	.388E-02	.756	.214E-02	.295E-02	-.1354
2.464	.961E-01	.268E-01	.671	.111E-01	.309E-02	.744	.817E-02	.228E-02	-.0976

TABLE XX

DIFFERENTIAL CROSS SECTIONS AT 2.9 GeV, 20°

p	$\frac{d^2\sigma}{d\Omega\ dp}$		p*	$\frac{d^2\sigma}{d\Omega^* dp^*}$		M_x	$\frac{d^2\sigma}{d\Omega^* dM}$		cosθ*
GeV/c	mb/(sr GeV/c)		GeV/c	mb/(sr GeV/c)		GeV	mb/(sr GeV)		
1.630	.289E-01	± .594E-01	.853	.953E-02	± .196E-01	.380	.292E-02	± .601E-02	-.7567
1.673	.992E-02	.245E-01	.841	.307E-02	.756E-02	.416	.104E-02	.257E-02	-.7330
1.720	.527E-01	.259E-01	.830	.152E-01	.749E-02	.448	.563E-02	.277E-02	-.7050
1.769	.132E-01	.121E-01	.820	.358E-02	.327E-02	.474	.142E-02	.130E-02	-.6745
1.822	.247E-01	.133E-01	.811	.626E-02	.337E-02	.496	.261E-02	.140E-02	-.6400
1.861	.194E-01	.120E-01	.806	.472E-02	.292E-02	.507	.202E-02	.125E-02	-.6133
1.918	.161E-01	.134E-01	.801	.368E-02	.307E-02	.519	.163E-02	.136E-02	-.5733
1.967	.277E-01	.103E-01	.798	.609E-02	.226E-02	.525	.273E-02	.101E-02	-.5383
2.014	.362E-01	.984E-02	.797	.767E-02	.208E-02	.527	.345E-02	.937E-03	-.5037
2.060	.212E-01	.112E-01	.798	.435E-02	.229E-02	.525	.195E-02	.103E-02	-.4695
2.119	.292E-01	.913E-02	.801	.579E-02	.181E-02	.519	.255E-02	.799E-03	-.4257
2.177	.233E-01	.780E-02	.806	.449E-02	.150E-02	.508	.193E-02	.646E-03	-.3827
2.223	.137E-01	.876E-02	.811	.260E-02	.166E-02	.495	.108E-02	.691E-03	-.3485
2.268	.216E-01	.660E-02	.818	.404E-02	.123E-02	.480	.162E-02	.494E-03	-.3163
2.322	.201E-01	.827E-02	.827	.370E-02	.153E-02	.456	.140E-02	.577E-03	-.2776
2.371	.149E-01	.607E-02	.836	.273E-02	.111E-02	.430	.964E-03	.392E-03	-.2431
2.420	.938E-02	.100E-01	.847	.171E-02	.182E-02	.399	.554E-03	.591E-03	-.2103
2.462	.203E-01	.821E-02	.856	.368E-02	.149E-02	.368	.109E-02	.441E-03	-.1830

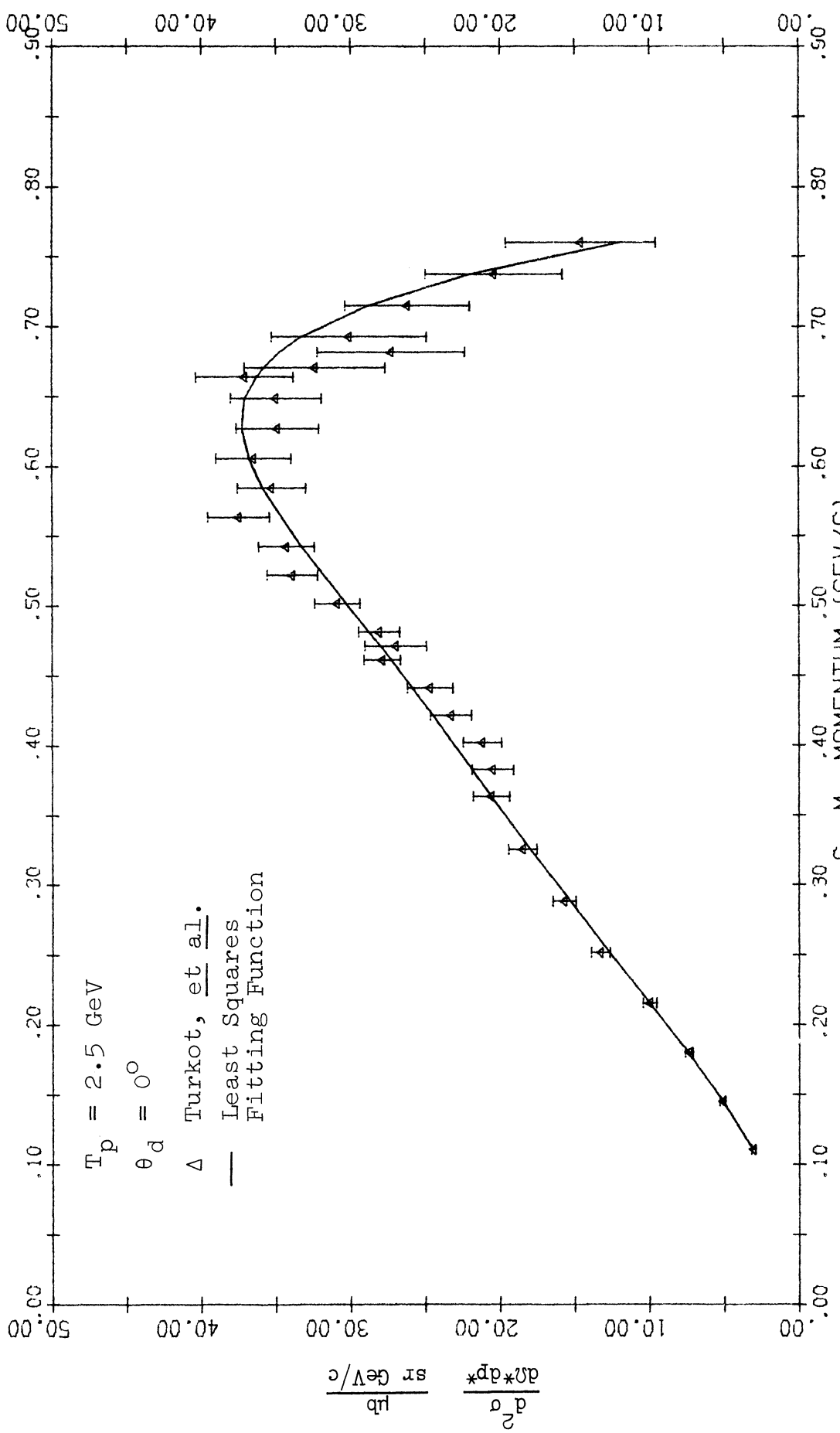

Fig. 48. C.m. differential cross section for deuteron production in p-p collisions vs. deuteron c.m. momentum from Turkot, et al.[12] T_p = 2.5 GeV, θ_d(lab) = 0°.

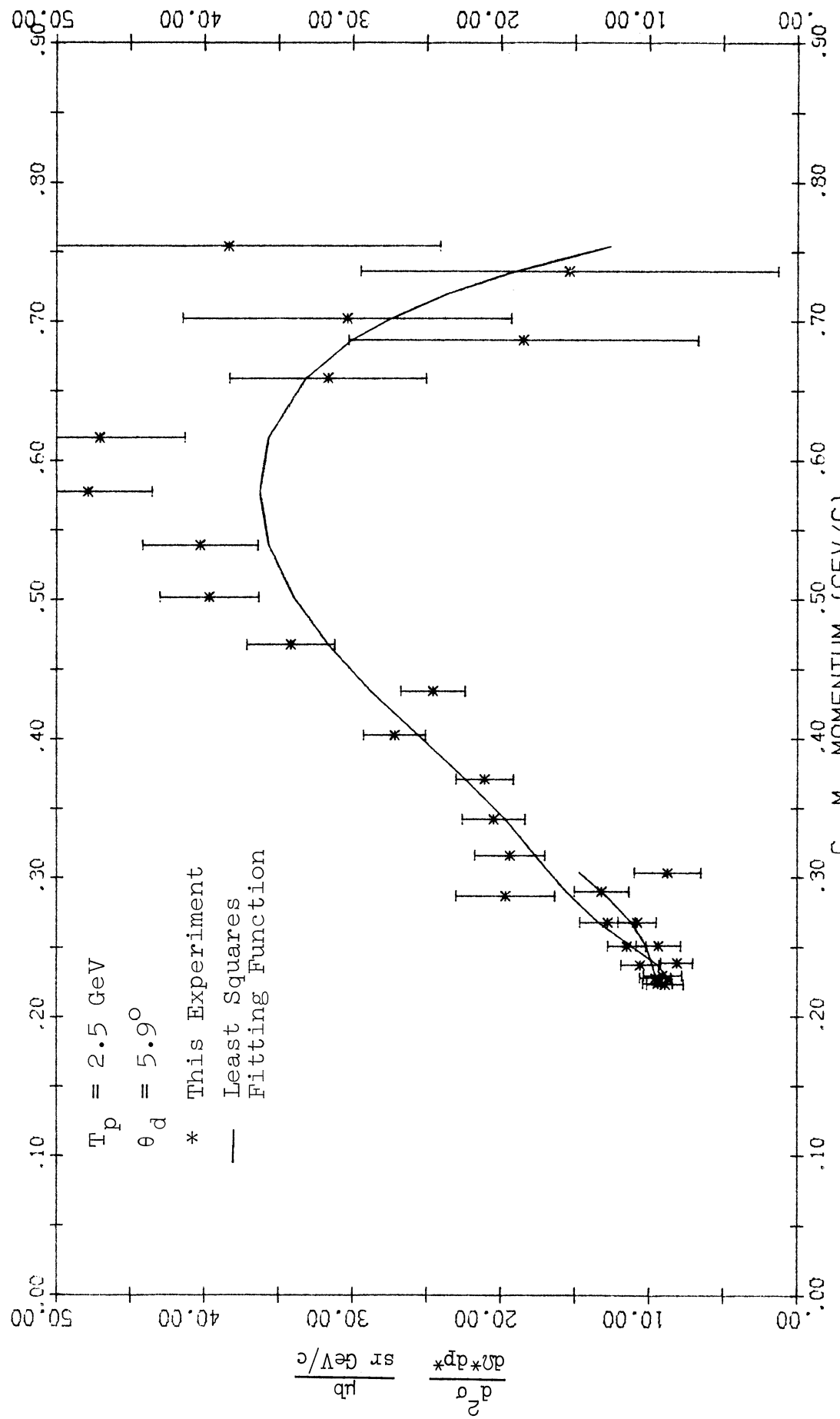

Fig. 49. C.m. differential cross section for deuteron production in p-p collisions vs. deuteron c.m. momentum. T_p = 2.5 GeV, θ_d(lab) = 5.9°.

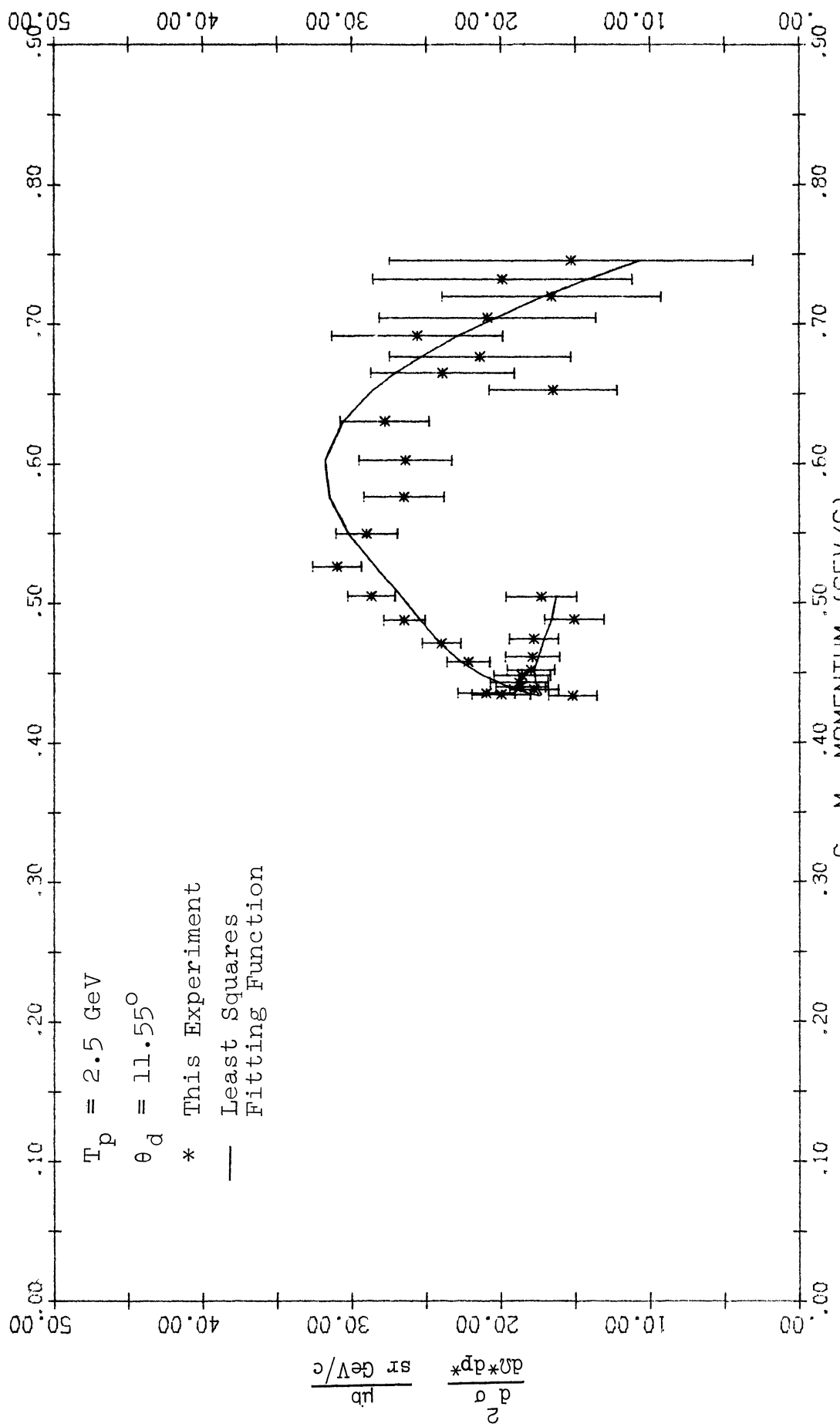

Fig. 50. C.m. differential cross section for deuteron production in p-p collisions vs. deuteron c.m. momentum. T_p = 2.5 GeV, θ_d(lab) = 11.55°.

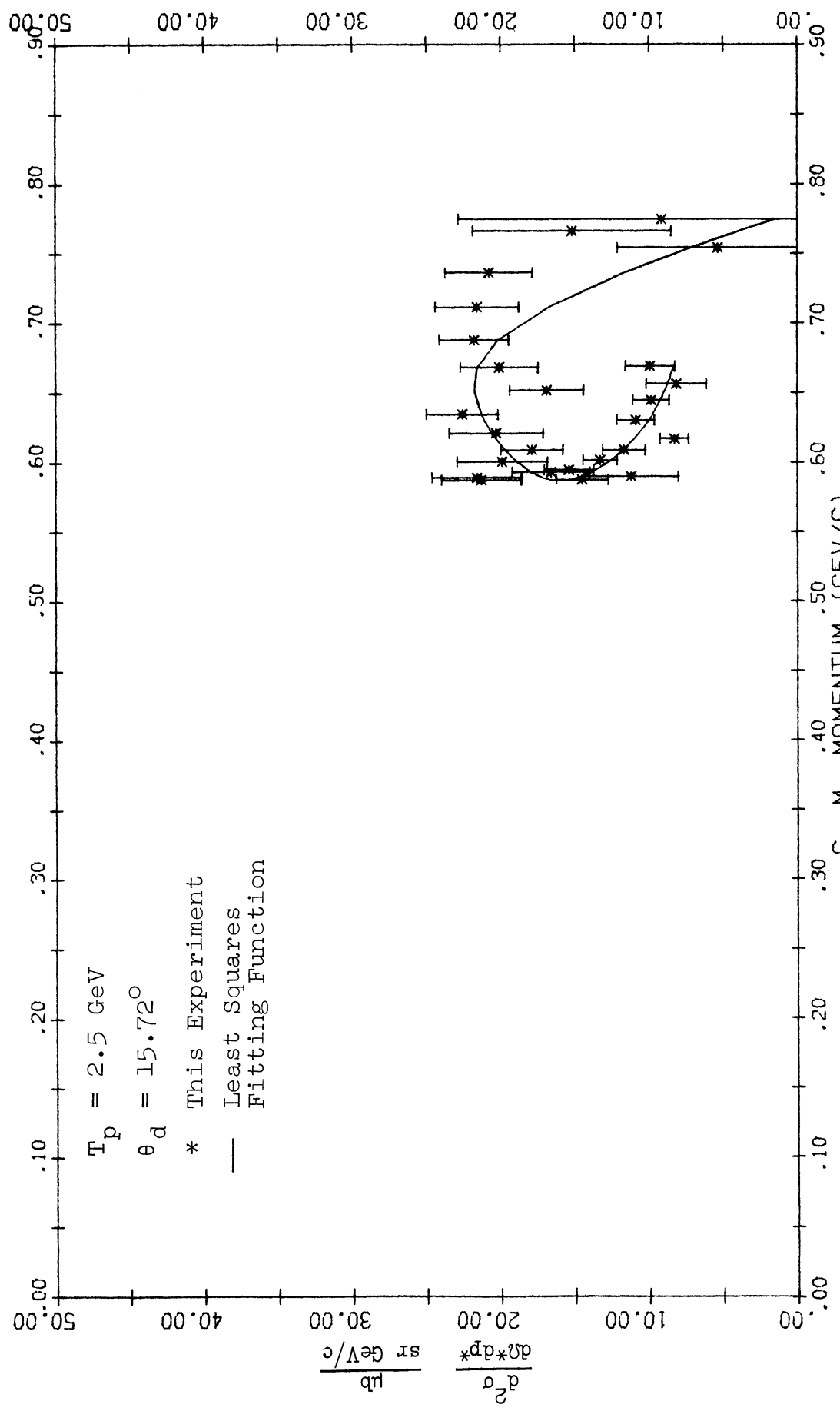

Fig. 51. C.m. differential cross section for deuteron production in p-p collisions vs. deuteron c.m. momentum. T_p = 2.5 GeV, θ_d(lab) = 15.72°.

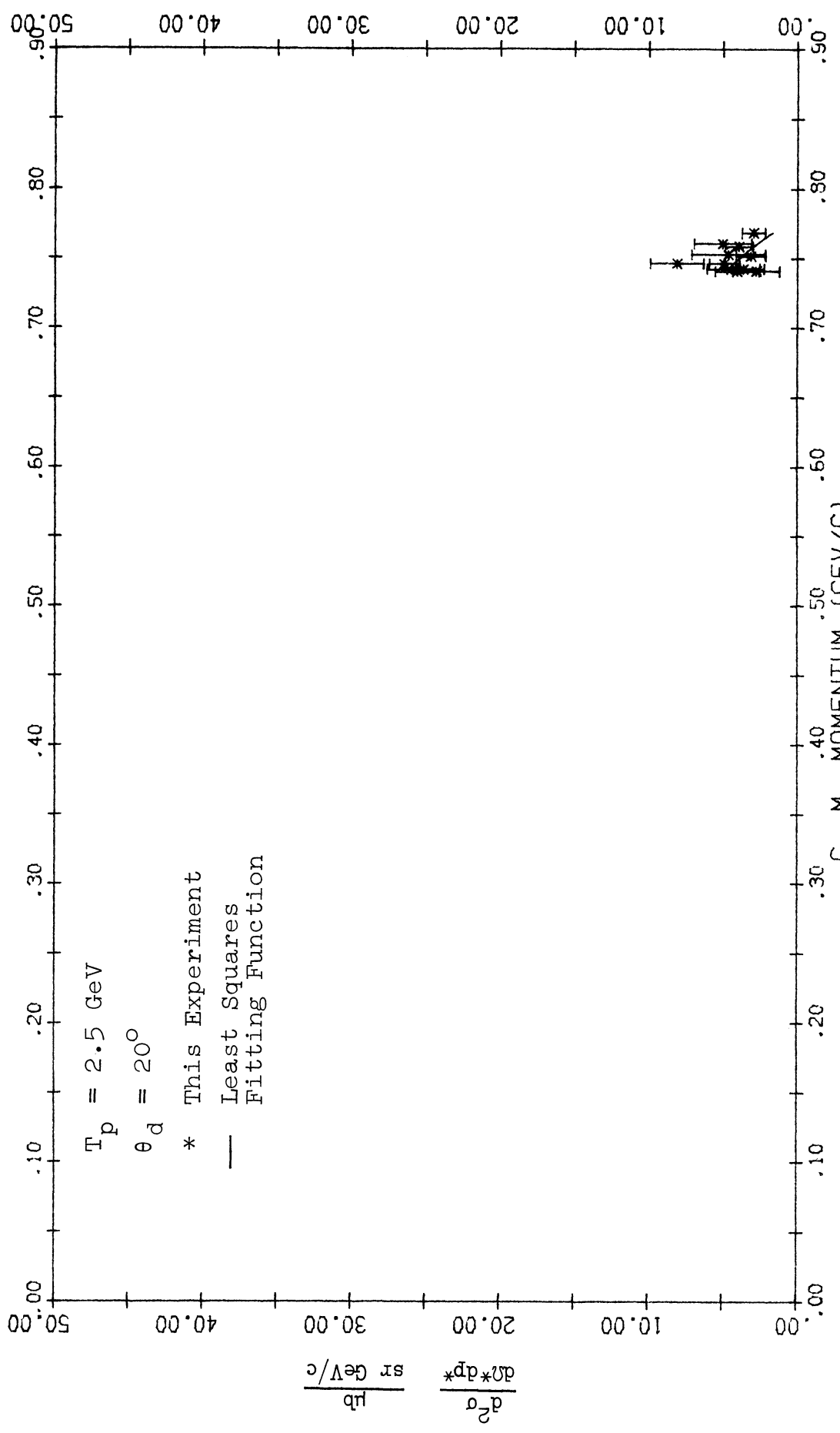

Fig. 52. C.m. differential cross section for deuteron production in p-p collision vs. deuteron c.m. momentum. T_p = 2.5 GeV, θ_d(lab) = 20°.

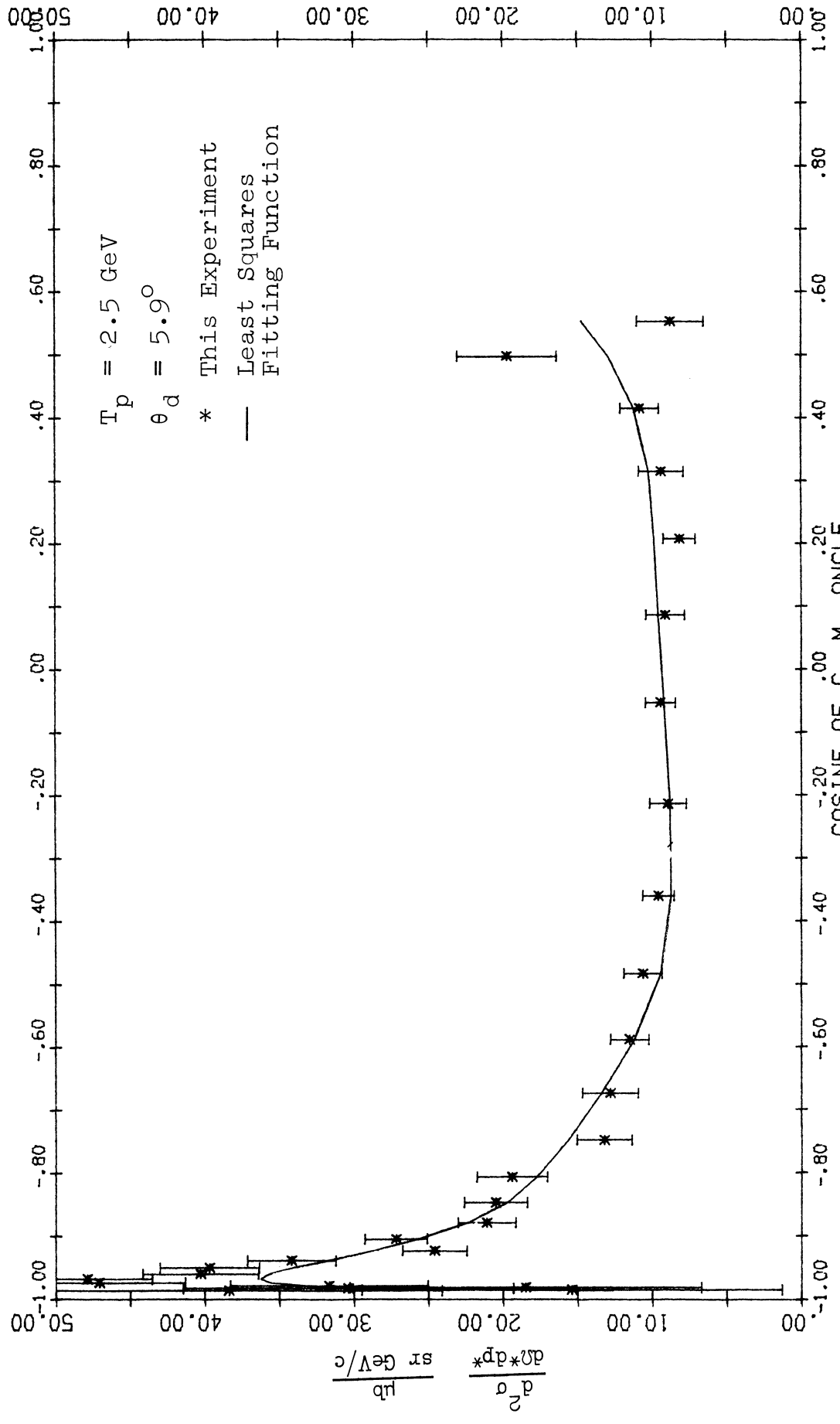

Fig. 53. C.m. differential cross section for deuteron production in p-p collision vs. the cosine of the deuteron c.m. production angle. T_p = 2.5 GeV, $\theta_d(lab)$ = 5.9°.

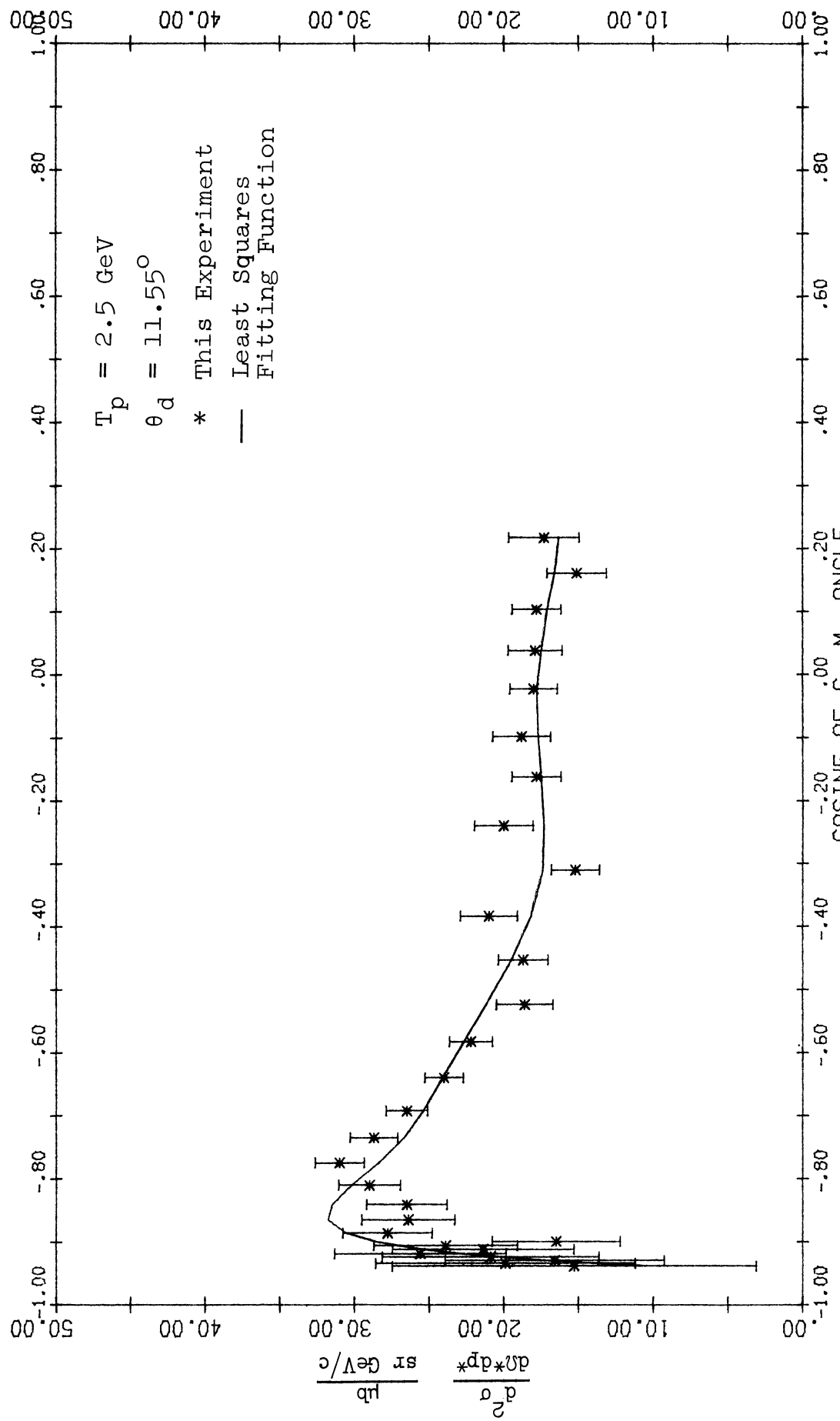

Fig. 54. C.m. differential cross section for deuteron production in p-p collisions vs. the cosine of the deuteron c.m. production angle. T_p = 2.5 GeV, $\theta_d(lab)$ = 11.55°.

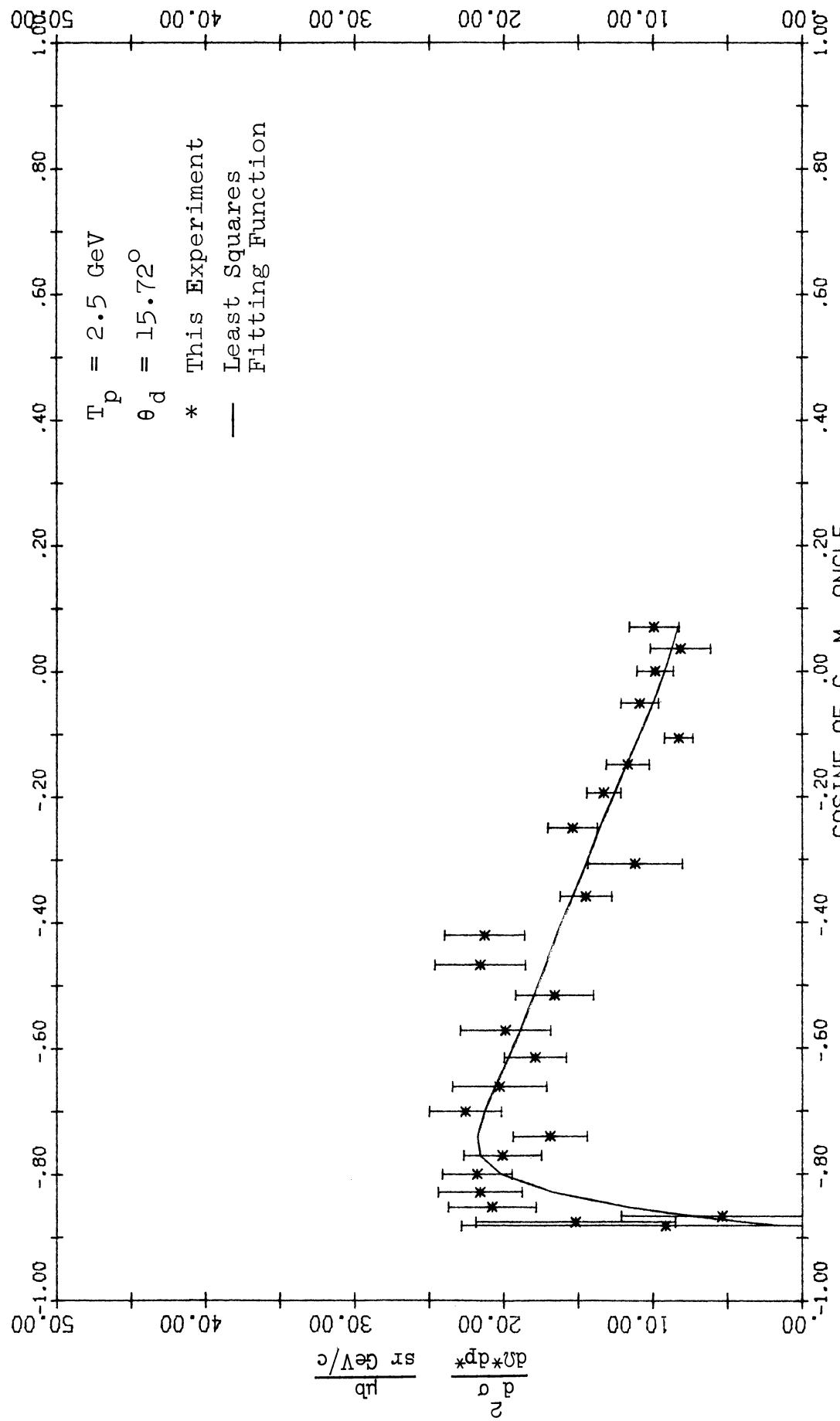

Fig. 55. C.m. differential cross section for deuteron production in p-p collisions vs. the cosine of the deuteron c.m. production angle. T_p = 2.5 GeV, θ_d(lab) = 15.72°.

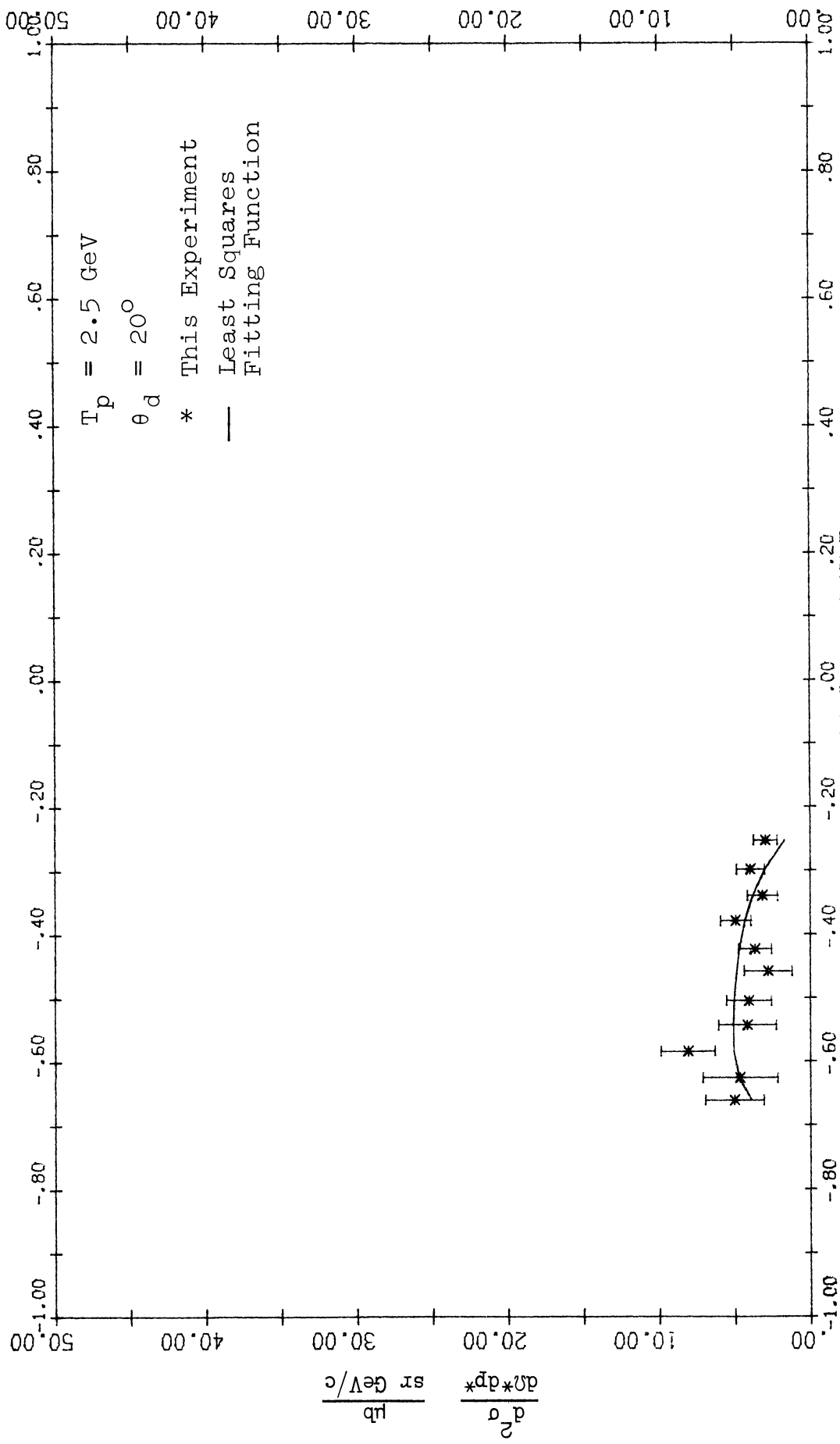

Fig. 56. C.m. differential cross section for deuteron production in p-p collisions vs. the cosine of the deuteron c.m. production angle. T_p = 2.5 GeV, $\theta_d(lab)$ = 20°.

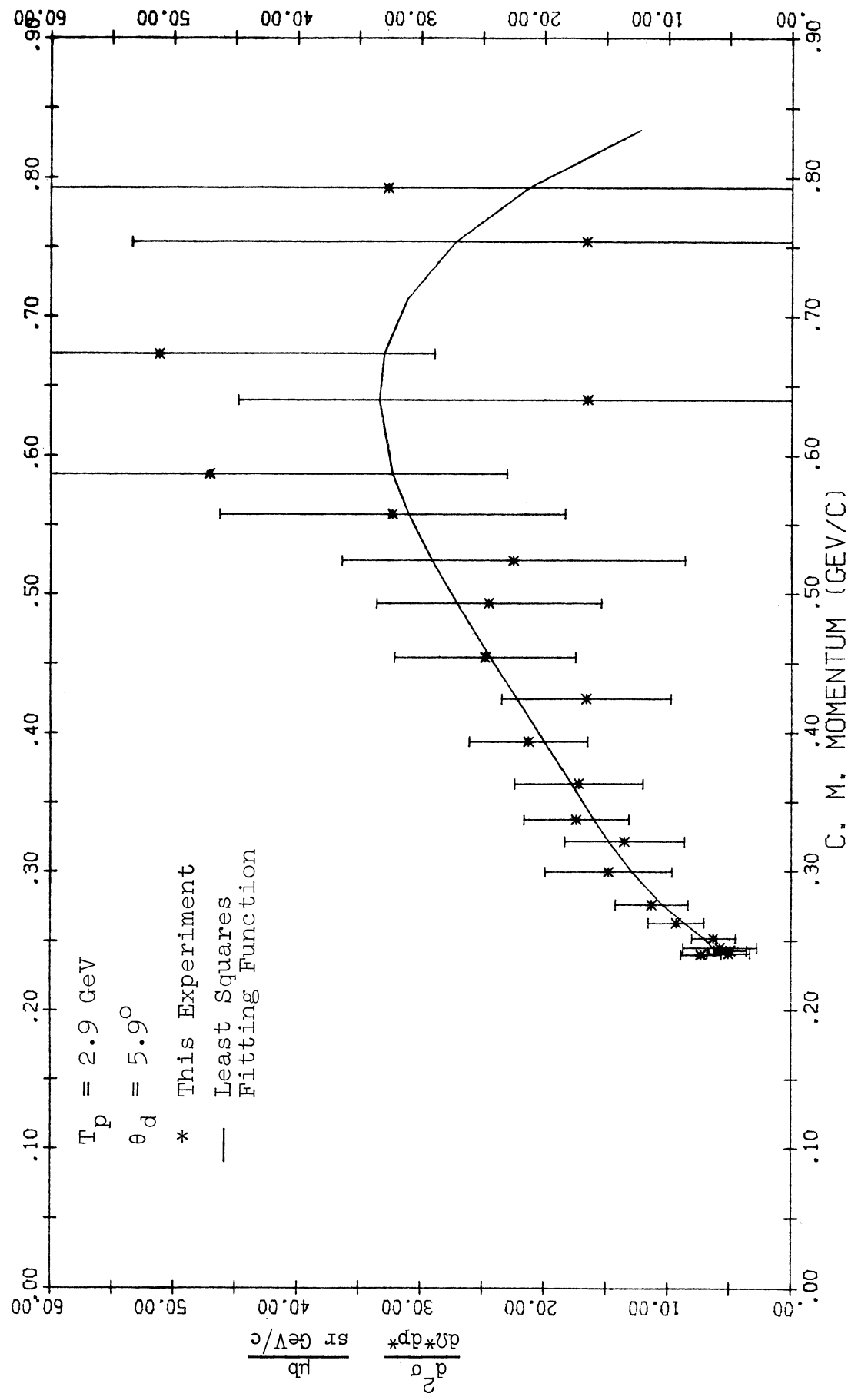

Fig. 57. C.m. differential cross section for deuteron production in p-p collisions vs. deuteron c.m. momentum. T_p = 2.9 GeV, θ_d(lab) = 5.9°.

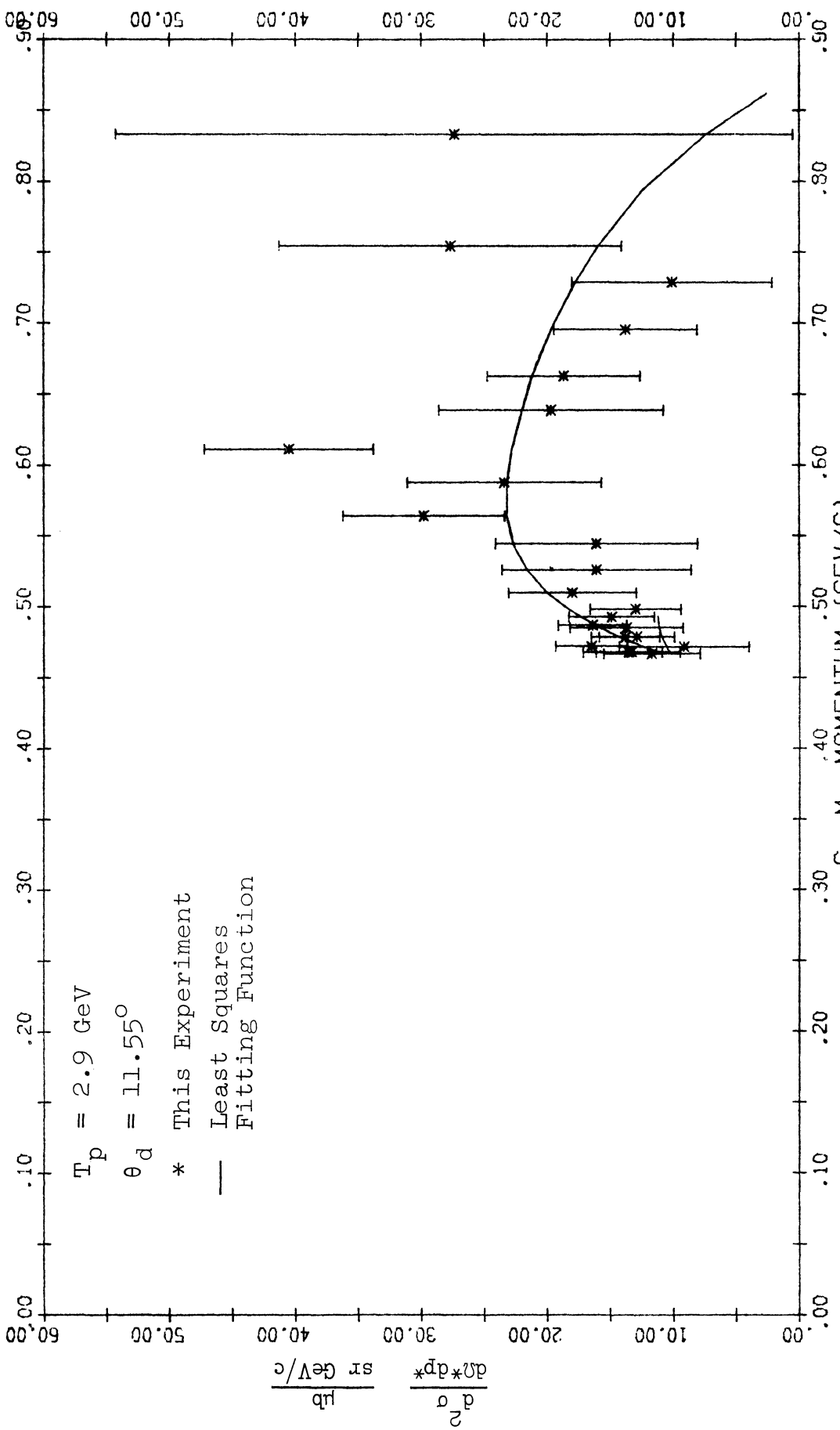

Fig. 58. C.m. differential cross section for deuteron production in p-p collisions vs. deuteron c.m. momentum. T_p = 2.9 GeV, θ_d(lab) = 11.55°.

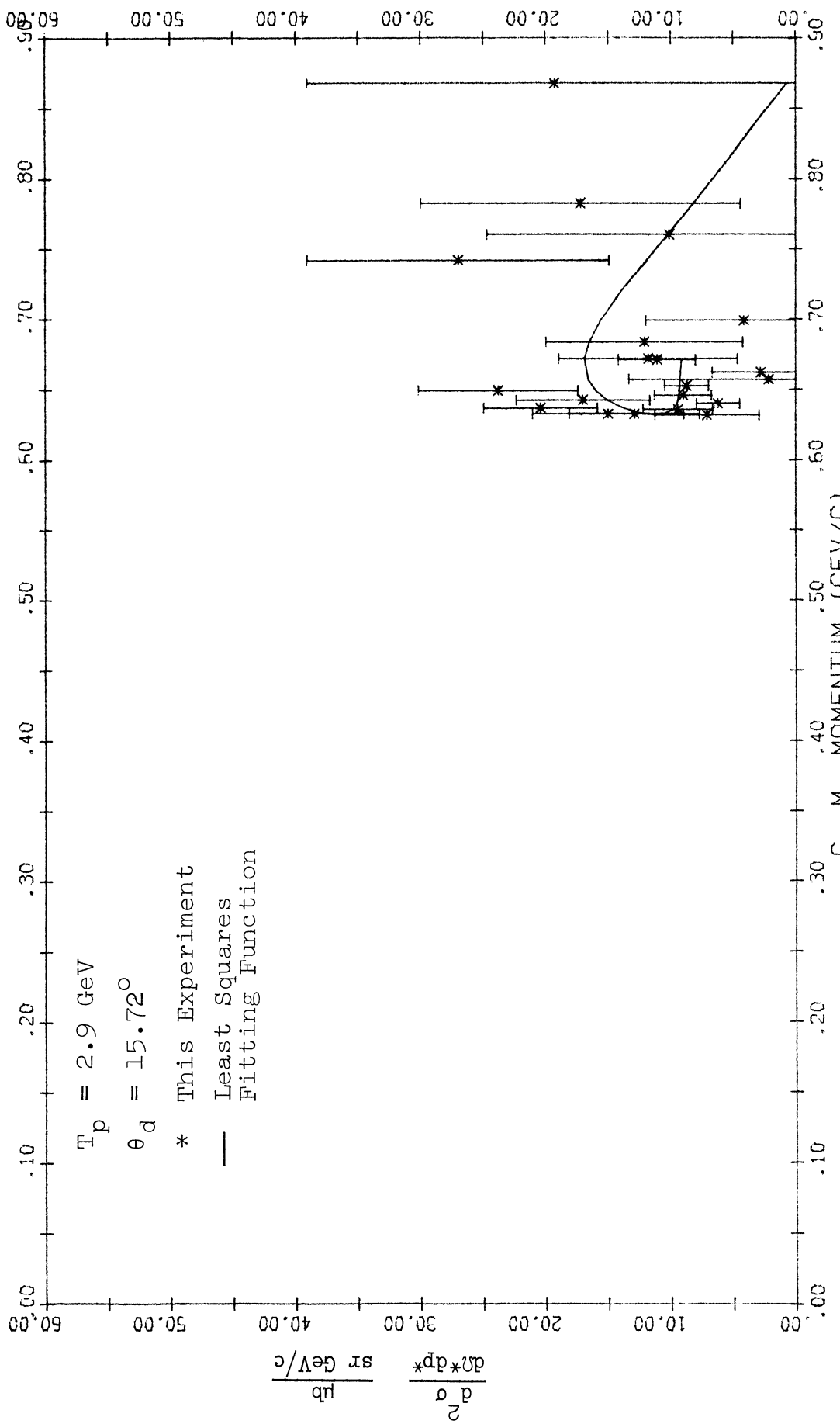

Fig. 59. C.m. differential cross section for deuteron production in p-p collisions vs. deuteron c.m. momentum. T_p = 2.9 GeV, θ_d(lab) = 15.72°.

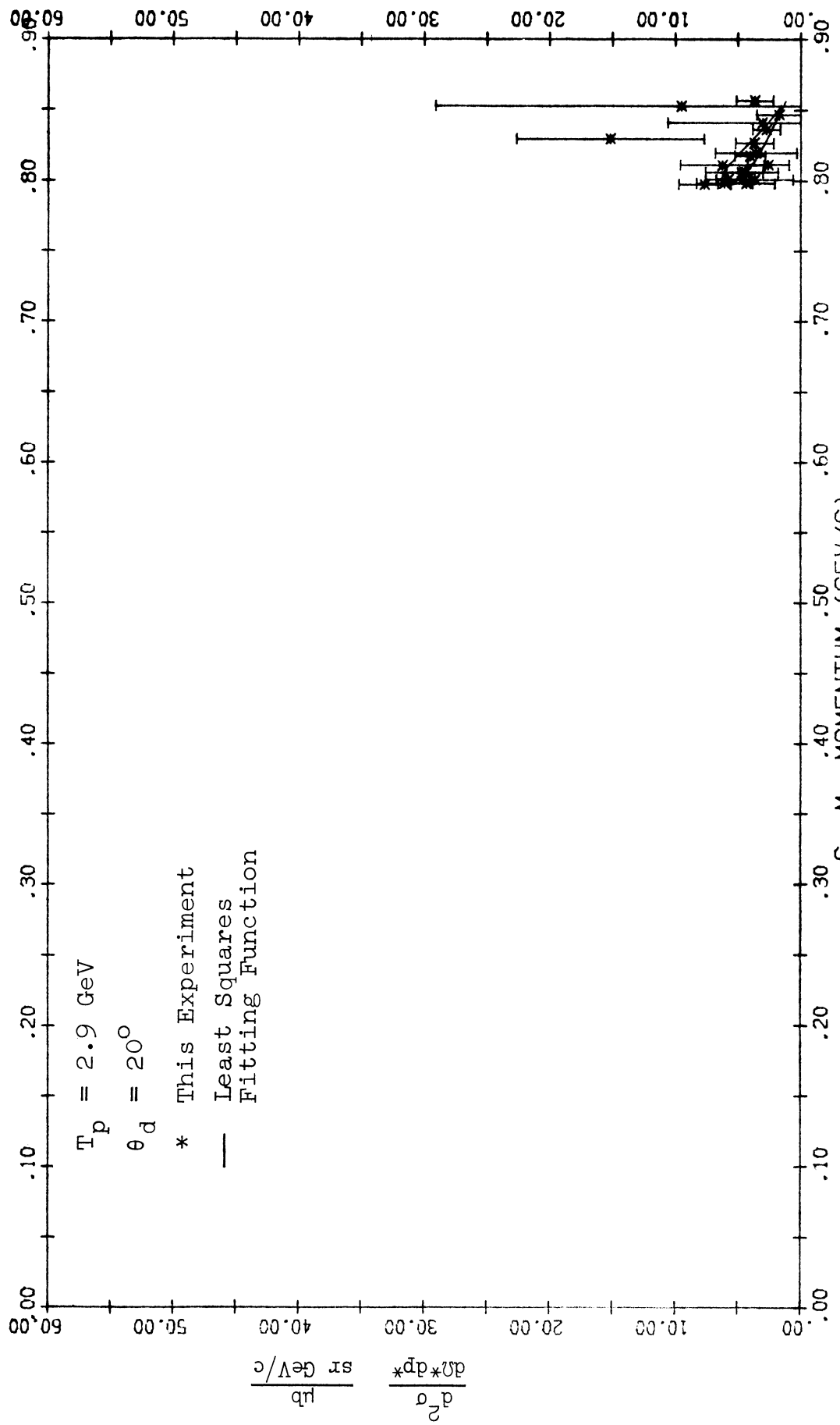

Fig. 60. C.m. differential cross section for deuteron production in p-p collisions vs. deuteron c.m. momentum. T_p = 2.9 GeV, θ_d(lab) = 20°.

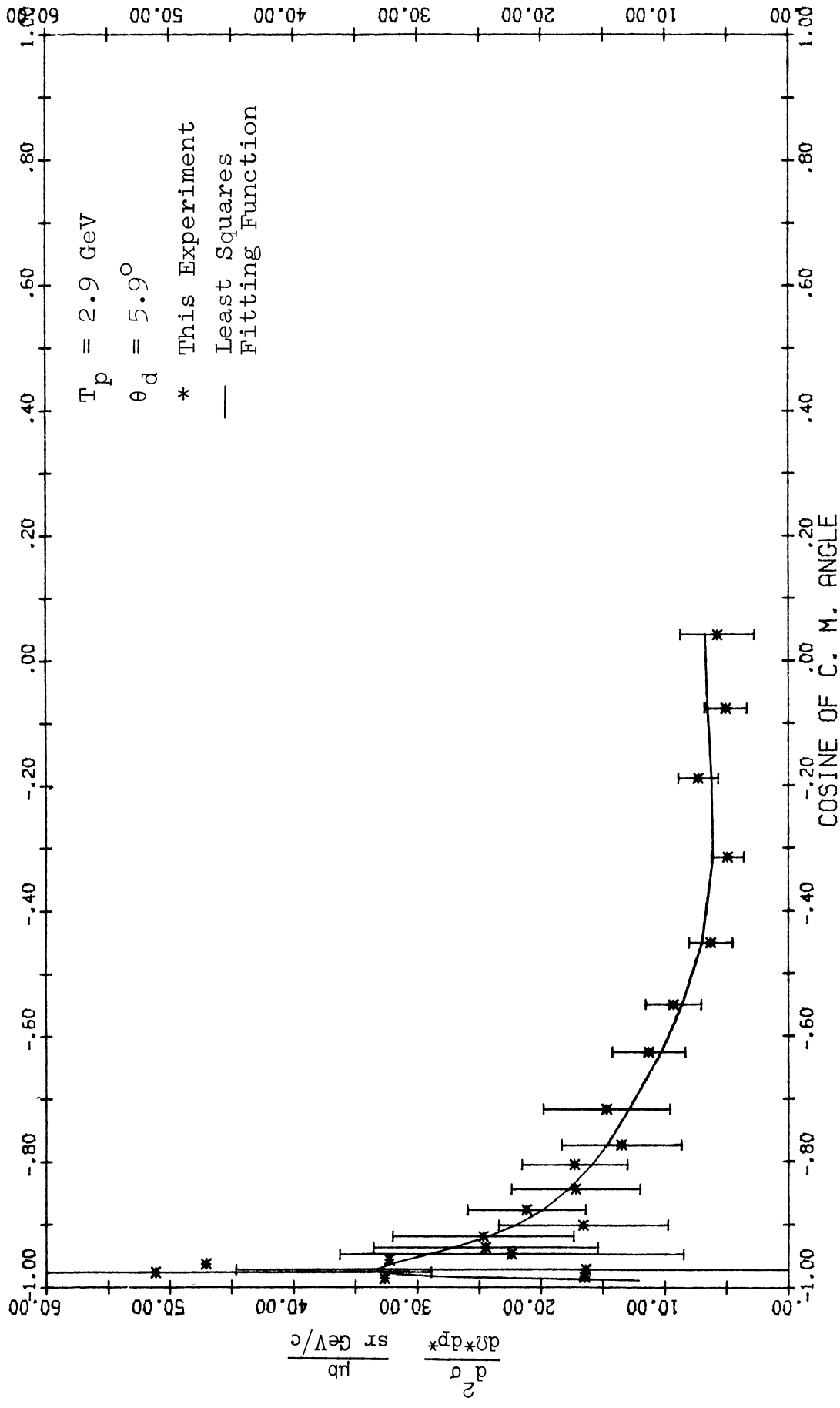

Fig. 61. C.m. differential cross section for deuteron production in p-p collisions vs. the cosine of the deuteron c.m. production angle. T_p = 2.9 GeV, $\theta_d(lab)$ = 5.9°. The error bars have been omitted from some points for the sake of clarity.

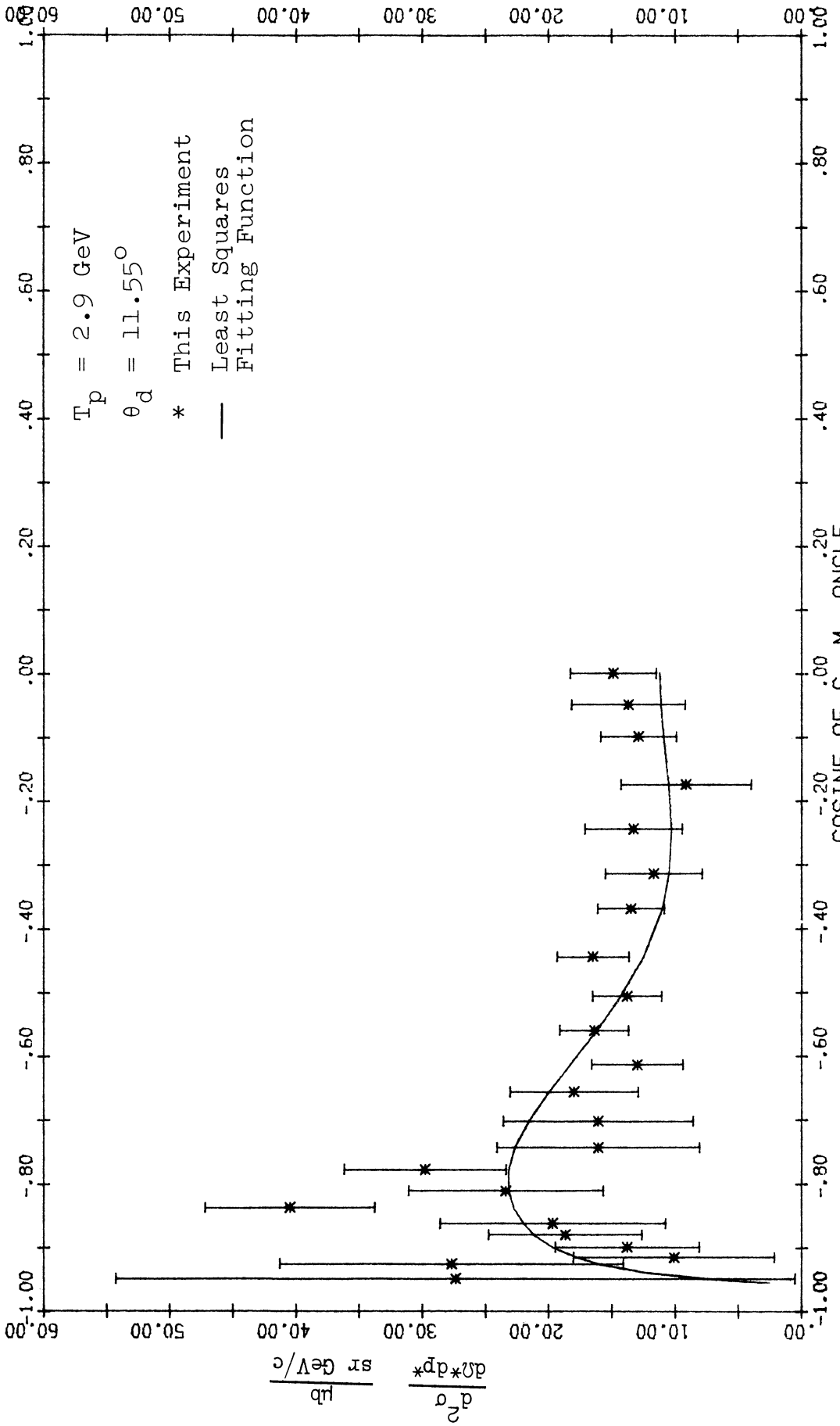

Fig. 62. C.m. differential cross section for deuteron production in p-p collisions vs. the cosine of the deuteron c.m. production angle. T_p = 2.9 GeV, $\theta_d(lab)$ = 11.55°.

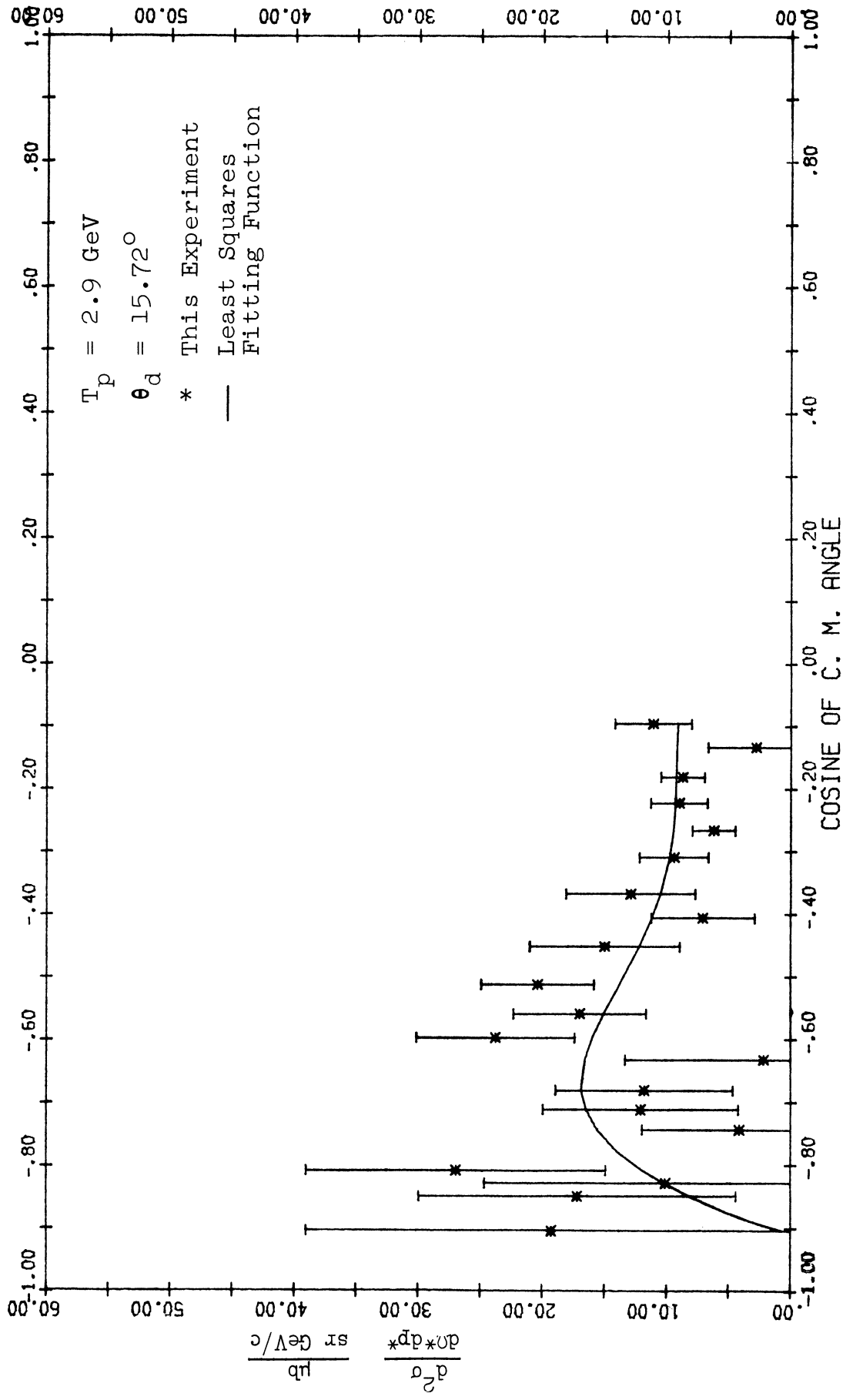

Fig. 63. C.m. differential cross section for deuteron production in p-p collisions vs. the cosine of the deuteron c.m. production angle. T_p = 2.9 GeV, θ_d(lab) = 15.72°.

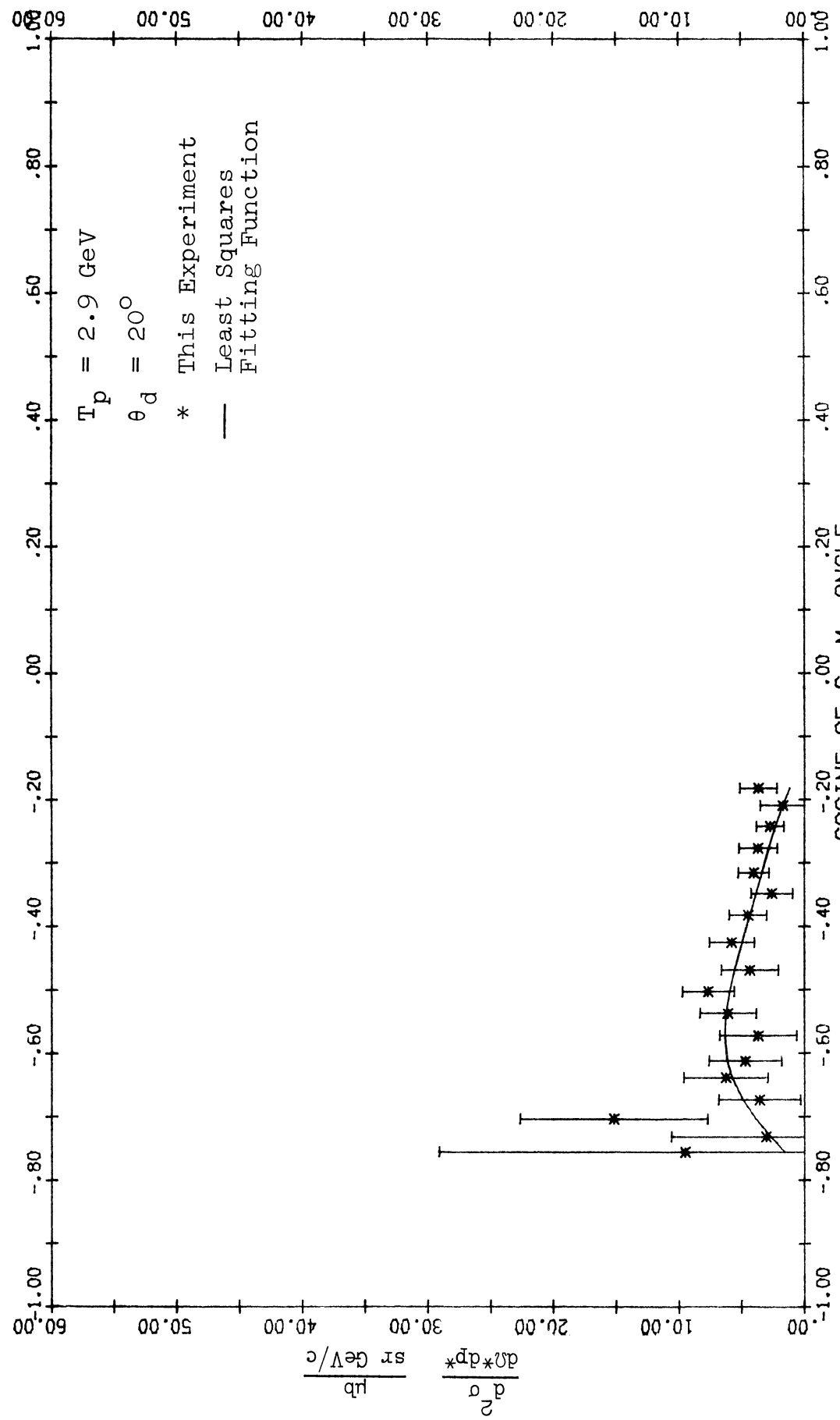

Fig. 64. C.m. differential cross section for deuteron production in p-p collisions vs. the cosine of the deuteron c.m. production angle. T_p = 2.9 GeV, θ_d(lab) = 20°.

LIST OF REFERENCES

1. O.E. Overseth, R.M. Heinz, L.W. Jones, M.J. Longo, D.E. Pellett, M.L. Perl, and F. Martin, Phys. Rev. Letters 13, 59(1964).

2. R.M. Heinz, "A Study of the Reaction $p + p \rightarrow d + \pi^+$ from 1 to 2.8 BeV" (Thesis), University of Michigan Technical Report No. 18, October 1964 (unpublished).

3. A.M. Eisner, E.L. Hart, R.I. Louttit, and T.W. Morris, Phys. Rev. 138, B670(1965).

4. E. Pickup, D.K. Robinson, and E.O. Salant, Phys. Rev. 125, 2091(1962).

5. E.L. Hart, R.I. Louttit, D. Luers, T.W. Morris, W.J. Willis, and S.S. Yamamoto, Phys. Rev. 126, 747(1962).

6. B. Sechi Zorn, Phys. Rev. Letters 8, 282(1962).

7. B. Sechi Zorn, Bull. Am. Phys. Soc. 7, 349(1962).

8. R. Barloutaud, J. Heughebaert, A. Leveque, J. Meyer, and R. Omnes, Phys. Rev. Letters 8, 32(1962).

9. A.R. Erwin, R. March, W.D. Walker, and E. West, Phys. Rev. Letters 6, 628(1961).

10. C.C. Peck, L.W. Jones, and M.L. Perl, Phys. Rev. 126, 1836(1962).

11. D.V. Bugg, A.J. Oxley, J.A. Zoll, J.G. Rushbrooke, V.E. Barnes, J.B. Kinson, W.P. Dodd, G.A. Doran, and L. Riddiford, Phys. Rev. 133, B1017(1964).

12. F. Turkot, G.B. Collins, T. Fujii, M.A.R. Kemp, J. Menes, J. Oostens, R.A. Carrigan, R.M. Edelstein, and N.C. Hien, "Deuteron Production in P-P Collisions in the Range 1.5 to 2.5 GeV," Sienna International Conference on Elementary Particles, September 1963 (unpublished).

13. F. Turkot, G.B. Collins, and T. Fujii, Phys. Rev. Letters 11, 474(1963).

14. A.N. Diddens, W. Galbraith, E. Lillethun, G. Manning, A.G. Parham, A.E. Taylor, T.G. Walker, and A.M. Wetherell, Nuovo Cimento 31, 961(1964).

15. R.A. Piroué and A.J.S. Smith, "Particle Production by 2.9-BeV Protons Incident on Beryllium and Platinum," Princeton-Pennsylvania Accelerator Report No. PPAD-589E, March 1966 (unpublished).

16. A.E Glassgold, Conference on Direct Interactions and Nuclear Reaction Mechanisms, Padua, 1962 (Gordon and Breach, New York, 1963), pp. 1114-1133.

17. R. Hagedorn, Phys. Rev. Letters 5, 276(1960).
R. Hagedorn, Nuovo Cimento 15, 434(1960).

18. R.M. Sternheimer and S.J. Lindenbaum, Phys. Rev. 123, 333(1961).
S.J. Lindenbaum and R.M. Sternheimer, Phys. Rev. 105, 1874(1957).

19. T. Yao, Phys. Rev. 134, B454(1964).

20. G.W. Bennett, "Cosmotron Proton Energy Measurement," Cosmotron Internal Report No. GWB-2, August 1962 (unpublished).

21. F. Eisler, "Magnet Characteristics," Cosmotron Internal Report No. FE-4, Rev. I, April 1963 (unpublished).

22. D.M. Ritson, Techniques of High Energy Physics, (Interscience Publishers, Ltd., London and New York, 1961), pp. 330, 449, 450.

23. R. Sugarman, F.C. Merritt, and W.A. Higinbotham, "Nanosecond Counter Circuit Manual, "Brookhaven National Laboratory Report BNL 711(T-248), February 1962 (unpublished).

24. W.T. Scott, Phys. Rev. 76, 212(1949).

25. A. Ashmore, "Multiple Scattering of Charged Particles" (Sec. VIII, High Energy and Nuclear Physics Data Handbook, The National Institute for Research in Nuclear Science, Rutherford High Energy Laboratory, Chilton (1963)).

26. H.A. Bethe, Phys. Rev. 89, 1256(1953).

27. G.Z. Moliere, Z. Naturforsch. 3a, 78(1948).

28. F.F. Chen, C.P. Leavitt, and A.A. Shapiro, Phys. Rev. 103, 211(1956).

29. D.V. Bugg, D.C. Salter, G.H. Stafford, R.F George, K.F. Riley, and R.J. Tapper, Phys. Rev. 146, 980(1966).

30. J. Orear, "Notes on Statistics for Physicists," University of California Radiation Laboratory Report UCRL-8417, August 1958 (unpublished).

31. J.R. Holt, J.C. Kluyver, and J.A. Moore, Proc. Phys. Soc. (London) 71, 781(1958).

32. H.A. Neal, Jr., "The Polarization Parameter in Elastic Proton-Proton Scattering from .75 to 2.84 GeV" (Thesis), University of Michigan Technical Report No. 23, April 1966 (unpublished), p. 19.

33. G. Moneti, "DALPS. A 7090 Program to Calculate the Boundary of Dalitz Plots and the Invariant Momentum Space for Three Particle Systems," Brookhaven National Laboratory Report No. F-96, August 1962 (unpublished).

T.E. Kalogeropoulos, "LIMS. A 7090 IBM Program for Effective Mass Distributions, Energy Spectra, and Angular Correlations, from the Invariant Momentum Space," Brookhaven National Laboratory Report No. F-89, August 1962 (unpublished).

34. P.M. Dauber, W.E. Slater, L.T. Smith, D.H. Stork, and H.K. Ticho, Phys. Rev. Letters 13, 449(1964).

35. W. Kienzle, B.C. Maglic, B. Levrat, F. Lefebvres, D. Freytag, and H.R. Blieden, Physics Letters 19, 438(1965).

36. L.B. Auerbach, T. Elioff, W.B. Johnson, J. Lach, C.E. Wiegand, and T. Ypsilantis, Phys. Rev. Letters 9, 173 (1962).

H.R. Blieden, D. Freytag, J. Geibel, A.R.F. Hassan, W. Kienzle, F. Lefebvres, B. Levrat, B.C. Maglic, J. Seguinot, and A.J. Smith, Physics Letters 19, 444(1965).

37. A.M. Poskanzer, L.P. Remsberg, S. Katcoff, and J.B. Cumming, Phys. Rev. 133, B 1507(1964).

J.B. Cumming, G. Friedlander, and C.E. Swartz, Phys. Rev. 111, 1386(1958).

38. J.B. Cumming, A.M. Poskanzer, and J. Hudis, Phys. Rev. Letters 6, 484(1961).

J.B. Cumming, J. Hudis, A.M. Poskanzer, and S. Kaufman, Phys. Rev. 128, 2392(1962).

39. W.H. Moore, "Absolute Polyethylene Foil Counting," Cosmotron Internal Report No. WHM-13, December 1963 (unpublished).

Unclassified

Security Classification

DOCUMENT CONTROL DATA - R&D

(Security classification of title, body of abstract and indexing annotation must be entered when the overall report is classified)

1. ORIGINATING ACTIVITY (Corporate author) The University of Michigan Department of Physics Ann Arbor, Michigan	2a. REPORT SECURITY CLASSIFICATION Unclassified 2b. GROUP

3. REPORT TITLE

DEUTERON PRODUCTION IN PROTON-PROTON COLLISIONS FROM 1.5 TO 3 GeV

4. DESCRIPTIVE NOTES (Type of report and inclusive dates)

Technical Report

5. AUTHOR(S) (Last name, first name, initial)

Pellett, David E.

6. REPORT DATE	7a. TOTAL NO. OF PAGES	7b. NO. OF REFS
August 1966	151	39

8a. CONTRACT OR GRANT NO.	9a. ORIGINATOR'S REPORT NUMBER(S)
Nonr-1224(23) b. PROJECT NO. NR-022-274 c. d.	03106-26-T 9b. OTHER REPORT NO(S) (Any other numbers that may be assigned this report) Technical Report No. 26

10. AVAILABILITY/LIMITATION NOTICES

Distribution of this document is unlimited.

11. SUPPLEMENTARY NOTES	12. SPONSORING MILITARY ACTIVITY
	Department of the Navy Office of Naval Research Washington, D. C.

13. ABSTRACT

The differential cross section for deuteron production in proton-proton collisions was measured for incident proton kinetic energies of 1.55, 2.5, and 2.9 GeV. Measurements were made at laboratory angles of 5.9°, 11.55°, 15.72°, and at the two higher energies, at 20° relative to the beam direction for deuteron laboratory momenta in the range 1.0-2.4 GeV/c.

The experiment was performed in an external proton beam of the cosmotron at Brookhaven National Laboratory. A system of scintillation and Cerenkov counters was used to identify deuterons by momentum analysis and time-of-flight techniques.

The differential cross sections are presented in the laboratory and center of mass (c.m) systems. Plots are given of the cross section versus the invariant mass of the system of particles formed with the deuteron in the collisions. Total cross sections were obtained by integrating a smooth function fitted to the c.m. data at each energy.

The deuteron distributions in the laboratory system were peaked at small angles relative to the beam direction. All deuterons were formed with momenta > 1.0 GeV/c.

The c.m. differential cross section distributions obtained at the three energies of this experiment showed a general similarity to one another. The cross section

(Concluded on next page)

DD FORM 1 JAN 64 1473

Unclassified

Security Classification

14. KEY WORDS	LINK A		LINK B		LINK C	
	ROLE	WT	ROLE	WT	ROLE	WT
Deuteron production Proton-proton collisions						

INSTRUCTIONS

1. ORIGINATING ACTIVITY: Enter the name and address of the contractor, subcontractor, grantee, Department of Defense activity or other organization *(corporate author)* issuing the report.

2*a*. REPORT SECURITY CLASSIFICATION: Enter the overall security classification of the report. Indicate whether "Restricted Data" is included. Marking is to be in accordance with appropriate security regulations.

2*b*. GROUP: Automatic downgrading is specified in DoD Directive 5200.10 and Armed Forces Industrial Manual. Enter the group number. Also, when applicable, show that optional markings have been used for Group 3 and Group 4 as authorized.

3. REPORT TITLE: Enter the complete report title in all capital letters. Titles in all cases should be unclassified. If a meaningful title cannot be selected without classification, show title classification in all capitals in parenthesis immediately following the title.

4. DESCRIPTIVE NOTES: If appropriate, enter the type of report, e.g., interim, progress, summary, annual, or final. Give the inclusive dates when a specific reporting period is covered.

5. AUTHOR(S): Enter the name(s) of author(s) as shown on or in the report. Enter last name, first name, middle initial. If military, show rank and branch of service. The name of the principal author is an absolute minimum requirement.

6. REPORT DATE: Enter the date of the report as day, month, year; or month, year. If more than one date appears on the report, use date of publication.

7*a*. TOTAL NUMBER OF PAGES: The total page count should follow normal pagination procedures, i.e., enter the number of pages containing information.

7*b*. NUMBER OF REFERENCES: Enter the total number of references cited in the report.

8*a*. CONTRACT OR GRANT NUMBER: If appropriate, enter the applicable number of the contract or grant under which the report was written.

8*b*, 8*c*, & 8*d*. PROJECT NUMBER: Enter the appropriate military department identification, such as project number, subproject number, system numbers, task number, etc.

9*a*. ORIGINATOR'S REPORT NUMBER(S): Enter the official report number by which the document will be identified and controlled by the originating activity. This number must be unique to this report.

9*b*. OTHER REPORT NUMBER(S): If the report has been assigned any other report numbers *(either by the originator or by the sponsor)*, also enter this number(s).

10. AVAILABILITY/LIMITATION NOTICES: Enter any limitations on further dissemination of the report, other than those imposed by security classification, using standard statements such as:

(1) "Qualified requesters may obtain copies of this report from DDC."

(2) "Foreign announcement and dissemination of this report by DDC is not authorized."

(3) "U. S. Government agencies may obtain copies of this report directly from DDC. Other qualified DDC users shall request through _____."

(4) "U. S. military agencies may obtain copies of this report directly from DDC. Other qualified users shall request through _____."

(5) "All distribution of this report is controlled. Qualified DDC users shall request through _____."

If the report has been furnished to the Office of Technical Services, Department of Commerce, for sale to the public, indicate this fact and enter the price, if known.

11. SUPPLEMENTARY NOTES: Use for additional explanatory notes.

12. SPONSORING MILITARY ACTIVITY: Enter the name of the departmental project office or laboratory sponsoring *(paying for)* the research and development. Include address.

13. ABSTRACT: Enter an abstract giving a brief and factual summary of the document indicative of the report, even though it may also appear elsewhere in the body of the technical report. If additional space is required, a continuation sheet shall be attached.

It is highly desirable that the abstract of classified reports be unclassified. Each paragraph of the abstract shall end with an indication of the military security classification of the information in the paragraph, represented as *(TS), (S), (C), or (U)*

There is no limitation on the length of the abstract. However, the suggested length is from 150 to 225 words.

14. KEY WORDS: Key words are technically meaningful terms or short phrases that characterize a report and may be used as index entries for cataloging the report. Key words must be selected so that no security classification is required. Identifiers, such as equipment model designation, trade name, military project code name, geographic location, may be used as key words but will be followed by an indication of technical context. The assignment of links, rules, and weights is optional.

DD Form 1473

ABSTRACT (Concluded)

was sharply peaked in the forward and backward directions for large c.m. momenta. The maximum became more broad as the momentum decreased until the cross section was almost isotropic. There was evidence of structure in the broad maximum at intermediate momenta.

The total deuteron production cross section decreased monotonically with incident proton kinetic energy from 310 ± 25 μb at 1.5 GeV to 137 ± 21 μb at 2.9 GeV. The interpolated value at 2.3 GeV was consistent with the statistical model prediction. The cross section for production of deuterons associated with two or more pions had a maximum near 2 GeV.

A search for pion resonances of unit isotopic spin in the mass range 400-1000 MeV through reactions of the form $p + p \rightarrow d + x^+$ yielded evidence for ρ production. At 2.5 GeV, the ρ production cross section was small ($\sigma_{total} \lesssim 9$ μb) and did not appear to be sharply peaked in the forward and backward directions. Upper limits were set for the production of the ζ (560 MeV) and the X^+ (960 MeV) resonances.

The laboratory distributions in momentum and angle of deuterons produced in proton-proton collisions at 2.9 GeV were found to be much different from those arising from proton-beryllium and proton-platinum collisions at the same energy. The total deuteron production cross section per nucleon was approximately six times greater in collisions of protons with beryllium than in collisions with other protons, indicating that specifically nuclear processes are at work in the former case.